

Dissertation zur Erlangung des Doktorgrades
der Fakultät für Chemie und Pharmazie
der Ludwig-Maximilians-Universität München

**Aggregation of Organozinc Species in Solution
and Their Reactivity**



Julia Elisabeth Fleckenstein

aus Würzburg

2011

Erklärung

Diese Dissertation wurde im Sinne von § 13 Abs. 3 bzw. 4 der Promotionsordnung vom 29. Januar 1998 (in der Fassung der sechsten Änderungssatzung vom 16. August 2010) von Herrn Prof. Dr. Konrad Koszinowski betreut.

Ehrenwörtliche Versicherung

Diese Dissertation wurde selbständige, ohne unerlaubte Hilfe erarbeitet.

München,

Julia Fleckenstein

Dissertation eingereicht am:

1. Gutachter Prof. Dr. Konrad Koszinowski
2. Gutachter Prof. Dr. Herbert Mayr

Mündliche Prüfung am: 16.12.2011

Acknowledgements

First, I would like to express my sincere gratitude to Prof. Dr. Konrad Koszinowski for giving me the opportunity to perform this thesis in his group. I have always appreciated the fruitful discussions, his support, his knowledge of chemistry and inspiring ideas.

Especially, I would like to thank Prof. Dr. Herbert Mayr for his continuous generous support and help.

Furthermore, I thank the board of examiners for reviewing this thesis and for their participation in my defense examination.

This work would not be possible without the help, support, collaboration, motivation, proof reading, and knowledge of the past and present co-workers of the Koszinowski and Mayr group. Special thanks to Petra Böhrer, Katharina Böck, Christina Müller and Alex Putau for their friendship and kindness. I also would like to thank my former students Areenan In-Iam, Katharina Böck and Philipp Schmid for their contribution to this work in course of their internships in the Koszinowski group. For the fruitful SFB collaboration and the all the interesting discussions I express my deepest gratitude to Dr. Matthias Schade and the Knochel group. I really would like to thank the analytical team of the LMU for their invaluable help, Sonja Kosak and, especially Dr. David Stephenson for his patience and time.

Additionally, I thank Prof. Dr. Dr. h.c. Dr. h.c. Helmut Schwarz for giving me the opportunity to stay in his group at the Technical University of Berlin, as well as Robert Kretschmer for his collaboration.

Finally, I would like to thank my family and Florian for their belief, motivation and love. Thank you very much!

Parts of the results of this thesis have been published in:

Microsolvated and Chelated Butylzinc Cations: Formation, Relative Stability, and Unimolecular Gas-Phase Chemistry

J. E. Fleckenstein, K. Koszinowski, *Chem. Eur. J.* **2009**, *15*, 12745.

Charged Tags as Probes for Analyzing Organometallic Intermediates and Monitoring Cross-Coupling Reactions by Electrospray Ionization Mass Spectrometry

M. A. Schade, J. E. Fleckenstein, P. Knochel, K. Koszinowski, *J. Org. Chem.* **2010**, *75*, 6848.

Lithium Organozincate Complexes LiRZnX_2 : Common Species in Organozinc Chemistry

J. E. Fleckenstein, K. Koszinowski, *Organometallics* **2011**, *30*, 5018.

Table of Contents

1	Abstract	1
2	Introduction	2
	2.1 <i>Organozinc Reagents</i>	2
	2.2 <i>Objectives</i>	5
3	Experimental Section	7
	3.1 <i>Electrospray Ionization Mass Spectrometry (ESI-MS)</i>	7
	3.1.1 Theory	7
	3.1.2 Experimental Part	10
	3.2 <i>Gas Chromatography</i>	12
	3.2.1 Instrument Overview	12
	3.2.2 Experimental Part	12
	3.3 <i>Synthesis</i>	15
	3.3.1 General Considerations	15
	3.3.2 Synthesis and Sample Preparation of Organozinc Reagents	17
	3.3.3 Synthesis and Sample Preparation of <i>iPrMgCl/LiCl</i>	21
	3.3.4 Synthesis of Geminal Diiiodides	23
	3.3.5 Preparation of Charged-Tagged Organozinc Reagents	27
	3.3.6 Preparation of Negishi Cross-Coupling Reactions with Butyl Zinc Reagents	28
4	Microsolvated Organozinc Cations	31
5	Organozinc Iodides in the Presence of Chelating Ligands	41

6	Formation of Lithium Organozincates	51
6.1	Lithium Organozincate Complexes $LiRZnX_2$	51
6.2	Comparison of Lithium Organozincate Complexes with $iPrMgCl/(LiCl)_n$	71
7	Characterization of the Simmons-Smith Reagent	75
8	Charged Tags as Probes for Monitoring Cross-Coupling Reactions by ESI-MS	81
9	Kinetic Analysis of Palladium-Catalyzed Negishi Cross-Coupling Reactions	94
10	Summary	108
11	References and Notes	112
12	Curriculum Vitae	122

1 Abstract

Organozinc intermediates were characterized by NMR spectroscopy, electrical conductivity measurements, and especially electrospray ionization (ESI) mass spectrometry as a particularly useful tool to probe ionic intermediates.

Solutions of butylzinc iodide in tetrahydrofuran, acetonitrile, and *N,N*-dimethylformamide were analyzed by ESI mass spectrometry. In all cases, microsolvated butylzinc cations $\text{ZnBu}(\text{solvent})_n^+$, $n = 1-3$, were detected. The parallel observation of butylzincate anions ZnBuI_2^- suggests that these ions result from disproportionation of neutral butylzinc iodide in solution. In the presence of simple bidentate ligands, chelated complexes $\text{ZnBu}(\text{ligand})^+$ formed quite readily. The gas-phase fragmentation of mass-selected $\text{ZnBu}(\text{ligand})^+$ led to the elimination of butene and formation of $\text{ZnH}(\text{ligand})^+$, whereas the micro-solvated cations $\text{ZnBu}(\text{solvent})_n^+$ lost the attached solvent molecules to produce bare ZnBu^+ . This behavior mimicked the activation of organozinc reagents by chelating ligands in solution. In this case, ESI mass spectrometric experiments were able to provide a consistent picture of how solvation and chelation stabilized the butylzinc cation.

However, ESI mass spectrometry is considered less suitable for quantitative analysis and thus offers only limited insight into the association and dissociation equilibria operative in solution. Therefore, a combination of ESI mass spectrometry, electrical conductivity measurements, and NMR spectroscopy was used to investigate the effect of LiCl on solutions of organyl zinc halides RZnX in tetrahydrofuran. The obtained results pointed to the formation of lithium organozincates $\text{Li}^+\text{RZnX}_2^-$ and the association constant derived for $\text{Li}^+\text{BuZnCl}_2^-$ also suggests that at synthetically relevant concentrations the lithium organozincate complex predominates.

After the characterization and determination of the association equilibria of these zinc reagents, their reactivity was investigated by kinetic measurements. ESI mass spectrometry was used to study the reactivity of organozinc iodides bearing a cationic quaternary ammonium group at a remote position. This approach permits a straightforward identification of the rate-limiting step of the probed Pd-catalyzed Negishi cross-coupling reaction and the determination of the corresponding second-order rate constant.

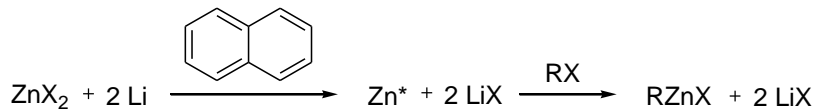
For further kinetic measurements, Pd-catalyzed Negishi cross-coupling reactions were carried out in solution and analyzed by gas chromatography. Here the influence of added lithium salts, different BuZnX compounds and concentrations of the reacting compounds was examined to gain information about the rate-limiting step. The observed results point to the oxidative addition as the rate-limiting step.

2 Introduction

2.1 Organozinc Reagents

Since prehistoric times zinc compounds have found practical uses, but not until the 14th century zinc was recognized as a metal.¹ In the middle of the 19th century the pioneering works of Edward Frankland^{2,3} marked the beginning of organozinc chemistry, as well as the birth of a larger field: organometallic chemistry.⁴ At first Frankland prepared diethylzinc by heating ethyl iodide with zinc metal in a sealed tube, which appeared to be a volatile colorless liquid that inflamed spontaneously upon contact with air.² Until the discovery of the Grignard reagents around 1900 organozinc compounds were used extensively as alkylating agents in organic chemistry.⁵ The organomagnesium reagents were found to be more reactive species toward a broad range of electrophiles, though and afforded generally higher yields compared to organozincs. Therefore, in the following years only a few reactions with zinc organometallics found synthetic applications such as the Reformatsky reaction⁶ and the Simmons-Smith cyclopropanation.⁷ Their revival began in 1936 with the work of Hunsdiecker who carried out reactions of alkyl iodides with zinc dust to obtain the corresponding alkyl zinc iodides.⁸ According to this work a broad range of organozinc iodides could be synthesized at often elevated temperature and in polar solvents.⁹

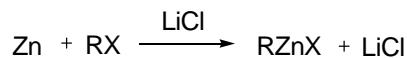
Further organozinc halides can be generated by the insertion of Zn into organic halides RX.¹⁰ As this reaction is relatively inefficient for commercially available Zn dust, several different ways of activating Zn have been developed.¹¹⁻¹⁵ Among these, for a long time arguably the most important was Rieke's method, which produces finely dispersed and highly active Zn* by the reduction of ZnX₂ by Li in the presence of catalytic amounts of naphthalene (Scheme 2.1.1).¹⁶ Unless the active Zn* metal is carefully washed, the finally obtained ethereal solution of RZnX contains substantial amounts of LiX.



Scheme 2.1.1. Rieke's method to activate zinc and its reaction with organozinc halides

More recently, Knochel and coworkers have demonstrated that stoichiometric amounts of LiCl greatly accelerate the insertion of Zn into organic halides, thus providing a very convenient and

practical access to organozinc halides (Scheme 2.1.2).¹⁷



Scheme 2.1.2. Preparation of organozinc halides by Knochel's method.

Although the most common syntheses of organozinc halides thus all produce these reagents in the presence of LiX, the possible role of the latter has been largely ignored¹⁸ until Knochel's work on LiCl-promoted Zn insertion reactions has put them into the spotlight.

Alternatively, a straightforward access to organozinc halides and diorganozinc compounds is given by transmetalation. The reaction of ethereal solutions of ZnX_2 with one or two equivalents of organolithium reagents produces RZnX and R_2Zn along with one or two equivalents of LiX, respectively (Eqs. 2.1.1 and 2.1.2). Similarly, organomagnesium compounds may also be used for transmetalation.

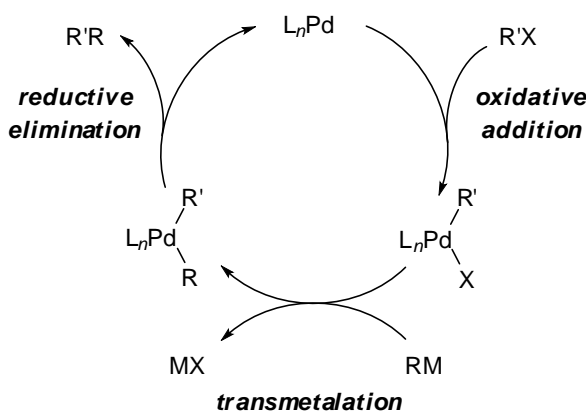


The outstanding advantages of these organozincs are the high tolerance of functionalities and the much improved chemoselectivity, compared to organolithium and organomagnesium compounds. Moreover, organozinc compounds are prone to undergo a large range of transmetalations due to the presence of empty low-lying *p*-orbitals that can interact with the *d*-orbitals of many transition metal salts.¹⁹ Therefore, they are ideally suited as reagents for cross-coupling reactions. Indeed, Negishi cross-coupling reactions²⁰ constitute one of the most important and versatile methods in contemporary organic synthesis.^{21,22} This transformation uses organozinc halides RZnX (or the corresponding diorganozinc species R_2Zn) as coupling reagents for organyl halides $\text{R}'\text{X}$ (Eq. 2.1.3), and hence strongly benefits from recently developed methods to access highly functionalized organozinc compounds.^{17,19}



Negishi cross-coupling reactions are generally believed to follow the catalytic cycle common to the whole family of palladium-catalyzed transformations.²³ The conventional catalytic cycle involves

the distinct elementary steps of oxidative addition, transmetalation, and reductive elimination (Scheme 2.1.3) and has been proven extremely useful for understanding the mechanism of palladium-catalyzed cross-coupling reactions and for their rational optimization.



Scheme 2.1.3. Conventional catalytic cycle of palladium-catalyzed cross-coupling reactions ($L = \text{ligand}$). In the case of Negishi cross-coupling reactions, $RM = R\text{ZnX}$ and ZnR_2 .

Elucidating the actual mechanism of Negishi cross-coupling reactions and determining the nature of the organozinc reagents involved is rather difficult. In particular, the ability of metal centers to switch between different oxidation or coordination states and to engage in dynamic equilibria can dramatically complicate the situation. Several analytical techniques have been used to address this problem. Highly detailed and valuable structural information is given by X-ray crystallography. However, this method does not provide direct insight into the behavior of reactive intermediates in solution. In contrast, spectroscopic techniques can directly probe dissolved organometallic species. While NMR, IR, UV-Vis, and X-ray spectroscopy are suitable for the identification of reactive organometallic intermediates, the information obtained by these methods is not always sufficient for a full characterization of the system under investigation. Particularly, the distinction between different coordination and aggregation states can be challenging. An alternative approach, which may help to overcome these problems by providing unambiguous stoichiometric information, relies on electrospray-ionization (ESI) mass spectrometry.²⁴ This method permits the transfer of ions from solution into the gas phase, thus allowing the sampling of dissolved charged organometallics *in situ*. It is therefore not surprising that ESI mass spectrometry has been applied to the analysis of numerous different organometallic systems. The successful detection of various charged organometallics, including rather labile ones,^{25,26} is consistent with the commonly accepted view

that ESI constitutes a relatively “soft” ionization technique, which transfers only limited amounts of energy into the probed ions and does not significantly change their nature.²⁷ This assumption forms the basis on which properties of the solution-phase system are deduced from gas-phase measurements.

2.2 Objectives

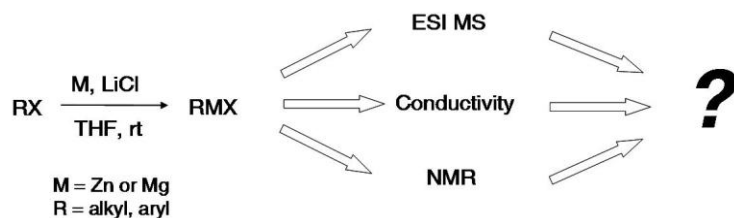
The present thesis seeks to gain a comprehensive understanding of the aggregation and reactivity of organozinc compounds. To this end, different aspects of organozinc chemistry are investigated.

The aim of the first project was to characterize butylzinc iodide compounds in the absence of LiCl via ESI mass spectrometry, with the intention to detect organozinc cations, as well as the already by Koszinowski and Böhrer detected organozinc anions.²⁸ The use of different solvents such as THF, DMF and CH₃CN and their influence on the stabilization of the organozinc species was sought to be examined as well (Chapter 4).

Next, an investigation of the heterolytic dissociation of butylzinc iodide in the presence of bidentate ligands such as 1,2-dimethoxyethane (**L1**), *N,N*-dimethyl-2-methoxyethylamine (**L2**), and *N,N,N',N'*-tetramethylethylenediamine (TMEDA) (**L3**) was attempted. The effect of added ligands to the stoichiometry and reactivity of organozinc compounds were sought to be explored by using ESI mass spectrometry and collision-induced dissociation (CID). (Chapter 5).

The influence of LiCl on several organozinc compounds, analyzed by ESI mass spectrometry, has already been reported by Koszinowski and Böhrer.²⁸ However, ESI mass spectrometry is considered less suitable for quantitative analysis and therefore, the determination of association and dissociation equilibria in solution is difficult. To solve this problem, different analytical methods such as NMR spectroscopy, electrical conductivity measurements and ESI mass spectrometry are applied to gain a more detailed picture of the influence of LiCl on organozinc compounds and the formation of zincates. Besides, LiCl does not only play an important role in organozinc chemistry but also in organomagnesium chemistry, thus the combination of mixed analytical methods may be employed for the analysis of an isopropylmagnesium chloride system as well (Chapter 6) (Scheme 2.2.1).

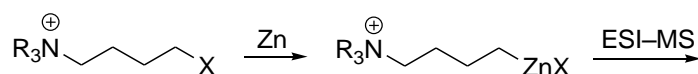
As a further project the zinc insertion reactions of geminal diiodides which were used in the well-known Simmons-Smith reaction, are planned to be analyzed by ESI mass spectrometry. More information of the supposed carbene like character of these diiodides will possibly be gained (Chapter 7).



Scheme 2.2.1. Insertion reaction of zinc or magnesium into RX analyzed by a combination of analytical methods.

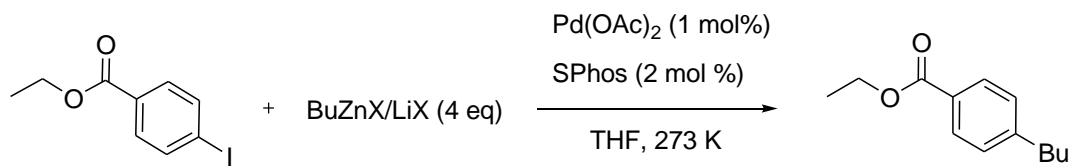
Further studies aim at the detection of organozinc compounds with an overall positive charge, which should not be on the zinc center, using ESI mass spectrometry.

These compounds may allow the observation not only of products, but also starting materials and hydrolysis products of the compounds involved in the zinc insertion reactions (Chapter 8) (Scheme 2.2.2).



Scheme 2.2.2 Synthesis of organozinc reagents bearing a charged tag for structure elucidation via ESI mass spectrometry.

At last, the influence of different LiX salts and butylzinc reagents on palladium-catalyzed Negishi cross-coupling reactions is studied (Scheme 2.2.3). The course of the reaction can be monitored by gas chromatography (Chapter 9).



Scheme 2.2.3. Model reaction investigated. SPhos = 2-dicyclohexylphosphino-2',6'-dimethoxybiphenyl.

3 Experimental Section

This chapter describes the methods of ESI mass spectrometry and gas chromatography in detail, the synthesis of the reagents and starting materials, including the sample preparation for the applied analyzing methods such as ESI mass spectrometry, electrical conductivity measurements, NMR spectroscopy and gas chromatography.

3.1 Electrospray Ionization Mass Spectrometry (ESI-MS)

3.1.1 Theory

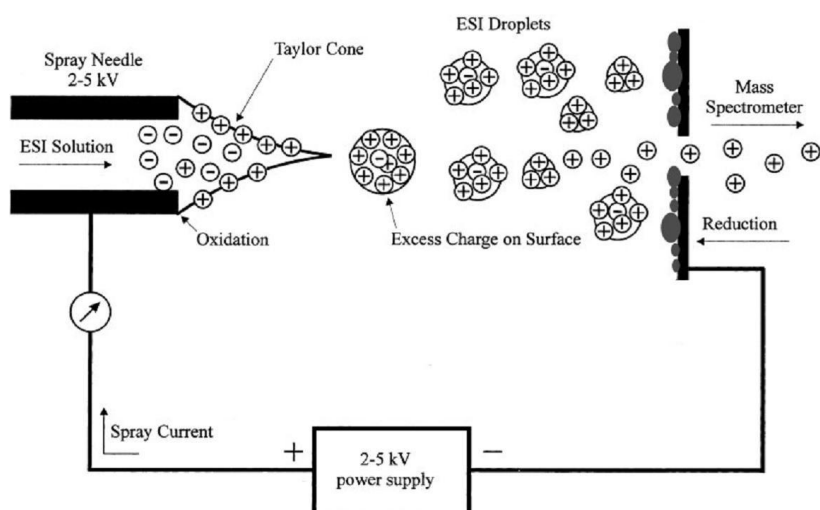
The basic principle of mass spectrometry is to generate ions from either inorganic or organic compounds, to separate these ions by their mass-to-charge ratio (m/z) and to detect them qualitatively and quantitatively by their respective m/z and abundance. The mass spectrometer consists of three different modules: an ion source, a mass analyzer and a detector. The prepared sample is introduced through an inlet to the ionization source. The analyte may be ionized by electric fields or by impacting energetic electrons, ions or photons. The source generates gas-phase ions, which are transferred to the mass analyzer for separation according to their mass-to-charge ratio. Static or dynamic electric or magnetic fields effect the ion separation. A detector registers and counts the arriving ions.²⁹

In this work two different instruments were applied using electrospray ionization (ESI) as ionization technique: a HCT quadrupole-ion trap mass spectrometer designed by Bruker Daltonik and a TSQ 7000 multistage mass spectrometer from Thermo-Finnigan.

Electrospray Ionization. In the 1960s Dole and co-workers³⁰ developed electrospray as a technique for mass spectrometry and the process was improved by Yamashita and Fenn who coupled an electrospray source to a quadrupole mass analyzer in the 1980s.³¹ The latter was recognized for his work by the award of the Nobel Prize for Chemistry (2002). Despite the widespread adoption of ESI-MS as a technique especially for biochemical compounds, the technique was still viewed as a “black box” and several mechanisms were proposed for the process of ionization.³²

A dilute solution of an analyte is pumped through a capillary at a very low flow rate (0.1-10 μ L/min) and a high voltage is applied (2-5kV) to the capillary (Scheme 3.1.1). The voltage, which can be

either negative or positive, depending on the analytes chosen, provides the electric field gradient required to produce charge separation at the surface of the liquid. From the capillary tip, known also as “Taylor cone” the liquid protrudes and when the solution reaches the Rayleigh limit (this is the point at which Coulombic repulsion of the surface charge is equal to the surface tension of the solution) droplets containing an excess of positive or negative charge, respectively, detach from the capillary tip. Through the atmosphere these droplets shift to the entrance of the mass spectrometer and generate ions. One proposed mechanism for the electrochemical process of the ionization is known as the ion evaporation, which follows the assumption that the increased charge density, due to the solvent evaporation, eventually causes Coulombic repulsion to overcome the liquid's surface tension and results in a release of ions from droplet surfaces.^{27,32} Regardless of the exact mechanism, ESI is a very soft means of ionization that causes little or no fragmentation of the sample.³²



Scheme 3.1.1. Schematic of the ionization electrospray process according to ref. 32.

Analyzers. Mass analyzers separate the ions according to their mass-to-charge ratio using either static or dynamic fields, and magnetic or electric fields. Several mass analyzers are currently available: quadrupoles, time-of-flight (TOF) analyzers, magnetic sectors and, both Fourier transform and quadrupole ion traps. Mass spectrometers that have more than one analyzer are called Tandem (MS/MS) mass spectrometers and can be used for structural and sequencing studies.²⁹ The mass spectrometers applied in this work operate with two different analyzers. The TSQ 7000 instrument runs with a tandem quadropole which spatially divides the ions and the HCT ion trap includes a 3D-ion trap which separates the ions temporally.

Tandem quadrupole analyzer of the TSQ 7000 instrument. The basic design of the TSQ 7000 instrument includes two independent mass analyzers (quadrupoles Q_1 and Q_2) arranged in tandem and separated by a collision cell (octopole O_1).

The quadrupoles consists of four parallel metal rods, set parallel to each other. Each opposing rod pair is connected together electrically, wheras a radio frequency voltage is applied between one pair of the rods and the other. A direct current voltage is then superimposed on the radio frequency voltage. Ions are accelerated out of the ion source along the z -axis of the quadrupole between the rods. They experience forces in the x and y directions that cause them to oscillate toward and away from the rods. If the oscillation is too large the ions collide with the rods and do not reach the detector. Therefore, only ions of a certain mass-to-charge ratio m/z will reach the detector for a given ratio of voltages. This permits selection of an ion with a particular m/z or allows the operator to scan for a range of m/z -values by continuously varying the applied voltage.

The first (Q_1) and the second quadrupole (Q_2) act as mass filters, and the octopole (O_1) in the middle is employed as a collision cell. This collision cell is a radio frequency-only octopole, using helium gas for collision induced dissociation of selected parent ions from Q_1 . Subsequent fragments are passed through to Q_2 where they may be filtered or fully scanned.

There are several operating modes available for the above described triple-quadrupole instrument:
(a) The m/z ratios of the ions were established by scanning the first quadrupole mass filter. The ions then passed an 18 cm long octopole ion guide and a second quadrupole mass filter, which were set to transmit before reaching the detector. (b) For probing the unimolecular gas-phase reactivity of an ion of a particular m/z ratio, the first quadrupole mass filter was used to mass-select this ion. The mass-selected ion then passed the octopole. Argon was added as collision gas into the octopole to study the unimolecular reactivity of a mass-selected ion in a collision induced dissociation (CID). The m/z ratios of the product ions formed by CID were then established by scanning the second quadrupole mass filter before the ions reached the detector.^{29,33}

3D-ion trap of HCT ion trap. Quadrupole ion traps use similar operating principles to those of the standard quadrupole mass analyzer. The ion trap consists of two conical lens or electrodes, and one “donut-shaped“ ring lens. The ions are held between the conical lenses that form the caps of the trap and the center of the ring electrode. By lowering and raising the voltages on the entrance and exit trap electrode, ions can pass into the trap, be stored for some period of time (μs up to s), and then released to the detector.^{29,34}

3.1.2 Experimental Part

Applied settings for the TSQ 7000 multistage mass spectrometer (Thermo-Finnigan)

Sample solutions ($c \approx 1\text{-}20 \text{ mM}$) were transferred into a gas-tight syringe and introduced into the ESI source of the instrument at flow rates of approx. $5\text{-}30 \mu\text{L min}^{-1}$ by means of a syringe pump. Particular care was taken to exclude or minimize contact of the organometallic samples with air. Traces of moisture or oxygen in the inlet system were eliminated by extensively flushing it with dry solvent (THF or DMF) before adding the organometallic sample. The sample solution entered the ESI source via a fused-silica tube (0.10 mm inner diameter). Stable electrospray conditions were usually achieved for ESI voltages ranging from 3.0 to 4.5 kV with nitrogen as a sheath gas (2.5 bar). The spray then passed through a heated capillary held at 333 K for THF solutions and 373 K for DMF solutions. This relatively low temperature yielded acceptable signal intensities while preventing excessive fragmentation of the potentially labile organozinc ions. Furthermore, the potential difference between the heated capillary and the following electrooptic lens was kept low to avoid strong acceleration of the ions and unwanted fragmentations due to energetic collisions with gas molecules present in the ESI source region. Similar ESI conditions were maintained for all experiments to ensure direct comparability.

For probing the unimolecular gas-phase reactivity argon (Linde, 99.998%) was used as collision gas in the octopole ($p(\text{Ar}) \approx 0.6 \text{ mtorr}$ as measured with a Convectron). The collision energy E_{LAB} was controlled by adjusting the voltage offset of the octopole. These energies cannot be easily converted to collision energies in the center-of-mass frame because multiple collisions are likely at the typical argon pressure applied. The vacuum chamber of the mass spectrometer was held at $T \approx 343 \text{ K}$, and it is assumed that this temperature also describes the distribution of the internal energy of the neutral reactants.

Applied settings for the HCT quadrupole-ion trap mass spectrometer (Bruker Daltonik).

Sample solutions ($c \approx 5\text{-}40 \text{ mM}$) were transferred into a gas-tight syringe and introduced into the ESI source of the instrument at flow rates of approx. $5 \mu\text{L min}^{-1}$. To prevent moisture from entering the source, it was kept closed between experiments and constantly purged with dry N_2 gas heated to 573 K. Nitrogen was used as sheath gas (0.7 bar backing pressure) and an ESI voltage of 3.0-4.0 kV was applied. The thus produced ions then passed a capillary, a skimmer, and two transfer octopoles before entering the quadrupole ion trap. Varying the voltage offsets of the capillary exit and the two transfer octopoles had significant effects. For most of the experiments, a

drying gas flow of 5.0 L min^{-1} of nitrogen heated to 373 K, a cap-exit voltage of $V_{\text{cap-exit}} = 113 \text{ V}$, a skimmer voltage of $V_{\text{skimmer}} = 40 \text{ V}$ and a voltage offset of the first and second transfer octopoles of $V_{\text{oct1}} = 12 \text{ V}$ and $V_{\text{oct2}} = 5 \text{ V}$, respectively, were applied. The ions were then transferred into the instrument's three-dimensional quadrupole ion trap filled with helium (Air Liquide, 99.999% purity, estimated pressure $p(\text{He}) \approx 2 \text{ mtorr}$). The helium-filled quadrupole ion trap was operated at trap drive values of 15-35. For the gas-phase fragmentation experiments, the mass-selected ions (typical isolation widths of 3-4 amu) were subjected to excitation voltages with amplitudes of V_{exc} and allowed to collide with the helium gas. Only fragment ions whose m/z ratio is larger than 27% of that of their parent ion can be detected efficiently in the ion trap. The Compass 1.3 software package was used to operate the ions in the trap to afford their detection in simple MS experiments and their mass-selection, kinetic excitation, and detection in CID experiments.

To avoid unwanted decomposition reactions, milder settings were used for the obtained spectra in Chapter 6 and 8.^{35,36} A drying gas temperature of 333 K, a capillary exit voltage of $V_{\text{cap-exit}} = 20 \text{ V}$, a skimmer voltage of $V_{\text{skimmer}} = 20 \text{ V}$, and a voltage offset of the first and second transfer octopoles of $V_{\text{oct1}} = 5 \text{ V}$ and $V_{\text{oct2}} = 1.7 \text{ V}$, respectively, were applied.

3.2 Gas Chromatography

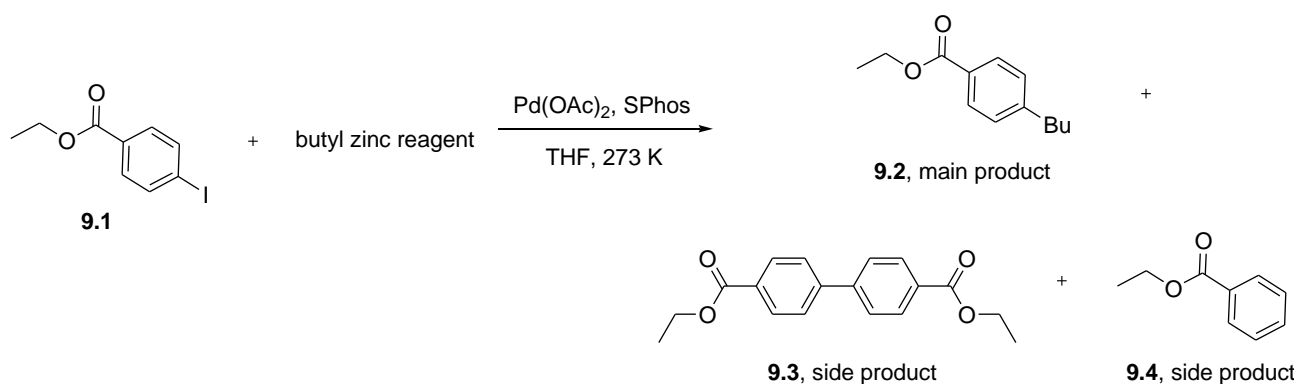
3.2.1 Instrument Overview

Gas chromatography is used in analytical chemistry for separating and analyzing mixtures of compounds that can be vaporized without decomposition. The gas chromatograph TRACE GC Ultra (Thermo Electron Corporation) was applied and the prepared samples were measured using an autosampler. As carrier gas nitrogen was used and the flow rate of the carrier gas was carefully controlled to ensure reproducible retention times and to minimize detector drift and noise.³⁷ The carrier gas entered the injector. The Merlin Microseal™ High Pressure Valve Septum acted as a junction through which the injector syringe needle may pass to deliver the sample into the injection port. The advantage of this septum is that it has no membrane, which can easily be destroyed and automatically opens at injection. After the injection of the analyte, it was vaporized in the heated injection port and carried into the column (diameter: 0.25 mm, length: 25 m, stationary phase: fused silica). The sample partitioned between the mobile and the stationary phases and it was separated into individual components. The column oven permitted a quick heating up and cooling down of the column inside, whereas the temperature capacity of the oven lies at 723 K, but the maximal temperature of the column should not be exceeded, which is about 553 K. The sample and the carrier gas passed now through a Flame Ionization Detector (FID), which is one of most widely used GC detectors and is characteristic for high sensitivity and robustness. FID responds to all organic compounds that burn in the oxy-hydrogen flame. This device measured the quantity of the sample and produced an electrical signal which went to a data system generating a chromatogram.³⁷

3.2.2 Experimental Part

As model reaction for the kinetic measurements, the cross-coupling of butylzinc reagents with ethyl 4-iodo-benzoate catalyzed by Pd(OAc)₂/SPhos was probed (Scheme 3.2.2.1).

Samples from the reaction mixture were treated with an aqueous solution of NH₄Cl and analyzed by gas chromatography with undecane as an internal standard (Figure 3.2.2.1).



Scheme 3.2.2.1 Negishi cross-coupling model reaction.

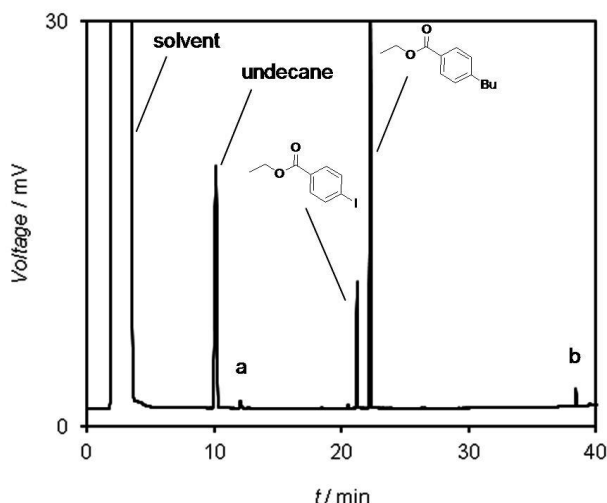


Figure 3.2.2.1 Example of a measured chromatogram with the TRACE GC Ultra. The peak labelled a was characterized as benzoic acid ethyl ester (**9.4**) and b as biphenyl-4,4'-dicarboxylic acid diethyl ester (**9.3**).

The abundances of reactant ethyl 4-iodo-benzoate (**9.1**), the cross-coupling product ethyl 4-butylbenzoate (**9.2**), the homo-coupling product biphenyl-4,4'-dicarboxylic acid diethyl ester (**9.3**) and the dehalogenation product benzoic acid ethyl ester (**9.4**) were determined by comparing their integrated measured peak areas (normalized to that of the internal standard) to calibration curves for authentic samples of these substances. Several calibration curves for the reagent **9.1** (Figure 3.2.2.2.A), product **9.2** (Figure 3.2.2.2.B) and the side products **9.3** and **9.4** (Figure 3.2.2.3) were prepared and the mean values were used for the calculations.

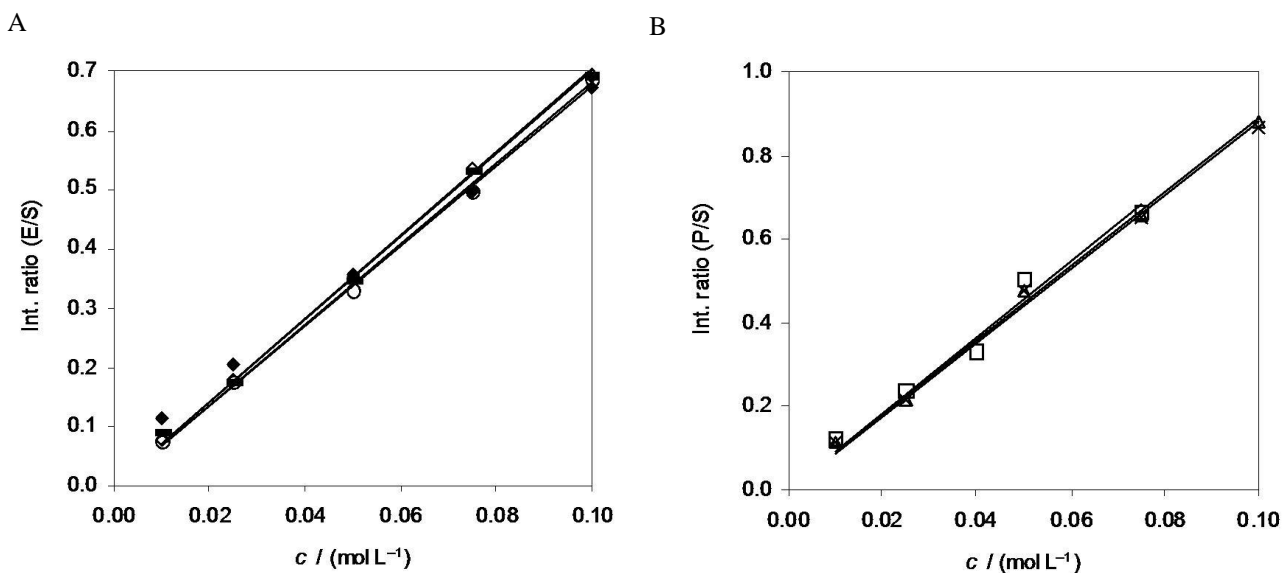


Figure 3.2.2.2.A. Calibration curves of the reactant ethyl 4-iodo-benzoate (**9.1**) determined by gas chromatograph analysis. The plot shows the integration area of the reactant ethyl 4-iodo-benzoate (E) divided by the integration area of the standard (S) versus the concentration of the reactant E. **B.** Calibration curves of the product 4-butyl-benzoic acid ethyl ester (**9.2**) determined by gas chromatograph analysis. The plot showed the integration area of the product 4-butyl-benzoic acid ethyl ester (P) divided by the integration area of the standard (S) versus the concentration of the product (P).

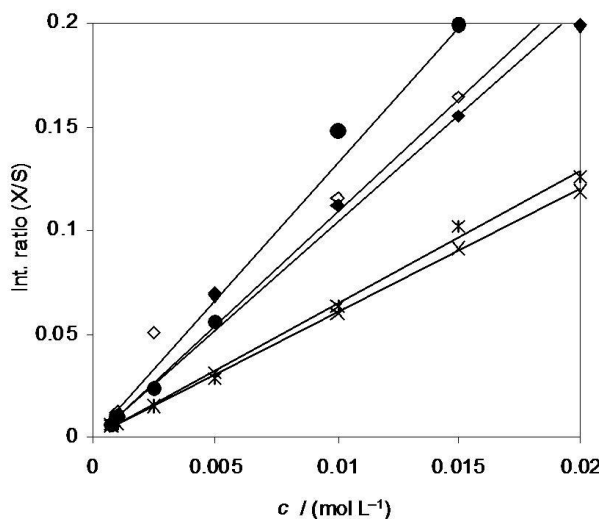


Figure 3.2.2.3 Calibration curves of the side products benzoic acid ethyl ester (**9.3**, labelled as a, crosses) and biphenyl-4,4'-dicarboxylic acid diethyl ester (**9.4**, labelled as b, open and filled diamonds and filled circles) determined by gas chromatograph analysis. The plot shows the integration area of the reagent X (X = reagent **9.3** or **9.4**) divided by the integration area of the standard (S) versus the concentration of the respective reagent X.

3.3 Synthesis

3.3.1 General Considerations

In all cases standard Schlenk techniques were applied in flame-dried glassware under an argon atmosphere to exclude moisture and oxygen. Gas-tight syringes were used to transfer exact quantities of solutions under the exclusion of moisture and oxygen.

Solvents

CH_3CN (acetonitrile) was refluxed over phosphorus pentoxide for 1 h, distilled twice, and stored over 3 Å molecular sieves under argon.

Et_2O (diethylether) was predried over CaCl_2 and dried with the solvent purification system SPS-400-2 from INNOVATIVE TECHNOLOGIES INC or was freshly distilled from sodium benzophenone ketyl under argon.

DMF (dimethylformamide) was used as received (Acros Organics, extra dry, over molecular sieves, water content < 50 ppm).

THF (tetrahydrofuran) was freshly distilled from sodium benzophenone ketyl under argon.

THF-d₈ (tetrahydrofuran) (euriso-top, 99.50% D) was distilled and stored over molecular sieves (4 Å) under argon at 278 K in the dark.

Analytical data

Infrared Spectroscopy. Infrared spectra were recorded from 4000-400 cm^{-1} on a Perkin 281 IR spectrometer. Samples were measured neat (ATR, Smiths Detection DuraSample IR II Diamond ATR). The absorption bands were reported in wave numbers (cm^{-1}) and labeled as vs = very strong, s = strong, m = medium, and w = weak.

Mass spectrometry. Mass spectra were recorded on a Finnigan MAT 95Q or Finnigan MAT 90 instrument for electron impact ionization (EI), as well as high resolution mass spectra (HRMS).

Chromatography. Flash column chromatography was performed using SiO_2 60 (0.04 - 0.063 mm, 230 - 400 mesh) from Merck. Thin layer chromatography (TLC) was performed using aluminium plates coated with SiO_2 (Merck 60, F-254). The spots were visualized by UV-light.

Nuclear Magnetic Resonance Spectroscopy. NMR spectra were recorded on Varian Mercury 200, Bruker AC 300, WH 400, or AMX 600 instruments. Chemical shifts are reported as δ -values in ppm relative to the solvent signal (in the case of THF-D₈: ¹H δ 1.73 ppm). At room temperature, ⁷Li NMR spectra were recorded with a 400-MHz JOEL EX-400 instrument, calibrated to LiCl in water. For the characterization of the observed signal multiplicities the following abbreviations are used: s (singlet), d (doublet), t (triplet), dd (doublet of doublet), dt (doublet of triplet), m (multiplet), q (quartet), quint (quintet), sext (sextet), as well as br (broad).

Electrical Conductivity Measurements. A classical method has been used here to study the status of ion association and solvation in electrolyte solutions. The knowledge of the state of association of the analyzed systems and their interactions with the solvent molecules is important for the understanding of reaction mechanisms. Such studies are perfectly complemented with non-quantitative ESI mass experiments.

The electrical conductivity measurements were performed with a CDM230 instrument (Radiometer Analytical) and a standard platinum-electrode cell (cell constant $\kappa_{\text{cell}} = 1 \text{ cm}^{-1}$) or a SevenMulti instrument (Mettler Toledo) and a stainless steel-electrode cell (InLab741, Mettler Toledo, $\kappa_{\text{cell}} = 0.1 \text{ cm}^{-1}$). Both instruments were calibrated against 0.100 M solutions of aqueous KCl.

Reagents

Commercially available reagents were used without further purification unless otherwise stated.

LiX (X = Cl, Br, I) was rigorously dried by prolonged heating under vacuum at 473 K. After cooling to 298 K dry THF ($c = 0.5 \text{ M}$) was added and the mixture was stirred for 24 h.

ZnX₂ (X = Cl, Br, I) was rigorously dried by prolonged heating under vacuum at 423 K. After cooling to 298 K dry THF ($c = 0.5 \text{ M}$ or 1.0 M) or diethylether ($c = 0.5 \text{ M}$ or 1.0 M) was added and the mixture was stirred for 24 h.

MgCl₂ was dried under vacuum at 573 K for several hours, anhydrous THF ($c = 0.5 \text{ M}$) was added and the mixture was stirred at 323 K for 20 h.

nBuLi was purchased as a solution in hexane from Chemetall GmbH (Frankfurt, Germany).

PhLi was purchased as a solution in dibutylether from Sigma-Aldrich Chemie GmbH (Steinheim, Germany).

NaHMDS and **LiHMDS** were purchased as a solution in THF (1.00 M) from Sigma-Aldrich Chemie GmbH (Steinheim, Germany).

The concentration of organolithium reagents was determined by titration with dibenzyl tosylhydrazone.³⁸

3.3.2 Synthesis and Sample Preparation of Organozinc Reagents

General Procedure 1 (GP1). Synthesis of organozinc halides RZnX via direct Zn insertion reaction.

A flask loaded with zinc dust (1.4 eq) was flame-dried under high vacuum and allowed to cool down under argon atmosphere. The procedure was repeated twice and the corresponding solvent was added. The zinc was activated by the addition of 1,2-dibromoethane (3 mol%) followed by a short boiling-up of the suspension, and of chlorotrimethylsilane (2 mol%), followed again by a short boiling-up. The substrate (1 eq) was added dropwise and the suspension was stirred overnight at room temperature. The remaining zinc powder was allowed to settle and iodometric titration³⁹ determined the yield of organozinc species of the supernatant solution.

Note that the thus produced organozinc reagents may contain small amounts of extra halide ions originating from the 1,2-dibromoethane and chlorotrimethylsilane additives (on the basis of the employed reagent quantities, maximum extra bromide and chloride contents of 0.09 and 0.03 eq, respectively, can be calculated). These extra halide ions presumably form ZnX_2 salts, which are supposed to have only small effects on organozinc halides other than reducing their stability.⁴⁰

Preparation of alkylzinc iodide RZnI ($\text{R} = \text{Me}, \text{iPr}, \text{Bu}$).

According to GP1, the zinc reagents were prepared from alkyl iodides RX ($\text{R} = \text{Me}, \text{iPr}, \text{Bu}$) (5.0 mmol, 1 eq) and Zn dust (7.0 mmol, 1.4 eq) in the corresponding solvent ($c = 1 \text{ M}$, THF, THF-D₈, acetonitrile, or DMF, respectively) at room temperature for 12 h. Titration against iodine³⁹ determined the yield of alkylzinc of the supernatant solution to 89% for THF, 96% of butylzinc iodide in acetonitrile, and 79% of butylzinc iodide in DMF (average of two independent experiments in each case).

Preparation of benzylzinc bromide BnZnBr .

Solutions of benzylzinc bromide or *m*-methylbenzylzinc bromide in THF were prepared according to the method of Berk et al.¹¹ A flame-dried Schlenk flask was charged with zinc dust (7.0 mmol, 1.4 eq) and dry THF ($c = 1 \text{ M}$). Then, 1,2-dibromoethane (3 mol%) was added and the mixture was

heated until evolution of bubbles of ethylene and darkening of the zinc surface indicated activation. The reaction mixture was cooled to 273 K and benzyl bromide or *m*-methylbenzyl bromide (5.0 mmol, 1 eq), respectively, was slowly added. The reaction mixture was allowed to warm up to room temperature and stirred for 12 h.

General Procedure 2 (GP2). Preparation of RZnX. LiCl-mediated zinc insertion.

RZnX/(LiCl)_{*n*} reagents were generated as described above (**GP1**), but with *n* equivalents of LiCl added (*n* = 0.125, 0.5, 1, 2, 5). A dry, argon-flushed Schlenk flask was charged with LiCl and heated with a heat gun under high vacuum for 5 min. The flask was flushed with argon and was allowed to cool down. The procedure was repeated twice followed by the typical procedure of **GP1**.

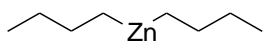
Preparation of BuZnI/LiCl.

BuZnI/(LiCl)_{*n*} reagents were generated from butyl iodide as described in **GP2**, with *n* equivalents of LiCl added (*n* = 0.125, 0.5, 1, 2, 5). The yield, determined by iodometric titration, amounted 92 to 98% for all buyl zinc species.

Preparation of BnZnBr/LiCl.

According to **GP2** BnZnBr/(LiCl)_{*n*} reagents were generated form benzyl bromide and *n* equivalents of LiCl (*n* = 0.5, 1, 2). The concentration was determined by iodometric titration (93-96% yield).

Synthesis of Bu₂Zn.⁴¹



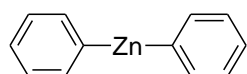
A flame-dried flask under argon atmosphere was charged with a solution of BuLi in hexane (2.4 M) and the solvent was removed at 273 K under reduced pressure. To the yellow residue was slowly added a solution of ZnCl₂ in diethyl ether (1.0 M, 0.5 eq) at 195 K before the reaction mixture was allowed to warm up to room temperature. After stirring for 15 h in the dark, the resulting suspension was subjected to centrifugation (1 h, 2000 rpm). The clear supernatant solution was separated and freed from diethyl ether under reduced pressure. Further purification could be achieved by distillation under high vacuum to give Bu₂Zn as a colorless oil (65% yield), whose ¹H NMR spectroscopic properties (¹H NMR (200 MHz, 296 K, C₆D₆) δ (ppm) 0.35 (t, *J* = 7.7 Hz, 4H, CH₂Zn), 1.08 (t, *J* = 7.2 Hz, 6H, CH₃), 1.45-1.63 (m, 4H CH₃CH₂), 1.78-1.93 (m, 4H

$\text{CH}_2\text{CH}_2\text{Zn}$) agreed with those reported in the literature reasonably well.⁴² Solutions of Bu_2Zn in THF or THF-D₈ (1.3 M, exact determination by iodometric titration),³⁹ respectively, were stored under argon in the dark and found stable to degradation for > 2 weeks.

Preparation of BuZnX and $\text{BuZnX}/(\text{LiX})_n$ via Bu_2Zn .

A combination of measured quantities of Bu_2Zn solutions (1 eq) with 1 eq of ZnX_2 ($\text{X} = \text{Cl}, \text{Br}, \text{I}$) in THF was stirred for 15 min to produce solutions of BuZnX . Reagents of $\text{RZnX}/(\text{LiX})_n$ were generated as described above, but with n equivalents of LiX added ($\text{X} = \text{Cl}, \text{Br}, \text{I}, \text{ClO}_4$ and $n = 0.5, 1, 2, 5$).

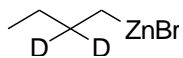
Synthesis of Ph_2Zn .



A flamed dried flask was charged with PhLi in Bu_2O (1.9 M) under argon. A solution of ZnCl_2 in diethyl ether (1.0 M, 0.5 eq) was slowly added at 223 K. After stirring for 3 h in the dark, the resulting suspension was subjected to centrifugation (30 min, 2000 rpm). The light-yellow colored solution was separated from the colorless precipitate and the solvent was removed under reduced pressure at 323 K. Sublimation (reduced pressure, 453 K) gave Ph_2Zn as a colorless powder (55% yield), whose ¹H NMR spectroscopic properties (¹H NMR (200 MHz, 296 K, THF-d₈) δ (ppm) 6.95-7.10 (m, 6H, ArZn), 7.66-7.71 (m, 4H, ZnCCH) agreed with those reported in literature.⁴³ Solutions of Ph_2Zn in THF (0.25 M) were stored under argon in the dark and found stable to degradation for > 3 weeks.

Preparation of PhZnBr and $\text{PhZnBr}/(\text{LiCl})_n$ via Ph_2Zn .

Solutions of PhZnBr were prepared by a combination of Ph_2Zn (1 eq) with ZnBr_2 (1 eq) and stirring for 24 h. $\text{PhZnBr}/(\text{LiCl})_n$ reagents were generated as described above, but with n ($n = 0.5, 1, 2$) equivalents of LiCl added.

Rieke zinc method. Preparation of 2-*D,D*-butylzinc bromide (5.2).

In a dry and argon flushed tube lithium granulates (42 mg, 6.0 mmol, 1.4 eq) and naphthalene (768 mg, 6.0 mmol) were placed in THF (3 mL) and stirred until the lithium was completely dissolved and the color of the reaction mixture changed to dark green. A solution of ZnCl₂ in THF (3 mL, 1.0 M) was added dropwise and stirred for 5 min. The reaction mixture was centrifuged and the supernatant was removed. Then the precipitation was washed with THF (5 ml), centrifuged and the liquid excess was dismissed again. This procedure was repeated 3 times to remove the lithium salts. A solution of 2-*D,D*-butyl bromide⁴⁴ in THF (2 mL, 1.0 eq) was added and the reaction mixture stirred overnight.

Sample Preparation of Organozinc Compounds RZnX/(LiCl)_n and Bu₂Zn/(LiCl)_n for Electrical Conductivity Measurements.

In a first set of experiments, the specific conductivities of solutions of BuZnI in THF containing variable amounts of LiCl were measured. Performing these experiments by titration of a solution of BuZnI with a solution of LiCl and monitoring the increase in conductivity proved impractical because of the occurrence of hydrolysis reactions, despite the use of flame-dried glassware and careful observation of Schlenk techniques (hydrolysis of > 25% of the original BuZnI as determined by iodometric titration of the sample solution). Instead, sample solutions of preformed BuZnX/(LiCl)_n (X = Cl, Br, I; n = 0, 0.50, 1.00, and 2.00, respectively, c = 0.157 M) in THF were analyzed (one data point per sample solution), which minimized the transfer of solutions via gas-tight syringes and reduced the extent of hydrolysis (as determined by iodometric titration for each sample solution).³⁹ The same method was also used for measurements of BnZnBr, PhZnBr, Bu₂Zn, ZnCl₂, and ZnBr₂ solutions containing various amounts of LiCl. In this way, the extent of hydrolysis could be reduced to less < 10% for the BuZnI and Bu₂Zn reagents and < 5% for the other organozinc samples.

In a second set of experiments, the specific conductivities of BuZnI/LiCl solutions in THF were measured at different concentrations. These experiments were performed by adding portions of BuZnI/LiCl stock solutions to pure THF and monitoring the increase in conductivity. Because for these measurements the occurrence of hydrolysis reactions could not be rigorously excluded, additional experiments analyzed solutions of BuZnI/LiCl at fixed concentrations of c = 5.2, 9.6, 22,

39, and 76 mM, respectively (one data point per sample solution). For the sample solutions with concentrations $c > 5.2$ mM, iodometric titration³⁹ showed that < 8% of the BuZnI was hydrolyzed whereas no reliable determination was possible for the lowest concentration. Control experiments also probed solutions of pure LiX in THF. All conductometric measurements were performed at 258.15 ± 0.10 K in order to slow down interfering hydrolysis reactions.⁴⁵

Sample Preparation of Organozinc Compounds $\text{BuZnX}/(\text{LiCl})_n$ and $\text{Bu}_2\text{Zn}/(\text{LiCl})_n$ for NMR Spectroscopy.

Defined quantities of BuZnX ($\text{X} = \text{Cl}, \text{Br}, \text{I}$) or Bu_2Zn , respectively, in THF-D₈ and a solution of LiCl in THF-D₈ were added through rubber caps into flame-dried NMR tubes filled with argon. To determine the exact concentration of intact BuZnX in the probed samples, the amount of BuH formed by hydrolysis (due to residual traces of moisture) was derived from the ratio of the integrated ¹H signals. Only ¹H NMR experiments with < 25% hydrolysis (with respect to the initial concentration of the butylzinc reagent) were considered for further analysis although the ¹H chemical shifts of samples with higher percentages of hydrolysis did not show significant deviations (at similar LiCl concentrations).

3.3.3 Synthesis and Sample Preparation of Organomagnesium Reagents

Synthesis of $i\text{PrMgCl}/(\text{LiCl})_n$.⁴⁶

Magnesium turnings (1.2 eq, 0.32 mol) and anhydrous LiCl ($n = 0.0, 0.5, 1.0$, and 2.0 eq), were placed in a dry three necked flask equipped with an argon inlet, a dropping funnel, and a thermometer. The magnesium was covered with a small amount of THF (20 mL) and a mixture of isopropyl chloride (1 eq, 0.3 mol) in THF (110 mL) was added dropwise at a temperature below 318 K to get a grey solution. The reaction mixture was stirred overnight at room temperature and the remaining magnesium was allowed to settle down. The concentration was determined by iodometric titration (90-95% yield).³⁹

Preparation of $\text{BuZnX}/(\text{MgCl}_2)_{0.5}$ solutions.

According to **GP1**, solutions of $\text{BuZnI}/(\text{MgCl}_2)_n$ could be prepared if 0.5 M MgCl_2 solutions instead of pure THF or THF-D₈, respectively, were employed. In the case of $\text{BuZnI}/\text{MgCl}_2$, the formation of a colorless precipitate in addition to remaining Zn powder indicated that not all of the MgCl_2 remained soluble. Titration of a hydrolyzed aliquot of the nominal $\text{BuZnI}/\text{MgCl}_2$ solution with

ethylenediaminetetraacetate determined the overall concentration of dissolved divalent metal to $c = 0.75$ M. Together with the iodometrically determined concentration of the active butylzinc species, this result indicated an approx. stoichiometry of $\text{BuZnI}/(\text{MgCl}_2)_{0.5}$ of the dissolved reagent. $\text{BuZnCl}/(\text{MgCl}_2)_{0.5}$ could be prepared from Bu_2Zn , ZnCl_2 and a 0.5 M MgCl_2 solution in THF and the stoichiometry was determined in an analogous manner.

Sample Preparation of $i\text{PrMgCl}/(\text{LiCl})_n$ and $\text{MgCl}_2/(\text{LiCl})_n$

Electrical Conductivity Measurements. Two different methods were used to prepare the $i\text{PrMgCl}/(\text{LiCl})_n$ solutions. The first measurements were performed by a titration of $i\text{PrMgCl}$ ($c = 0.150$ M) with a solution of LiCl and the increase in conductivity was monitored. For the second set of experiments, preformed solutions of $i\text{PrMgCl}/(\text{LiCl})_n$ ($n = 0.0, 0.5, 1.0$, and 2.0 , respectively, $c = 0.150$ M) were analyzed. Both procedures revealed a high amount of hydrolysis reactions. Concentrations up to 45% lower than the starting concentrations were determined by iodometric titrations, despite Schlenk techniques and the use of dried reagents and glassware. This problem was solved by increasing the concentration up to $c = 0.300$ M and analyzing preformed solutions of $i\text{PrMgCl}/(\text{LiCl})_n$. In this way, the extent of hydrolysis could be reduced to less < 10%. All conductometric measurements were performed at 258.15 ± 0.10 K and 298.15 ± 0.10 K. Additional experiments of $\text{MgCl}_2/(\text{LiCl})_n$ ($n = 0.0, 0.5, 1.0$, or 2.0 , $c = 0.300$ M) were accomplished by a titration experiment of MgCl_2 with a solution of LiCl at 298.15 ± 0.10 K.

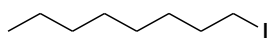
NMR Spectroscopy. In a first set of experiments, NMR spectra of $i\text{PrMgCl}$ in THF-D_8 containing variable amounts of LiCl were measured. Performing these experiments by titration of a solution of $i\text{PrMgCl}$ with a solution of LiCl in THF-D_8 proved impractical because of the occurrence of hydrolysis reactions (hydrolysis of > 50% of the original $i\text{PrMgCl}$ concentration as determined by iodometric titration of the sample solution). Instead, sample solutions of preformed $i\text{PrMgCl}/(\text{LiCl})_n$ ($n = 0.0, 1.0$, and 5.0 , respectively, $c = 0.300$ M) in THF-D_8 were analyzed, which reduced the extent of hydrolysis (as determined by iodometric titration for each sample solution).³⁹ Additionally, solutions of preformed $\text{BuZnX}/(\text{MgCl}_2)_{0.5}$ ($X = \text{Cl}, \text{I}$; $n = 0$ and 0.5 , $c \approx 0.040$ M) in THF-D_8 were analyzed.

3.3.4 Synthesis of Geminal Diiodides

General Procedure 3 (GP3). Preparation of the precursor reagents 1-iodooctane and (3-iodopropyl)-benzene.⁴⁷

The respective alcohol was dissolved in dichloromethane and then triphenylphosphine (1.10 eq) and imidazole (4.00 eq) were added at room temperature. After the addition of iodine (1.10 eq) at 273 K the reaction mixture turned yellow and was stirred for 10 min. The reaction mixture was allowed to warm up to room temperature and after 2 h stirring the reaction mixture was quenched with saturated aqueous ammonium chloride solution. The reaction solution was extracted 3 times with CH₂Cl₂ and the combined organic layers were washed with saturated ammonium carbonate solution and dried over MgSO₄. Removal of the solvent *in vacuo* and purification of the crude product via flash-chromatography (silica, CH₂Cl₂) afforded the analytically pure product.

1-Iodoctane (7.1)



According to **GP3**, octan-1-ol (542 mg, 4.16 mmol, 0.84 g/mL) was allowed to react with imidazole (1.13 g, 16.16 mmol), triphenylphosphine (1.20 g, 4.58 mmol) and iodine (1.16 g, 4.58 mmol) in CH₂Cl₂ (20 mL) for about 2 h. Flash column chromatographical purification (silica, CH₂Cl₂) gave **7.1** as an orange oil (530 mg, 2.22 mmol, 53%).

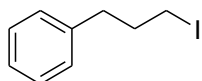
¹H-NMR (300 MHz, CDCl₃) δ (ppm) = 0.88 (t, *J* = 6.0 Hz, 3H, CH₃), 1.01-1.60 (m, 10H, CH₂), 1.82 (quint, *J* = 7.5 Hz, 2H, CH₂CH₂I), 3.19 (t, *J* = 7.1 Hz, 2H, CH₂I).

¹³C-NMR (75 MHz, CDCl₃) δ (ppm) = 7.56 (CH₂I), 14.25 (CH₃), 22.78 (CH₂CH₃), 28.67 (CH₂-Gruppe), 29.25 (CH₂-Gruppe), 30.67 (CH₂), 30.67 (CH₂), 31.91 (CH₂), 33.72 (CH₂CH₂I).

MS (70 eV, EI): *m/z* (%): 240 (M⁺, 7), 155 (C₂H₄I⁺, 12), 113 (C₈H₁₇⁺, 15), 71 (C₅H₁₁⁺, 100).

HRMS *m/z*: calc. for C₈H₁₇I 240.0375, found 240.0370.

IR (ATR): $\tilde{\nu}$ (cm⁻¹) = 721 (w), 1170 (m), 1204 (m), 1465 (m), 2853 (s), 2924 (vs), 2956 (m).

3-Iodopropylbenzene (7.2)

3-Phenylpropan-1-ol (6.08 g, 44.70 mmol, 1.01 g/mL) was allowed to react with imidazole (12.18 g, 178.68 mmol), triphenylphosphine (15.89 g, 49.17 mmol) and iodine (12.49 g, 49.17 mmol) in CH₂Cl₂ (200 mL) for about 2 h, according to **GP3**. Flash column chromatographical purification (silica, CH₂Cl₂) afforded **7.2** as an orange oil (7.71 g, 31.34 mmol, 70%)

¹H-NMR (300 MHz, CDCl₃) δ (ppm) = 2.25 (quint, *J* = 7.0 Hz, 2H, CH₂CH₂I), 2.75 (t, *J* = 7.3 Hz, 2H, Ar-CH₂), 3.19 (t, *J* = 6.8 Hz, 2H, CH₂I,), 7.39-7.16 (m, 5H, ArH).

¹³C-NMR (75 MHz, CDCl₃) δ (ppm) = 6.13 (CH₂I), 34.61 (CH₂CH₂I), 35.93 (ArCqCH₂), 125.89 (ArCH para), 128.21 (ArCH), 128.30 (ArCH), 140.12 (ArCq).

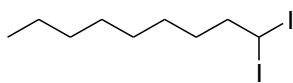
MS (70 eV, EI): *m/z* (%): 246 (M⁺, 35), 119 (C₉H₁₁⁺, 26), 91 (C₇H₇⁺, 100).

HRMS *m/z*: calc. for C₉H₁₁I 245.9905, found 245.9901.

IR (ATR): $\tilde{\nu}$ (cm⁻¹) = 696 (s), 739 (m), 1212 (m), 1453 (m), 1496 (m), 1871 (w), 2933 (m), 3026 (m).

General Procedure 4 (GP4). Formation of geminal diiodides with NaHMDS as base.⁴⁸

In a dry argon-flushed Schlenk-flask a solution of CH₂I₂ (5.00 eq) in THF was added dropwise to a solution of sodium hexamethyldisilazide (NaHMDS) (5.00 eq) in THF and ether at 183 K in an ethanol/liquid nitrogen bath. The color of the reaction solution changed from yellow to red-orange. Note that when the reaction mixture was brown, the addition of the diiodomethane was too fast and no geminal-diiodide was formed. After 20 min, a solution of the iodide in THF was added dropwise. The reaction mixture was allowed to warm slowly to room temperature over 16 h in the dark. Water was added and the mixture was extracted with CH₂Cl₂. The combined organic layers were washed with water and dried over MgSO₄. The solvent was removed under reduced pressure and purification by flash chromatography furnished the geminal diiodides.

1, 1-Diiodononane (7.3)

According to **GP4**, the NaHDMS solution (14.47 g, 78.95 mmol, 1.00 M in THF, 5.00 eq) in THF (47.00 mL) and ether (126.00 mL) was allowed to react with diiodomethane (21.15 g, 78.95 mmol, 3.33 g/mL, 5.00 eq) in THF (19.00 mL) and 1-iodooctane (**7.1**) (3.79 g, 15.79 mmol, 1.32 g/mL) in THF (32.00 mL). Purification by flash chromatography (silica, isohexane) yielded **7.3** as dark red oil (4.80 g, 12.65 mmol, 80%).

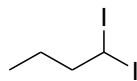
¹H-NMR (300 MHz, CDCl₃) δ (ppm) = 0.88 (t, *J* = 6.8 Hz, 3H, CH₃), 1.15-1.50 (m, 13H, CH₂), 2.28-2.43 (m, 2H, CH₂CHI₂), 5.11 (t, *J* = 6.5 Hz, 1H, CHI₂).

¹³C-NMR (75 MHz, CDCl₃) δ (ppm) = -24.83 (CHI₂), 14.26 (CH₃), 22.79 (CH₂CH₃), 27.77 (CH₂-Gruppe), 29.30 (CH₂), 29.46 (CH₂), 31.93 (CH₂), 31.96 (CH₂), 48.47 (CH₂CHI₂).

MS (70 eV, EI): *m/z* (%): 380 (M⁺, 5), 155 (C₂H₄I⁺, 12), 253 (C₉H₁₈I⁺, 38), 69 (C₅H₉⁺, 100).

HRMS *m/z*: calc. for C₉H₁₈I₂ 379.9498, found 379.9496.

IR (ATR): $\tilde{\nu}$ (cm⁻¹) = 618 (m), 721 (w), 1180 (m), 1119 (m), 1463 (m), 2851 (s), 2922 (vs), 2953 (m).

1, 1-Diiodobutane (7.4)

The NaHDMS solution (8.25 g, 45.00 mmol, 1.00 M in THF, 5.00 eq) in THF (27.00 mL) and ether (72.00 mL) was mixed with diiodomethane (12.05 g, 45.00 mmol, 3.33 g/mL, 5.00 eq) in THF (14.00 mL) and 1-iodopropane (1.53 g, 9.00 mmol, 1.78 g/mL) in THF (18.00 mL), according to **GP4**. Purification by flash chromatography (silica, isohexane) gave **7.4** as dark red oil (0.85 g, 2.74 mmol, 30%).

¹H-NMR (600 MHz, CDCl₃) δ (ppm) = 0.96 (t, *J* = 7.4 Hz, 3H, CH₃), 1.40-1.50 (m, 2H, CH₂CH₃), 2.26-2.40 (m, 2H, CH₂CHI₂), 5.13 (t, *J* = 6.6 Hz, 1H, CHI₂).

¹³C-NMR (75 MHz, CDCl₃) δ (ppm) = -25.50 (CHI₂), 12.18 (CH₂CH₃), 25.33 (CH₃), 50.36

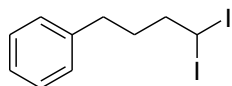
(CH_2CHI_2) .

MS (70 eV, EI): m/z (%): 310 (M^+ , 23), 183 ($C_4H_8I^+$, 100), 55 ($C_4H_7^+$, 90).

HRMS m/z : calc. for $C_4H_8I_2$ 309.8715, found 309.8714.

IR (ATR): $\tilde{\nu}$ (cm^{-1}) = 616 (w), 744 (m), 869 (w), 1071 (m), 1101 (vs), 1190 (m), 1234 (m), 1248 (m), 1460 (m), 2870 (s), 2928 (s), 2957 (vs).

4,4-Diiodobutylbenzene (7.5)



According to **GP4**, the NaHDMS solution (5.50 g, 30.00 mmol, 1.00 M in THF, 5.00 eq) in THF (18.00 mL) and ether (48.00 mL) was allowed to react with diiodomethane (8.04 g, 30.00 mmol, 3.33 g/mL, 5.00 eq) in THF (7.00 mL) and 3-iodopropylbenzene (**7.2**) (1.48 g, 6.00 mmol) in THF (12.00 mL). Flash column chromatographical purification (silica, isohexane) afforded **7.5** as an orange oil (1.54 g, 4.01 mmol, 67%)

1H -NMR (300 MHz, $CDCl_3$) δ (ppm) = 1.85-1.71 (m, 2H, $CH_2CH_2CHI_2$), 2.33-2.45 (m, 2H, CH_2CHI_2), 2.68 (t, 2H, J = 7.6 Hz, CH_2Cq), 5.11(t, J = 6.6 Hz, 1H, CHI_2), 7.12-7.41 (m, 5H, ArH).

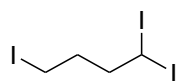
^{13}C -NMR (75 MHz, $CDCl_3$) δ (ppm) = -26.00 (CHI_2), 33.58 (CH_2), 33.95 (CH_2), 47.72 (CH_2CHI_2), 126.25 (ArCH para), 128.50 (ArCH), 128.62 (ArCH), 141.36 (ArCq).

MS (70 eV, EI): m/z (%): 386 (M^+ , 28), 131 ($C_{10}H_{11}^+$, 100).

HRMS m/z : calc. for $C_{10}H_{12}I_2$ 385.9028, found 385.9007.

IR (ATR): $\tilde{\nu}$ (cm^{-1}) = 696 (ss), 748 (m), 1087 (s), 1452 (m), 1495 (m), 1745 (w), 2854 (m), 2936 (m), 3024 (m).

Preparation of 1,1,4-Triiodobutane (7.6) with LiHMDS as base.⁴⁹



In a dry argon-flushed Schlenk flask lithium hexamethyldisilazide (LiHMDS) (279 mg, 1.67 mmol, 1.00 M in THF) was added drowise over 15 min into a solution of diiodomethane (447 mg, 1.67 mmol, 3.33 g/mL) and 1,3-diiodopropane (1.22 g, 4.11 mmol) in THF (14.00 mL) at 153 K

(pentane/nitrogen bath). The solution was allowed to reach room temperature over 16 h. Saturated aqueous ammonium chloride solution was added and the mixture was extracted three times with *tert*-butyl methyl ether. The combined extracts were washed with sodium thiosulfate solution (20%) and twice with water. The organic layers were dried over MgSO₄, concentrated *in vacuo* and purification with isohexane and silica afforded the product **7.6** as dark red oil (410 mg, 0.93 mmol, 56%).

¹H-NMR (300 MHz, CDCl₃) δ (ppm) = 1.89-2.09 (m, 2H, CH₂CH₂I), 2.42-2.58 (m, 2H, CH₂CHI₂), 3.22 (t, *J* = 6.7 Hz, 2H, CH₂I), 5.15 (t, *J* = 6.3 Hz, 1H, CHI₂).

¹³C-NMR (75 MHz, CDCl₃) δ (ppm) = -29.20 (CHI₂), 3.26 (CH₂I), 35.30 (CH₂), 48.62 (CH₂).

MS (70 eV, EI): *m/z* (%): 436 (M⁺, 2), 309 (C₄H₇I₂⁺, 100), 181 (C₄H₆I⁺, 30), 155 (C₂H₄I⁺, 15), 55 (C₄H₇⁺, 65),

HRMS *m/z*: calc. for C₄H₇I₃ 435.7682, found 435.7685.

IR (ATR): $\tilde{\nu}$ (cm⁻¹) = 617 (m), 753 (s), 804 (m), 971 (m), 1079 (vs), 1123 (m), 1166 (m), 1196 (s), 1225 (vs), 1253 (m), 1284 (m), 1423 (s), 1434 (s), 2832 (m), 2887 (s), 2931 (s), 2981 (m).

Preparation of geminal diiodozinc species

According to **GP1**, the zinc reagents were prepared from 1,1-diiodononane (**7.3**), and 1,1-triodobutane (**7.6**) (5.00 mmol, 1.00 eq) using Zn dust (7.00 mmol, 1.40 eq) in DMF.

3.3.5 Preparation of Charged-Tagged Organozinc Reagents

Synthesis of charge-tagged precursors

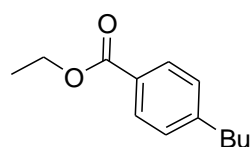
According to known literature procedures ammonium substituted alkyl iodides, dimethylbenzyl-(4-iodobutyl)-ammonium iodide (**8.2**), triethyl-(4-iodobutyl)-ammonium iodide (**8.3**) and tributyl-(4-iodobutyl)-ammonium iodide (**8.4**), were prepared.⁵⁰ A flask was charged with 1,4-diiodobutane (*n* = 0.032 mol, 1 eq) and diethylether (50 mL). The corresponding tertiary amine (*n* = 0.138 mol, 4.3 eq) was added slowly and the reaction mixture was stirred for 24 h at room temperature. The colorless precipitate was washed with diethylether/ethanol (10:1) and filtrated. The yield amounted to 38% for **8.3**, 18% for **8.4** and 25% for **8.5**.

Synthesis of charge-tagged organozinc species.

According to the typical procedure **GP1**, a flask was flame-dried under high vacuum and allowed to cool down under argon atmosphere. The procedure was repeated twice and Zn dust (1.4 eq) and 1.00 mL of solvent (THF, CH₃CN or DMF for reagent **8.3** and THF for reagent **8.6**) was added. Then 1.0 eq of (*p*-iodophenyl)-trimethylammonium iodide (**8.6**) or triethylammonium butyl iodide (**8.3**) respectively, was added and the resulting suspension was stirred for 14 h at 323 K for reagent **8.6** or for 12 h at room temperature for reagent **8.3**, respectively.

Sample preparation for Negishi cross-coupling experiments analyzed by ESI mass spectrometry.

A flame-dried flask was charged with (*p*-iodophenyl)-trimethylammonium iodide (**8.6**) and dry CH₃CN under argon atmosphere. To the resulting 2 mM solution benzylzinc bromide or *m*-methylbenzylzinc bromide (1.2 or 2.0 equiv), respectively, and Pd(dba)₂/2 tfp (bis(dibenzylideneacetone)palladium/ 2 tri-2-furylphosphine; 0.05, 0.10, or 1.0 eq wih respect to the palladium compound) were added at 253 K.

3.3.6 Preparation of Negishi Cross-Coupling Reactions with Butyl Zinc Reagents**Preparation of 4-butyl-benzoic ethyl ester (**9.2**)**

The zinc reagent BuZnCl/LiCl (10.00 mL, 4.90 mmol, 0.49 mM in THF), prepared from Bu₂Zn, ZnCl₂ and LiCl, was added to a solution of 4-iodobenzoic ethyl ester (1.16 g, 0.71 mL, 4.20 mmol), Pd(OAc)₂ (4.70 mg, 0.021 mmol, 0.5 mol%) and SPhos (2-dicycolhexylphosphino-2',6'-dimethoxybiphenyl, 17.22 mg, 0.042 mmol, 1.0 mol%) in THF (5.50 mL). The reaction mixture was stirred for 12 h at room temperature, a saturated NH₄Cl solution was added and extracted with ether (3 times). The combined organic layers were washed with an aqueous sodium thiosulfate solution and dried over Na₂SO₄. The solvent was removed under reduced pressure and purification of the crude product by flash chromatography furnished **9.2** as a colorless oil (1.46 g, 3.36 mmol, 80%).

¹H-NMR (300 MHz, CDCl₃) δ (ppm) = 0.93 (t, J = 7.4 Hz, 3H, C_{Ar}C₃H₆CH₃), 1.36-1.26 (m, 5H, OCH₂CH₃, C_{Ar}C₂H₄CH₂CH₃), 1.66-1.56 (m, 2H, C_{Ar}CH₂CH₂C₂H₅), 2.66 (t, J (H,H) = 7.7 Hz, 2H, C_{Ar}CH₂C₃H₇), 4.35 (q, J = 7.1 Hz, 2H, OCH₂CH₃), 7.23 (d, J = 8.1 Hz, 2H, C_{Ar}H), 7.95 (d, J = 8.2 Hz, 2H, C_{Ar}H).

¹³C-NMR (75 MHz, CDCl₃) δ (ppm) = 14.1 (C_{Ar}C₃H₆CH₃), 14.5 (OCH₂CH₃), 22.5 (C_{Ar}C₂H₄CH₂CH₃), 33.5 (C_{Ar}CH₂CH₂C₂H₅), 35.9 (C_{Ar}CH₂C₃H₇), 60.9 (OCH₂CH₃), 128.2 (CqC₄H₉), 128.5 (CHCqC₄H₉), 129.7 (CHCqCOO), 148.5 (CqCOO), 166.9 (CO).

MS (70 eV, EI): m/z (%): 206 (M⁺, 39), 161 (C₁₁H₁₃O⁺, 100), 91 (C₇H₇⁺, 35).

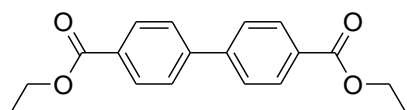
HRMS m/z : calc. for C₁₃H₁₈O₂ 435.7682, found 435.7685.

IR (ATR): $\tilde{\nu}$ (cm⁻¹) = 703 (m), 759 (m), 850 (m), 1021 (m), 1103 (vs), 1176 (s), 1270 (vs), 1610 (m), 1714 (s), 2860 (w), 2872 (w), 2930 (m), 2957 (m).

Preparation of 4-(ethoxycarbonyl)phenylzinc iodide

RZnI/(LiCl)_n reagents (R = 4-(ethoxycarbonyl)phenyl) were generated as described in **GP2**, with 1 equivalent of LiCl added. The yield, determined by iodometric titration, amounted to 57%.

Preparation of biphenyl-4,4'-dicarboxylic acid diethyl ester (**9.3**)^{51,52}



A dry and argon flushed Schlenk flask was charged with palladium acetate Pd(OAc)₂ (0.5 mg, 0.002 mmol, 1 mol%), SPhos (1.7 mg, 0.004 mmol, 2 mol%) and 4-(ethoxycarbonyl)phenylzinc iodide (5.0 mL, 2.9 mmol, 0.57 M in THF). After stirring the mixture for 5 min, ethyl 4-iodobenzoate (614 mg, 0.37 mL, 2.2 mmol) was added dropwise. The reaction mixture was stirred for 2 days under inert gas at room temperature. Then the reaction mixture was quenched with saturated NH₄Cl solution and extracted with ether (4 times). The combined organic phases were washed with an aqueous sodium thiosulfate solution and dried over Na₂SO₄. Purification of the crude residue obtained after evaporation of the solvents by flash chromatography (isohexane, silica) yielded biphenyl-4,4'-dicarboxylic acid diethyl ester (**9.3**) (550 mg, 1.85 mmol, 84%) as colorless solid.

¹H-NMR (300 MHz, CDCl₃) δ (ppm) = 1.42 (t, *J* = 7.1 Hz, 6H, OCH₂CH₃), 4.41 (q, *J* = 7.2 Hz, 4H, OCH₂CH₃), 7.69 (d, *J* = 8.3 Hz, 4H, C_{Ar}H), 8.14 (d, *J* = 8.2 Hz, 4H, C_{Ar}H).

¹³C-NMR (75 MHz, CDCl₃) δ (ppm) = 14.4 (2C, OCH₂CH₃), 61.1 (2C, OCH₂CH₃), 127.2 (2C, CqCqCH), 130.1 (2C, Cq), 130.2 (2C, COCqCH), 144.3 (2C, COCq), 166.3 (CO).

MS (70 eV, EI): *m/z* (%): 298 (M⁺, 56), 253 (C₁₆H₁₃O₃⁺, 100), 225 (C₁₅H₁₃O₂⁺, 19), 152 (C₁₂H₁₀⁺, 34).

HRMS *m/z*: calc. for C₁₈H₁₈O₄ 298.1205, found 298.1210.

IR (ATR): $\tilde{\nu}$ (cm⁻¹) = 696 (s), 752 (vs), 845 (vs), 1022 (s), 1107 (s), 1265 (vs), 1604 (m), 1702 (s), 2902 (w), 2930 (w), 2960 (w), 2979 (w), 2992 (w).

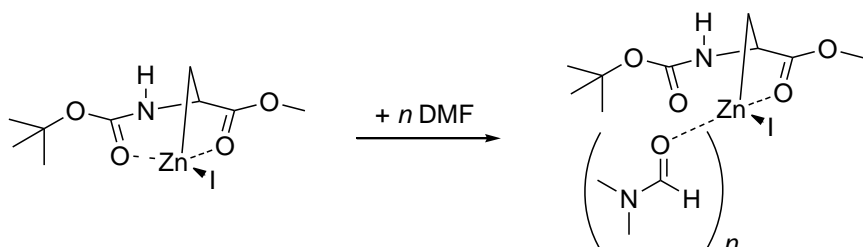
General procedure 5 (GP5) for Negishi cross-coupling reactions analyzed by gas chromatography.

A flame-dried flask under Ar atmosphere was charged with ethyl 4-iodo-benzoate (0.15 mmol, 1.0 eq), the butylzinc reagent (0.60 mmol, 4.0 eq), and *n*-undecane (0.15 mmol, 1.0 eq) as internal standard in a total volume of 1.35 mL of THF. The resulting solution was stirred and held at 273 ± 1 K by means of a circulating water/ethanol bath. A solution (0.15 mL) of Pd(OAc)₂ (1 mol%) and SPhos (2 mol%) was quickly added at time zero of the kinetic measurement. Samples from the reaction mixture were taken at defined times and quickly treated with an aqueous solution of NH₄Cl. After extraction with diethyl ether and filtration through glass wool, the resulting organic layers were analyzed by gas chromatography (Thermo Electron Corporation, Trace GC Ultra). The abundances of all reagents were determined by comparing their integrated measured peak areas (normalized to that of the internal standard) to calibration curves for authentic samples of these substances (see Chapter 3.2). The kinetic measurements were routinely performed in duplicate.

4 Microsolvated Organozinc Cations

Introduction

As mentioned above, organozinc compounds are important reagents in organic synthesis.⁵³ They show a high chemoselectivity and tolerance of functional groups.^{54,55} Besides, their use is not only restricted to relatively inert solvents, such as hydrocarbons and ethers, but they can also be handled in acetonitrile^{11,56,57} and *N,N*-dimethylformamide (DMF),⁵⁸ which greatly extends their scope. Recent progress in the application of functionalized alkylzinc iodides has partially relied on the empirical observation that dipolar aprotic solvents are beneficial both for preparation and solution stability of the reagents.⁵⁹ A good example was the use of DMF for reactions of amino acid-derived alkylzinc reagents.⁶⁰ ¹³C-NMR experiments provided evidence that DMF coordinated to zinc, influencing intramolecular coordination by the carbonyl oxygen atoms of both the ester and carbamate protecting group. This effect may have an influence of the stabilization of β -aminoalkylzinc iodides towards elimination (Scheme 4.1).⁶¹



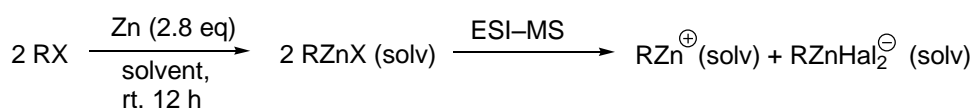
Scheme 4.1. Addition of DMF to zinc reagent in THF-d₈.

Caggiano and co-workers found only very recently that organozinc compounds can form ionic species in polar solvents. They provided evidence that alkylzinc iodides can partially undergo heterolytic dissociation in DMF to produce alkylzinc cations, which are stabilized by solvation.⁶² Similarly, Koszinowski and Böhrer reported on the observation of benzylzinc cations and anions in solutions of benzylzinc bromide in tetrahydrofuran (THF).^{28b} The group of Driess found related organozinc cations produced upon addition of B(C₆F₅)₃ to the solutions of organozinc compounds in THF.⁶³ All of these studies employed electrospray ionization (ESI) mass spectrometry, which has become one of the leading methods to characterize charged organometallic species.²⁵ Taking advantage of this technique the dissociation reaction of alkylzinc iodides in THF, acetonitrile and DMF was systematically investigated. Moreover, the unimolecular gas-phase chemistry of the resulting RZn(solvent)⁺ was studied and hereby provided detailed insight into the way how the

coordination of single solvent molecules modulated organometallic reactivity.

Results and Discussion

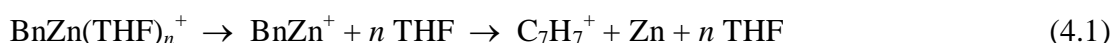
Preparatory studies started with benzylzinc bromide in THF as a model system. The studied solutions of benzylzinc bromide in THF and RZnI ($R = Me, iPr$, and Bu) in different solvents (THF, DMF, and acetonitrile) were prepared via a Zn insertion reaction and subjected to analysis by ESI mass spectrometry (Scheme 4.2).



$R = Me, iPr, Bu, Bn$

Scheme 4.2. Solutions of zinc insertion reactions into RX analyzed by ESI mass spectrometry.

Benzylzinc bromide in THF. Solutions of benzylzinc bromide in THF ($c = 5$ mM) afforded $BnZn(THF)^+$ as major ion upon cation-mode ESI employing the HCT ion trap. In addition $BnZn(THF)_2^+$ and $C_7H_7^+$ were detected (Figure 4.1.A) Collision-induced dissociation (CID) of $BnZn(THF)_n^+$ resulted in the sequential loss of the THF molecules and subsequent fragmentation into $C_7H_7^+$ and neutral Zn, Eq. 4.1 with $n = 1$ and 2 (Figure 4.1.B).



Formation of $C_7H_7^+/Zn$, rather than C_7H_7/Zn^+ is consistent with the known thermochemical data for the system ($IE(C_7H_7) = 7.25$ eV⁶⁴ < $IE(Zn) = 9.39$ eV⁶⁵). For detailed information of the anion-mode spectra see Chapter 6.1.

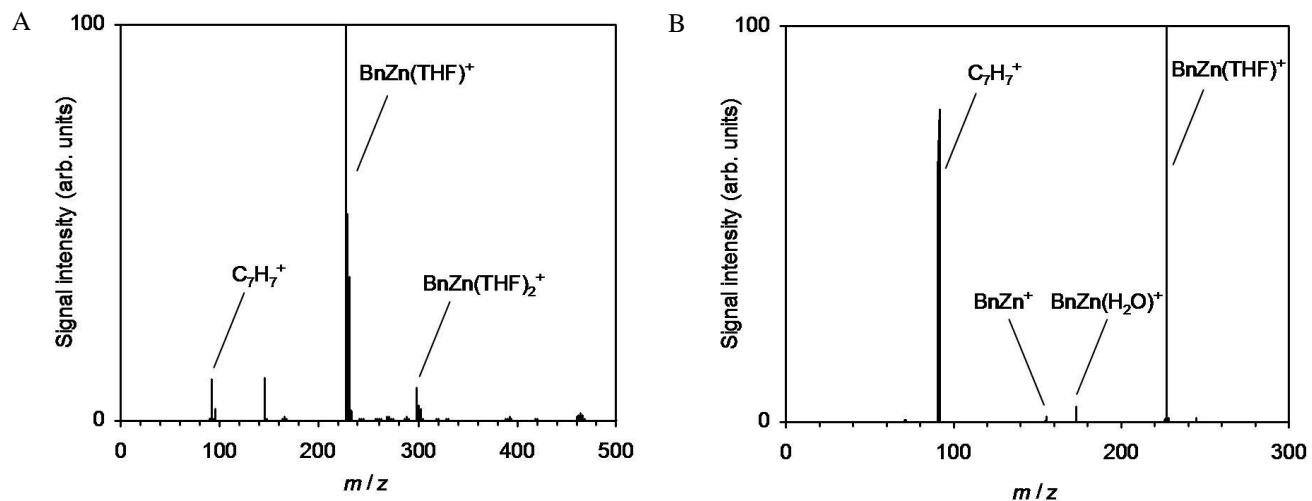
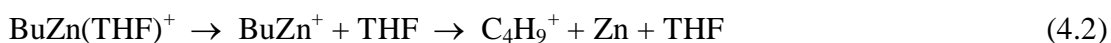


Figure 4.1.A. Cation-mode ESI mass spectrum of a 5 mM solution of benzylzinc bromide in THF measured with the HCT ion trap. **B.** Mass spectrum of mass-selected $\text{Bn}^{64}\text{Zn}(\text{THF})^+$ ($m/z = 227$) and its fragment ions produced upon collision-induced dissociation ($V_{\text{exc}} = 0.26$ V, HCT ion trap).

RZnI in THF. Next, the solutions of different alkylzinc species ($\text{R} = \text{Me}$, $i\text{Pr}$, and Bu) were analyzed. Cation-mode ESI mass spectrometry of solutions of butylzinc iodide in THF showed almost exclusively mononuclear $\text{BuZn}(\text{THF})^+$ over a wide range of concentrations ($c(\text{BuZnI}) = 5\text{-}40$ mM) and for different ESI conditions (Figure 4.2.A. Top). The identity of this mononuclear zinc species was confirmed by gas-phase fragmentation of the selected ion and the characteristic isotopic pattern (Figure 4.2.B).

Upon CID, $\text{BuZn}(\text{THF})^+$ lost the THF molecule to yield bare BuZn^+ , which dissociated into a C_4H_9^+ cation and Zn (Eq. 4.2 and Figure 4.2.A. Bottom).



The observed fragmentation pattern is again in accordance with thermochemistry ($IE(\text{C}_4\text{H}_9) = 8.02$ eV⁶⁶ < $IE(\text{Zn}) = 9.39$ eV). The generated C_4H_9^+ species most likely correspond to the more stable tertiary butyl cation formed upon rearrangement from the linear primary butyl cation. In addition the CID experiment showed significant amounts of $\text{BuZn}(\text{H}_2\text{O})^+$. This species originated from a bimolecular reaction with unavoidable traces of background water present in the ion trap.

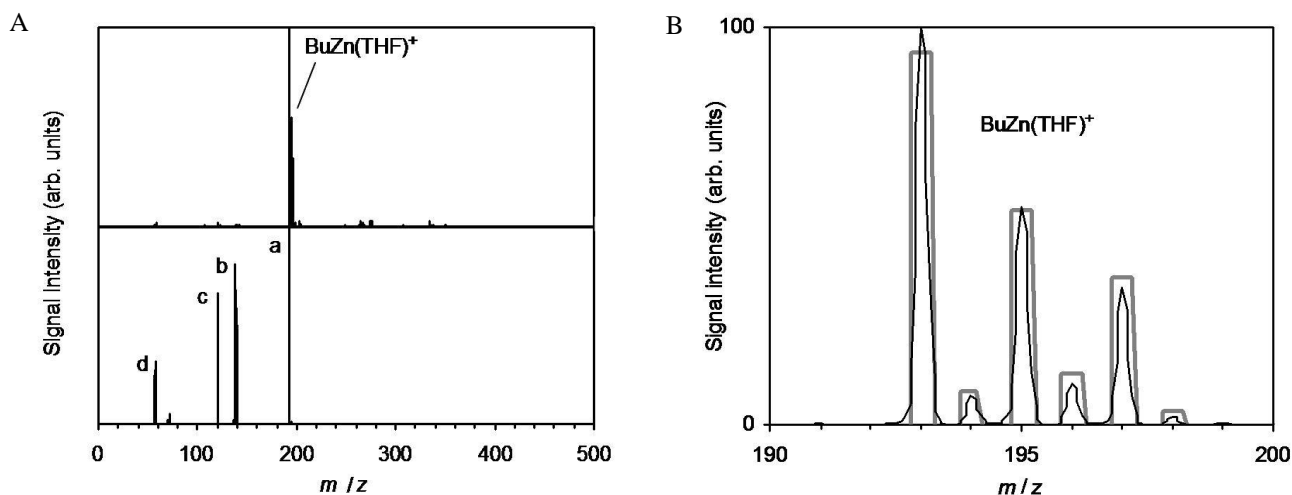


Figure 4.2.A. Top. Cation-mode ESI mass spectrum of a 5 mM solution of butylzinc iodide in THF measured with the HCT ion trap. **A. Bottom.** Cation-mode ESI mass spectrum of mass-selected a) $\text{Bu}^{64}\text{Zn}(\text{THF})^+$ (m/z 193) and its fragment ions produced upon collision induced dissociation ($V_{\text{exc}} = 0.30$ V, HCT ion trap): c) $\text{Bu}^{64}\text{Zn}^+$ and d) C_4H_9^+ . The ion b) $\text{Bu}^{64}\text{Zn}(\text{H}_2\text{O})^+$ originated from an ion-molecule reaction with background water. **B.** Cation-mode ESI mass spectrum of a 5 mM solution of butylzinc iodide in THF measured with the HCT ion trap (black) and the predicted isotopic pattern of $\text{Bu}^{64}\text{Zn}(\text{THF})^+$ (grey).

Upon CID, $\text{BuZn}(\text{H}_2\text{O})^+$ lost the water molecule to yield bare BuZn^+ (Eq. 4.3).



Obviously the gaseous butylzinc cation did not have an appreciable tendency toward hydrolysis, as the water molecule bound to the BuZn^+ as an intact ligand proven by elimination of H_2O . As recently reported by Koszinowski and Böhrer, the gas-phase reactivity of $\text{Bu}_n\text{ZnCl}_{3-n}^-$ ($n = 1-3$) was rather low.^{30a} Only Bu_3Zn^- and Bu_2ZnCl^- underwent proton transfer from formic acid at measurable rates. It is expected that the positive charge of BuZn^+ decreased the reactivity toward proton donors even further.

Solutions of methylzinc iodide and isopropylzinc iodide in THF ($c = 5$ mM) afforded $\text{RZn}(\text{THF})^+$ ($\text{R} = \text{Me}$ and $i\text{Pr}$) as major ions upon cation-mode ESI with the HCT ion trap. In addition, $\text{RZn}(\text{THF})_2^+$ and $\text{ZnI}(\text{THF})_n^+$ ($n = 1$ and 2) were detected and the fragmentation behavior of the mass-selected compounds were similar to the pattern of the butylzinc species.

Anion-mode ESI of solutions of butylzinc iodide in THF produced only relatively small amounts of the organozincate BuZnI_2^- (Figure 4.3).⁶⁷ Instead, the purely inorganic complex ZnI_3^- prevailed, whose signal intensity increased with time. As the concentrations of the organometallic reagents employed are quite low, even minor residual contaminations by water and/or oxygen became important. In addition, smaller amounts of $\text{ZnI}_{3-n}\text{Br}_n^-$ ($n = 1$ and 2)⁶⁸, were also detected. Similar spectra were obtained for solutions of methylzinc iodide and isopropylzinc iodide in THF.

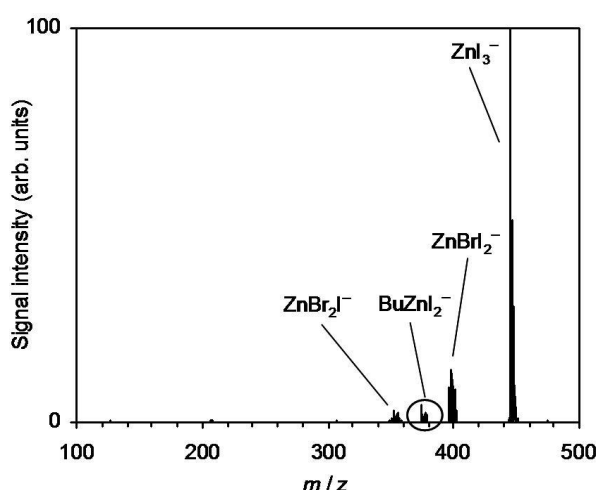


Figure 4.3. Anion-mode ESI mass spectrum of a 5 mM solution of butylzinc iodide in THF measured with the HCT ion trap.

Butylzinc iodide in acetonitrile. Solutions of butylzinc iodide in acetonitrile ($c = 5 \text{ mM}$) were analyzed with the HCT ion trap. Cation-mode ESI mass spectra afforded $\text{BuZn}(\text{CH}_3\text{CN})^+$ as the major ion. Additionally, $\text{BuZn}(\text{CH}_3\text{CN})_2^+$, $\text{ZnI}(\text{CH}_3\text{CN})_n^+$ ($n = 1$ and 2), BuZn^+ , and C_4H_9^+ were observed (Figure 4.4).

CID experiments of $\text{BuZn}(\text{CH}_3\text{CN})^+$ confirmed that BuZn^+ and C_4H_9^+ resulted from the fragmentation of the mass-selected complex (Eq. 4.4)



For the studies of solutions of butylzinc iodide in THF identical settings were applied and no spontaneous fragmentation occurred. Thus, these observations point to a lower intrinsic stability of $\text{BuZn}(\text{CH}_3\text{CN})^+$ compared to $\text{BuZn}(\text{THF})^+$.

Anion-mode ESI mass spectrometry of solutions of BuZnI in acetonitrile showed only inorganic complexes and thus indicated the occurrence of hydrolysis and/or oxidation reactions.

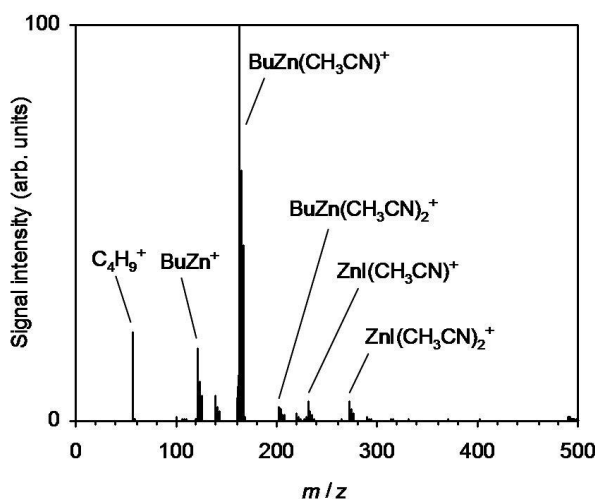


Figure 4.4. Cation-mode ESI mass spectrum of a 5 mM solution of butylzinc iodide in acetonitrile measured with the HCT ion trap.

Butylzinc iodide in DMF. Only, the TSQ instrument was used for the studies of solutions of butylzinc iodide in DMF to exclude cross-contamination. It was found that DMF solutions gave rise to extremely long-lasting contaminations and they were deliberately not introduced in the HCT instrument. DMF-containing ions were observed with high signal intensities, even after day-long flushing of the TSQ ESI-source with THF at elevated temperature. The complete removal of DMF from the ESI source was quite difficult because of the high boiling point and the substantial Lewis basicity.⁶⁹

Cation-mode ESI mass spectrometry of solutions of butylzinc iodide in DMF ($c = 1\text{-}4 \text{ mM}$) showed the formation of BuZn(DMF)_3^+ as the most prominent ion, while BuZn(DMF)_2^+ , ZnI(DMF)_3^+ , and Na(DMF)_3^+ were present in much lower abundance (Figure 4.5.A.). These results agree with the findings of Caggiano et al., who subjected solutions of pentylzinc iodide in DMF to analysis by ESI mass spectrometry.⁶² The number of solvent molecules bound to the $\text{C}_5\text{H}_{11}\text{Zn}^+$ center of the observed $\text{C}_5\text{H}_{11}\text{Zn(DMF)}_n^+$, $n = 1\text{-}3$, could be controlled by adjusting the ESI conditions. CID experiments, conducted in this work, showed the stepwise loss of DMF molecules from BuZn(DMF)_3^+ leading to BuZn^+ , followed by the dissociation into C_4H_9^+ + Zn^+ (Eq. 4.5, $n = 1\text{-}3$).



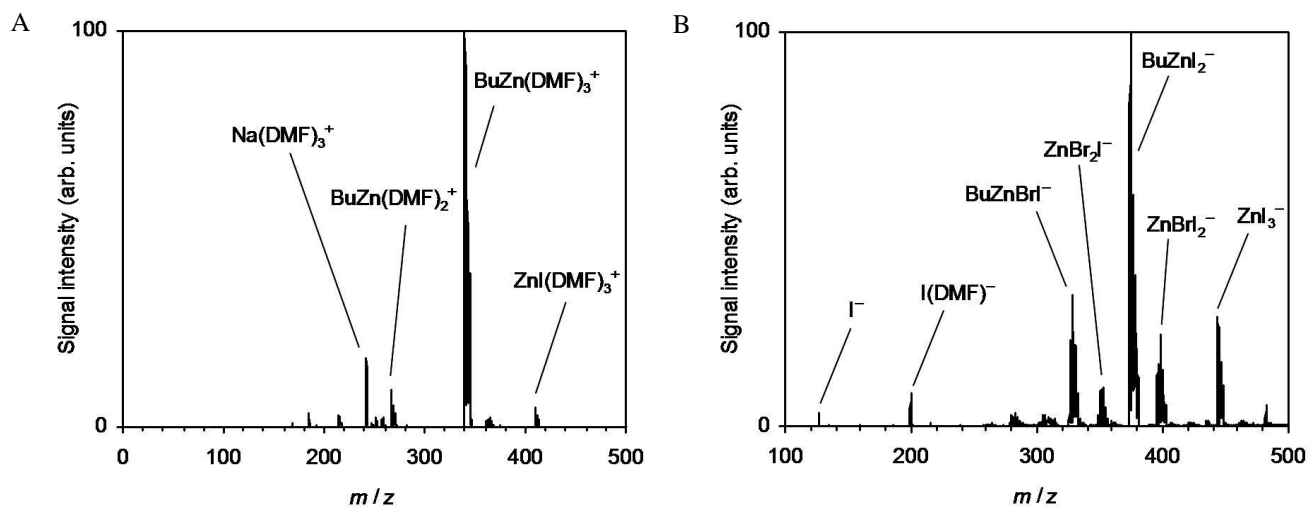
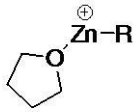
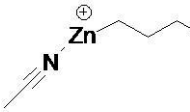
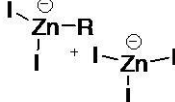
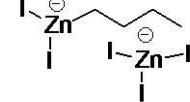


Figure 4.5.A. Cation-mode ESI mass spectrum of a 1 mM solution of butylzinc iodide in DMF measured with the TSQ 7000 instrument. The solvated Na^+ ion resulted from the drying of the THF solvent over sodium benzophenone ketyl. **B.** Anion-mode ESI mass spectrum of a 4 mM solution of butylzinc iodide in DMF measured with the TSQ instrument.

Solutions of butylzinc iodide in DMF afforded BuZnI_2^- as base peak upon anion-mode ESI mass spectra with the TSQ 7000 instrument (Figure 4.5.B). In their study on the related system pentylzinc iodide in DMF, Caggiano et al. observed neither the corresponding nor any other organozincate anion. Instead they only found inorganic species of the type $\text{Zn}_n\text{I}_{2n+1}^-$, $n = 1-3$.⁶² Preparatory experiments demonstrated that the detection of organozincate anions could depend strongly on the design of the ESI source used and the applied ESI conditions. This dependence could help to explain why Caggiano et al. did not observe $\text{Zn}(\text{C}_5\text{H}_{11})\text{I}_2^-$ nor any other organozincate anion. It is considered as unlikely that butyl- and pentylzinc iodide could significantly differ in their solution chemistry in DMF or their tendency to form organozincate anions. In addition, less intense signals for the analogous complex BuZnBrI^- as well as for the inorganic anions $\text{BuZnI}_n\text{Br}_{n-1}^-$ ($n = 1-3$) and $\text{I}(\text{DMF})_n^-$ ($n = 0$ and 1) were observed. The observation of $\text{I}(\text{DMF})^-$ was remarkable because it is the single micro-solvated anion encountered in the present study. One has to consider that this finding does not necessarily point to an intrinsically higher affinity of DMF toward anions (in comparison to THF and acetonitrile) but that it might simply result from the different ESI conditions in the TSQ 7000 instrument.

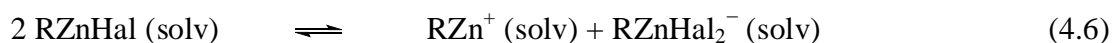
In summary main signals of various alkylzinc experiments are shown in table 4.1.

Table 4.1. Heterolytic dissociation of microsolvated alkylzinc halides in THF, CH₃CN, and DMF probed by ESI mass spectrometry. The main species of interest are shown.

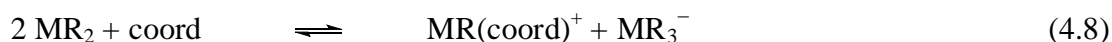
Solvent	THF	CH ₃ CN	DMF
Cations			
Anions			

R = Me, iPr, Bu

Comparison of solvent effects. In all three solvents investigated (THF, CH₃CN, and DMF), microsolvated mononuclear BuZn⁺ cations were observed. These findings suggest that solvated organozinc cations may spontaneously form in solution to a significant degree. The situation is best understood for the case of DMF, for which Caggiano et al. performed density-functional theoretical calculations.⁶² Focussing on methylzinc iodide as model system, Caggiano et al. found that heterolytic cleavage of the Zn-I bond could occur in the presence of three DMF molecules. The latter stabilized the generated ZnCH₃⁺ cation via *O*-coordination, thus acting as Lewis bases and providing the driving force for the overall reaction. In contrast, the simultaneously released I⁻ did not experience a comparable stabilization upon interaction with DMF, which is only a poor Lewis acid. In accordance with this assessment, the anion-mode ESI mass spectra measured for the butylzinc iodide solution showed only small amounts of I⁻ and I(DMF)⁻. It seems more plausible that I⁻ bound to remaining neutral alkylzinc iodide instead, despite the lower concentration of the latter in comparison to the solvent DMF. Like other dicoordinated organozinc species, alkylzinc iodides can be considered as typical Lewis acids.⁷⁰ The organozincate ion expected to result from this coordination indeed formed the base peak in the anion-mode ESI mass spectra obtained for butylzinc iodide in DMF. The heterolytic dissociation of organozinc halides in this solvent thus actually appears to correspond to a disproportionation reaction (Eq. 4.6).



Related processes were reported by Richey and coworkers, who extensively studied the reactions of strongly coordinating agents, such as crown ethers, azacrown ethers, and cryptands with organomagnesium^{71,72} and organozinc compounds.⁷³ Relying on ¹H-NMR spectroscopy, these authors could establish the occurrence of disproportionation reactions in benzene and ethers (Eqs. 4.7 and 4.8, M = Mg and Zn, and coord = coordination agent).^{71,72,73}



Although these equilibria often lied essentially completely on the side of the ionic products in the case of magnesium,^{76,77c} disproportionation usually was less efficient in the case of zinc. Unlike ¹H-NMR spectroscopy, ESI mass spectrometry does not allow straightforward quantitation and thus the degree of disproportionation of butylzinc iodide in DMF currently could not further be specified.

For THF and acetonitrile, an analogous behavior to that of DMF is assumed although for the former the stabilizing effect of coordination was weaker. In BuZn(CH₃CN)⁺, this interaction between the solvent molecule and the ZnBu⁺ center is weakened to such an extent that partial fragmentation occurs during the ESI process. As expected, the observed stability order of ZnBu(DMF)⁺ > BuZn(THF)⁺ > BuZn(CH₃CN)⁺ corresponds to the relative positions of the three different solvents in well-established Lewis basicity scales.⁷⁴

Interestingly, a parallel trend was observed in the macroscopic stability of the highly diluted butylzinc iodide solutions toward decomposition by hydrolysis and/or oxidation. While DMF solutions were stable for > 4 h, THF solutions had lifetimes of 1 - 2 h, and in acetonitrile, degradation occurred on a time scale of approximately 30 min. The different stability of butylzinc iodide in the three solvents was also evident from the relative amounts of organozincates visible in the anion-mode ESI mass spectra: BuZnI₂⁻ prevailed for DMF, appeared as minor peak for THF, and was absent for acetonitrile. A plausible explanation might be the involvement of Lewis-acidic organozinc species in the degradation reactions. The reactivity of these species should be lowered to a greater extent in more Lewis-basic solvents. The inferred Lewis-acidic organozinc species need not be free cations because the concentration of the latter, at least in acetonitrile, was probably not

overly high. As discussed above, neutral organozinc halides behaved as Lewis acids as well. Similar situations might also apply to other reactions of organozinc reagents.

Conclusion

Summing up, ESI mass spectrometric analysis of solutions of butylzinc iodide in THF, acetonitrile, and DMF resulted in the detection of micro-solvated $\text{BuZn}(\text{solvent})_n^+$ cations in all cases. In the THF and DMF experiments, the organozincate anion ZnBuI_2^- could also be observed. Similar results were obtained for the experiments of BnZnBr and RZnI ($\text{R} = \text{Me}, i\text{Pr}$) in THF. It is proposed that these ions form in solution by disproportionation of neutral RZnX . The main driving force for this reaction is believed to be the coordination of the Lewis-basic solvent molecules to the RZn^+ cation. For the butylzinc iodide experiments in different solvents the ability of the solvents to ionize the zinc species decreased in the order DMF > THF > acetonitrile. Gas-phase experiments provided additional insight on the stabilization of the RZn^+ cation by different solvents. Upon fragmentation, the micro-solvated $\text{RZn}(\text{solvent})_n^+$ cations lost the attached solvent molecules to form bare RZn^+ , which further dissociated into a R^+ cation and neutral Zn. The same behavior was also found for $\text{RZn}(\text{H}_2\text{O})^+$, which originated from the reaction of RZn^+ with background water. To gain further insight into the interaction of organozinc cations with different Lewis bases, the effect of chelating ligands, described in the following chapter, was investigated.

5 Organozinc Halides in the Presence of Chelating Ligands

Introduction

In Chapter 4 solvated alkylzinc cations⁷⁵ and organozincates^{28a,28b} were studied using ESI mass spectrometry. It is assumed that these ions result from a disproportionation reaction of neutral alkylzinc iodide in solution. DFT calculations have suggested that coordination of DMF to alkylzinc iodides could partially induce cleavage of the zinc-iodine bond to form a tight ion pair.⁶² The observed alkylzinc cation was not as easily protonated as the neutral alkylzinc iodide,⁶² providing a credible explanation for the high tolerance of alklyzinc iodides toward acidic protons.

In addition, organozinc compounds can be favorably combined with chiral ligands to achieve enantioselective chemical reactions. In particular, the enantioselective addition of diethylzinc to aldehydes is of enormous importance.⁷⁶ Until now, the effect of added ligands on the stoichiometry and reactivity of organozinc compounds is not fully understood. Thus, ESI mass spectrometry was chosen to investigate the heterolytic dissociation of butylzinc iodide in the presence of 1,2-dimethoxyethane (**L1**), *N,N*-dimethyl-2-methoxyethylamine (**L2**), and *N,N,N',N'*-tetramethylethylenediamine (TMEDA, **L3**). These ligands, although not being equal to crown ethers or cryptands in terms of coordination ability, mimicked the binding motif of practically highly important chiral ligands.^{76,77} In addition, diamine **L3** itself has been demonstrated to enhance the nucleophilic reactivity of diethylzinc toward benzaldehyde, in contrast to glycol ether **L1**, which had no effect.⁷⁸ Next the relative stabilities of the formed $\text{BuZn}(\text{ligand})^+$ complexes were probed by competition experiments and analysis of their unimolecular gas-phase reactivity. To gain more information about the unimolecular gas-phase reaction of butylzinc iodide solutions of deuterated butylzinc species were considered as well.

Results and Discussion

The concentration of butylzinc iodide in THF, $c(\text{BuZnI}) \approx 5 \text{ mM}$, was held constant and the amount of the added ligand varied between 1 and 5 equivalents. Both the chelating ligand and THF then competed for the limited number of binding sites at the BuZn^+ cations.

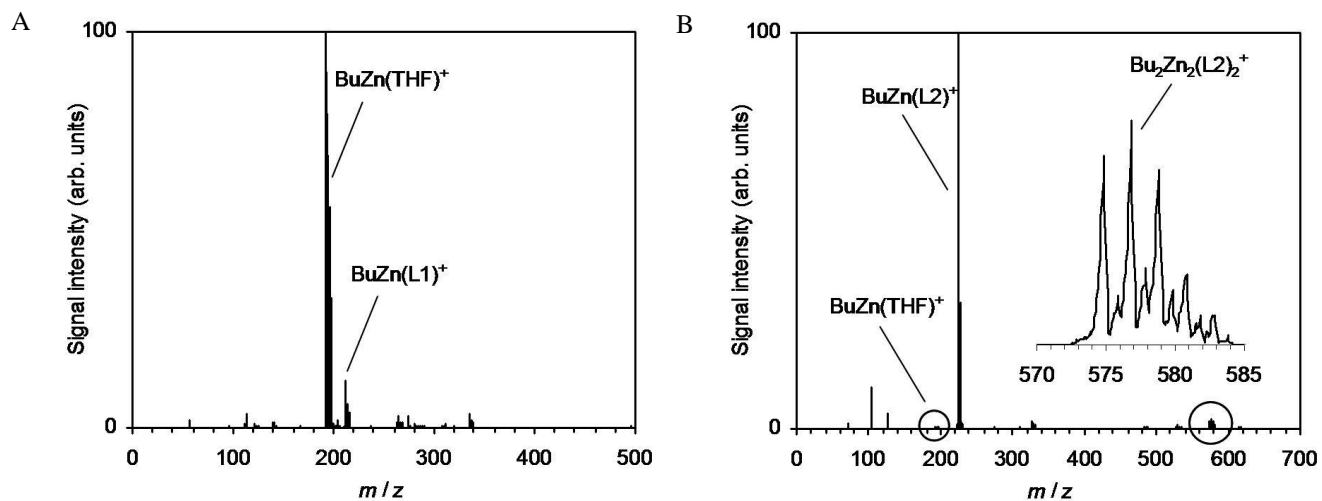


Figure 5.1.A. Cation-mode ESI mass spectrum of a solution of butylzinc iodide and 1,2-dimethoxyethane (ligand **L1**) in a ratio of 1:1 ($c = 5 \text{ mM}$) in THF measured with the HCT ion trap. **B.** Cation-mode ESI mass spectrum of a solution of butylzinc iodide and *N,N*-dimethyl-2-methoxyethylamine (ligand **L2**) in a ratio of 1:1 ($c = 5 \text{ mM}$) in THF measured with the HCT ion trap. Inset: Enlarged part of the mass spectrum showing the isotopic pattern of $\text{Zn}_2\text{Bu}_2\text{I}(\text{L2})_2^+$.

Although the effective concentration of the THF solvent exceeded that of the chelating ligand by approximately three orders of magnitude, cation-mode ESI mass spectrometry proved the extensive formation of $\text{BuZn}(\text{ligand})^+$ complexes. For the glycol ether **L1** (Figure 5.1.A), the signal intensity of $\text{BuZn}(\text{ligand})^+$ was still smaller than that of $\text{BuZn}(\text{THF})^+$ but both for the aminoether **L2** (Figure 5.1.B) and the diamine **L3** (Figure 5.2.A. Top) just the opposite held true.

These results demonstrated the enormous stabilization that the interaction with chelating ligands can provide to organozinc cations and thus echo the findings of Richey and coworkers.⁷⁸ At the same time, differences between the individual ligands are noticeable (Figure 5.2.B). For $\text{BuZn}(\text{L1})^+$, a relatively smaller signal intensity was observed, which implied that the interaction of the glycol ether **L1** with the butyl zinc cation is not as strong as that of ligands **L2** and **L3** with BuZn^+ .

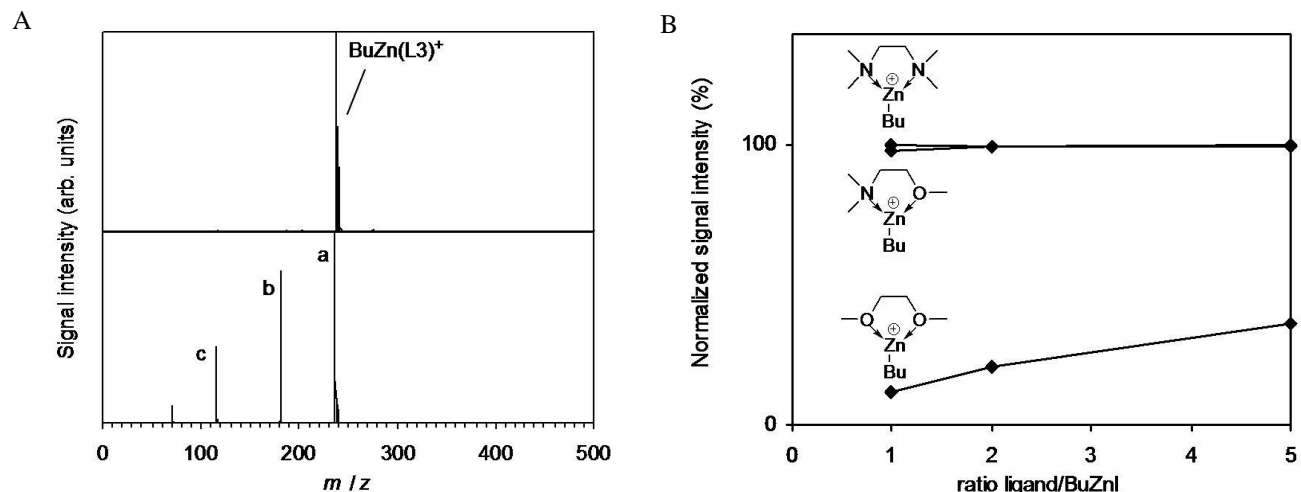


Figure 5.2.A. Top. Cation-mode ESI mass spectrum of a solution of butylzinc iodide and TMEDA (ligand **L3**) in a ratio of 1:1 ($c = 5 \text{ mM}$) in THF. **A. Bottom.** Cation-mode ESI mass spectrum of mass-selected a) $\text{Bu}^{64}\text{Zn}(\text{L3})^+$ ($m/z = 237$) and its fragment ions produced upon collision-induced dissociation ($V_{\text{exc}} = 0.35 \text{ V}$, HCT ion trap): b) $\text{ZnH}(\text{L3})^+$ and c) $(\text{L3}-\text{H})^+$. The fragment at $m/z = 70$ apparently resulted from cleavage of the backbone of ligand **L3**. **B.** Normalized signal intensities of the chelate complexes $\text{BuZn}(\text{ligand})^+$ as derived from cation-mode ESI mass spectra of solutions of butylzinc iodide and ligands **L1-L3** in THF ($c(\text{BuZnI}) = 5 \text{ mM}$, ratio ligand/ $\text{BuZnI} = 1:1$, $2:1$, and $5:1$). The normalized signal intensity of $\text{BuZn}(\text{ligand})^+$ was calculated as $I_{\text{norm}}(\text{BuZn}(\text{ligand})^+) = I(\text{BuZn}(\text{ligand})^+)/[I(\text{BuZn}(\text{ligand})^+) + I(\text{BuZn}(\text{THF})^+)]$.

To achieve a more direct comparison between the three different chelating ligands, THF solutions of butylzinc iodide containing two of the ligands together were also probed. The experiments combining the glycol ether **L1** with **L2** or **L3** (Figures 5.3.A. and 5.3.B), respectively, showed essentially no $\text{BuZn}(\text{L1})^+$ and thus again indicate a lower affinity of **L1** toward the ZnBu^+ center in comparison to **L2** and **L3**.

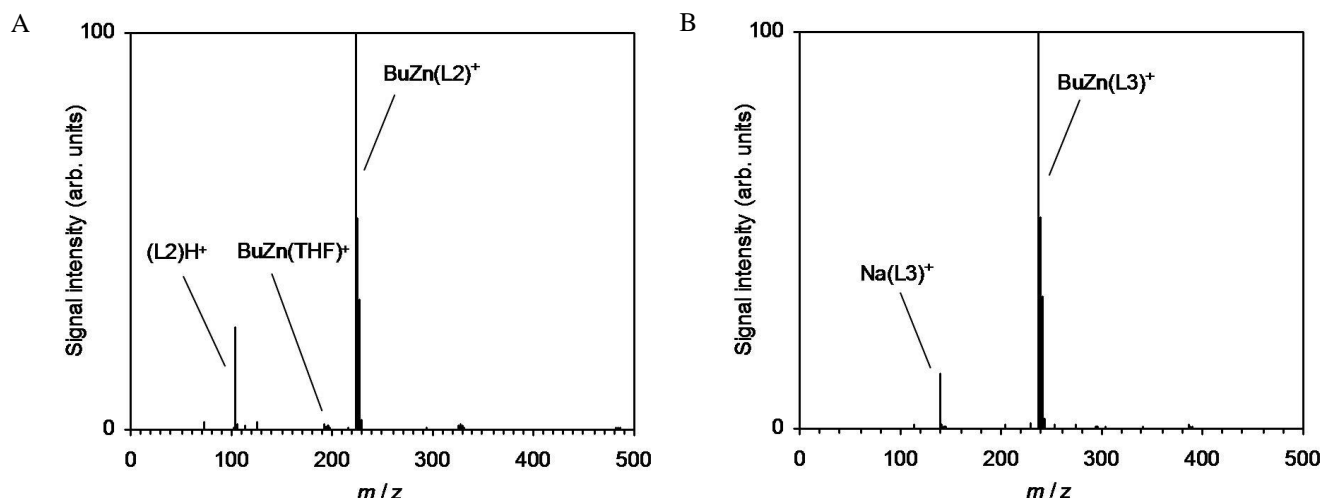
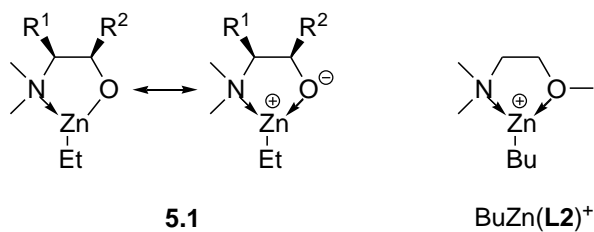


Figure 5.3.A. Cation-mode ESI mass spectrum of a solution of butylzinc iodide, 1,2-dimethoxyethane (**L1**), and *N,N*-dimethyl-2-methoxyethylamine (**L2**) in a ratio of 1:1:1 ($c = 5 \text{ mM}$) in THF measured with the HCT ion trap. Note that essentially no signal intensity was observed for the complex $\text{Bu}^{64}\text{Zn}(\text{L1})^+ (m/z = 211)$. **B.** Cation-mode ESI mass spectrum of a solution of butylzinc iodide, 1,2-dimethoxyethane (**L1**), and *N,N,N',N'*-tetramethylethylenediamine (**L3**) in a ratio of 1:1:1 ($c = 5 \text{ mM}$) in THF measured with the HCT ion trap. Note that essentially no signal intensity was observed for the complex $\text{Bu}^{64}\text{Zn}(\text{L1})^+ (m/z = 211)$. The solvated Na^+ ions resulted from the drying of the THF solvent over sodium benzophenone ketyl.

Direct competition between **L2** and **L3** resulted in higher signal intensities for $\text{BuZn}(\text{L3})^+$ than for $\text{BuZn}(\text{L2})^+$, but it was refrained from a rigorous quantitative analysis because of the complicating effect of the present protonated ligands, $\text{H}(\text{L2})^+$ and $\text{H}(\text{L3})^+$. In general, differences in ESI signal intensities do not necessarily reflect actual concentration differences in solution but may also arise from deviating ESI response factors of the different species.⁷⁹ In the present case, however, the two complexes $\text{ZnBu}(\text{L2})^+$ and $\text{ZnBu}(\text{L3})^+$ seemed so similar that comparable ESI response factors could be assumed. Accordingly, it is inferred that the observed relative signal intensities of $\text{ZnBu}(\text{L2})^+$ and $\text{BuZn}(\text{L3})^+$ roughly mirror their relative concentrations in solution and, thus, that the diamine **L3** binds to the ZnBu^+ center more strongly than the aminoether **L2**. Therefore, it was consistently found that the dimethylamino function stabilizes the butylzinc cation better than the methoxy function does. Richey and coworkers reached similar conclusions in their study of the complexation of organozinc cations by polyethers and polyamines.^{73c}

The different relative affinities of oxygen- and nitrogen-containing functional groups toward the

BuZn^+ moiety are of particular interest in the context of enantioselective catalysis. The chiral ligands typically employed in the asymmetric addition of diethylzinc to aldehydes feature a 1,2- or 1,3-aminoalcohol motif. The key intermediates in these transformations were commonly believed to be mono- and dimeric ethylzinc aminoalcoholates, which formed upon deprotonation of the aminoalcoholate and concomitant release of ethane.⁷⁶ For the case of chiral ligands with an 1,2-aminoalcohol motif, the resulting monomeric key intermediates of the type **5.1** are closely mimicked by the $\text{BuZn}(\text{L2})^+$ complex. The analogy between **5.1** and $\text{BuZn}(\text{L2})^+$ becomes most evident if the former is considered an ethylzinc cation stabilized by an amino and an alcoholate function. Because the anionic alcoholate function in **5.1** should bind to the ZnEt^+ center more strongly than the neutral methoxy group in $\text{BuZn}(\text{L2})^+$, the overall stabilization achieved in **5.1** will be even higher than for the model complex $\text{BuZn}(\text{L2})^+$. Of course, such a tight binding between the organozinc center and the chiral ligand is essential for achieving a high asymmetric induction. The observation that the model complex $\text{BuZn}(\text{L2})^+$ formed in THF even at low concentrations of the aminoether **L2** suggests that intermediates of type **5.1** will also be quite stable in this relatively polar solvent. Although most asymmetric additions of diethylzinc to aldehydes are performed in non-polar hydrocarbons, numerous examples are known for which high enantioselectivities could be also obtained in THF.⁷⁷



Interestingly, small amounts of the dinuclear aminoether complex $\text{Bu}_2\text{Zn}_2\text{I}(\text{L2})_2^+$ (Figure 5.1.B) were observed, which correspond to the cationic analogue of the supposed dimeric ethylzinc aminoalcoholate intermediates. Similarly, the dinuclear diamine complex $\text{Bu}_2\text{Zn}_2\text{I}(\text{L3})_2^+$ was detected in low signal intensities. The fact that these putatively rather labile dinuclear complexes survived the ESI process suggests once more that the ESI conditions applied were quite gentle. At the same time, it shows that mass spectrometry is ideally suited to differentiate between various aggregation states of ionic organometallic species.

Anion-mode ESI mass spectra obtained for THF solutions of butylzinc iodide with added ligands **L1-L3** were qualitatively similar to those recorded without added ligands (see above). Obviously, the chelating ligands did not bind to organozincate (or any other) anions. However, the addition of

the strongly binding ligands **L2** and **L3** significantly increased the signal intensity of ZnBuI_2^- (Figure 5.4.A and 5.4.B).

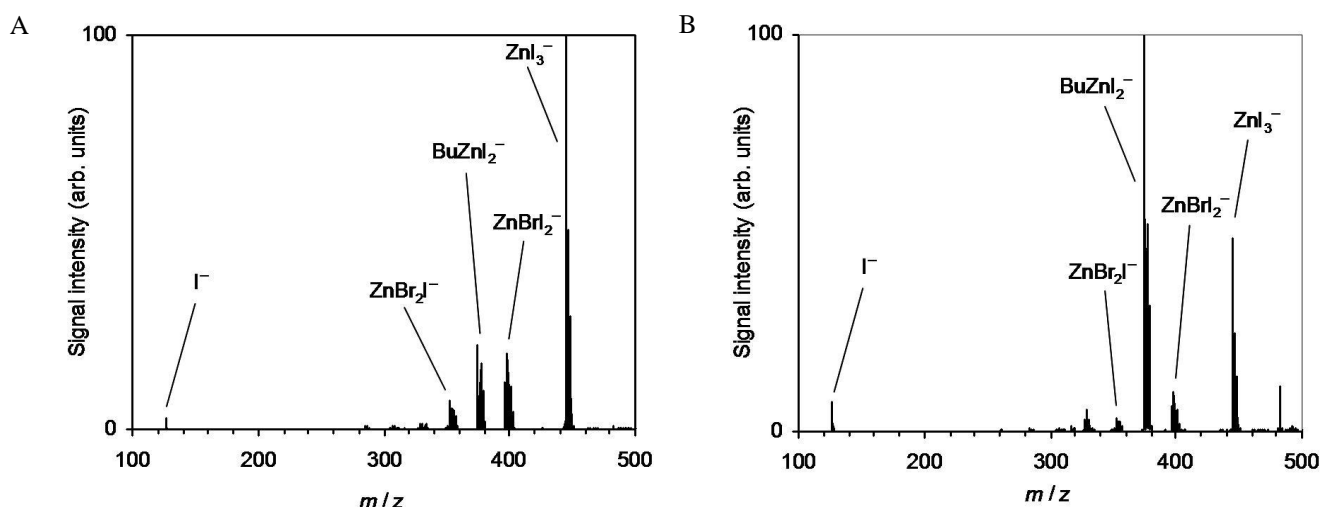


Figure 5.4.A. Anion-mode ESI mass spectrum of a solution of butylzinc iodide and *N,N*-dimethyl-2-methoxyethylamine (**L2**) in a ratio of 1:2 ($c = 5 \text{ mM}$) in THF measured with the HCT ion trap. **B.** Anion-mode ESI mass spectrum of a solution of butylzinc iodide and *N,N,N',N'*-tetramethylethylenediamine (**L3**) in a ratio of 1:2 ($c = 5 \text{ mM}$) in THF measured with the HCT ion trap.

This observation is fully in line with the inferred operation of a disproportionation equilibrium, which is shifted toward the side of ionic products in the presence of strongly chelating ligands, Eq. 5.1.



Unimolecular gas-phase chemistry of chelated butylzinc cations. After having explored the stability of the BuZn(ligand)^+ complexes (ligand = **L1** - **L3**) in solution, finally the unimolecular gas-phase chemistry of these species was investigated. In analogy to the relatively facile desolvation of the micro-solvated BuZn(solvent)_n^+ complexes (see Chapter 4) one might expect CID of BuZn(ligand)^+ to lead to simple ligand loss, Eq. 5.2.



However, this fragmentation pathway occurred only for the glycol-ether complex $\text{BuZn}(\textbf{L1})^+$ and, in this case, only to a minor extent (note that the main part of the BuZn^+ fragment apparently undergoes a bimolecular consecutive reaction with background water to form the simultaneously observed $\text{BuZn}(\text{H}_2\text{O})^+$ cation, see Chapter 4). Instead, all three complexes eliminated butene upon CID to produce the chelated hydridozinc cations ZnH(ligand)^+ , Eq. 5.3 (Figure 5.2.A. Bottom for ligand = **L3**).



Obviously, the cleavage of the covalent zinc-carbon and carbon-hydrogen bonds in this reaction is more favorable than the loss of the chelating ligand. This finding highlights once again the strong interaction of the chelating ligands, particularly **L2** and **L3**, with BuZn^+ . At the same time, it shows how the chelating ligands change the reactivity of the organometallic species. While bare BuZn^+ produced cationic and, thus, electrophilic C_4H_9^+ upon CID, the chelate complexes $\text{BuZn}(\text{ligand})^+$ released neutral butene, an, admittedly weak, nucleophile. This ligand-induced switch in gas-phase reactivity strikingly resembled the situation in solution, where only the addition of a chelating ligand, such as **L3** or an aminoalcohol, activated diethylzinc for the nucleophilic addition to benzaldehyde.⁷⁸ The glycol ether **L1** failed to activate diethylzinc in solution,⁷⁸ and in the gas-phase, too, it has a weaker effect than **L2** and **L3**, as $\text{BuZn}(\textbf{L1})^+$ produced *both* butene and the C_4H_9^+ cation upon CID.

Apart from these parallels to solution chemistry, the butene elimination from the cationic $\text{BuZn}(\text{ligand})^+$ complexes, Eq. 5.3, also resembles the previously reported loss of butene from the gaseous ZnBu_3^- anion.^{28a} It seems likely that both these fragmentations proceed as β -hydride eliminations although only relatively few examples of this type of mechanism are known for organozinc compounds.⁸⁰ The participation of d-orbitals in reactions lowers the barriers, so β -hydride eliminations occur particularly easily for coordinatively unsaturated transition metal species. The effect of this participation can also be seen from the efficiency of the reverse reactions, the olefin insertions into transition metal hydrides. Though less readily, main group and post-transition metal complexes also undergo β -hydride eliminations. Interestingly, not all of these transformations corresponded to unwanted, non-productive side reactions. In the semiconductor industry, one of the most important methods for the preparation of thin metal layers is metallo-organic chemical vapor deposition, which in many instances involved β -hydride eliminations. For example, the formation of zinc layers from deposited Et_2Zn has been suggested to proceed

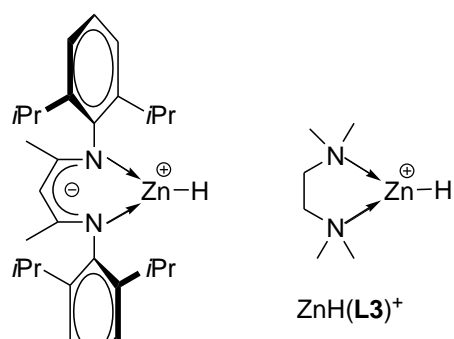
according to this reaction type.⁸¹

To test whether the butene elimination from the cationic BuZn(ligand)^+ complexes, Eq. 5.3, really corresponds to β -hydride eliminations, deuterium labelling of an alkyl reagent was employed. In this experiment⁸², a solution of 2-*D,D*-butylzinc bromide (**5.2**) in THF was prepared via the Rieke zinc method.^{16,44} An aliquot was diluted in THF and after addition of TMEDA **L3** ($c = 5 \text{ mM}$, ratio 1:1) subjected to analysis by ESI mass spectrometry. Cation-mode ESI mass spectrometry of these solutions in THF showed almost exclusively mononuclear 2-*D,D*- BuZn(L3)^+ ($m/z = 239/241/243$). This assignment is based on the agreement with the calculated pattern of $\text{ZnC}_{10}\text{H}_{23}\text{D}_2\text{N}_2^+$. Upon CID, a consistent loss of a neutral fragment of $\Delta m = 57$, which corresponds to $\text{C}_4\text{H}_7\text{D}$, was observed, Eq. 5.4.



This fragmentation pattern is the proof of the operation of a β -hydride elimination. The virtual absence of neutral C_4H_8 and $\text{C}_4\text{H}_6\text{D}_2$ fragments shows the extremely high selectivity of this process.

Apart from the mechanism itself, the ZnH(ligand)^+ fragment ions resulting from CID of the BuZn(ligand)^+ complexes are of interest. While a manifold of zinc hydride compounds is known,⁸³ only a limited number of them are monomeric. A structurally well-characterized example of such a monomeric zinc hydride is given by the recently reported hydridozinc complex **5.3**.⁸⁴



5.3

In this complex, the ZnH moiety is stabilized by a chelating β -diketiminate ligand, thus giving rise to a trigonal coordination of the zinc center. A similar geometric situation can be expected for

$\text{ZnH}(\text{L3})^+$ and the other two $\text{ZnH}(\text{ligand})^+$ complexes observed in the present work. Further fragmentation reactions of $\text{BuZn}(\text{L2})^+$ and $\text{BuZn}(\text{L3})^+$ involved hydride transfers from the ligand to the zinc center and thus generated neutral butylzinc hydride, Eqs. 5.5 and 5.6.



The concomitantly formed cations presumably correspond to iminium species. This fragmentation pathway was particularly prominent for the aminoether complex $\text{BuZn}(\text{L2})^+$.

Conclusion

In summary, the addition of bidentate chelating ligands to THF solutions of butylzinc iodide largely displaced THF from the coordination sphere of the metal center and formed preferentially mononuclear chelate complexes $\text{BuZn}(\text{ligand})^+$. Gas-phase experiments provided additional insight into the stabilization of the BuZn^+ cation by the ligands investigated and resulted in the fragmentation of the complexes $\text{BuZn}(\text{ligand})^+$ by elimination of butene and formation of the hydrido zinc cations $\text{ZnH}(\text{ligand})^+$. The mechanisms of the butene elimination corresponding to a β -hydride elimination are confirmed by the fragmentation pattern of the deuterated butylzinc species $2-D,D\text{-BuZn}(\text{L3})^+$. The behavior of the $\text{BuZn}(\text{ligand})^+$ cations are in stark contrast to the micro-solvated $\text{BuZn}(\text{solvent})_n^+$ cations, which lost the attached solvent molecules to form bare BuZn^+ and further dissociated into a C_4H_9^+ cation and neutral Zn. This observation proves that the chelating ligands bound much more strongly to the zinc center than the probed solvents in Chapter 4. Moreover, it suggests that the energy gained from the chelation exceeded the barrier associated with the elimination of butene. These results resemble the activating effect of chelating ligands on dialkylzinc in solution, which is of crucial importance for the nucleophilic alkylation of aldehydes. Furthermore the competition and CID experiments showed that the ability of the three different ligands to stabilize and ionize the zinc species supposedly decreased in the order **L3 > L2 > L1**. ESI mass spectrometric and gas-phase experiments are able to provide a consistent picture of how solvation and chelation stabilized the butylzinc cation and controlled its reactivity on a molecular level. For rather labile systems, such as the micro-solvated organometallic ions probed here, a careful control of the ESI conditions thus was mandatory. Furthermore, ESI mass spectrometry alone could not achieve reliable quantitation of the species of interest in the present work. Hence,

the equilibrium constants of the inferred disproportionation reactions are still not known in this case just as the extent to which the ionization of alkylzinc halides occurs. Therefore alternative analytical methods will be needed to address these issues in the future.

6 Formation of Lithium Organozincates

6.1 Lithium Organozincate Complexes LiRZnX_2

Introduction

The most common syntheses of organozinc halides produce these reagents in the presence of LiX salts, as described above. The possible role of these LiX salts has been largely ignored¹⁸ until Knochel's work on LiCl -promoted Zn insertion reactions has put them into the spotlight.^{17,19} Koszinowski and Böhrer have recently used ESI mass spectrometry to characterize organozinc intermediates²⁸, whereas these studies pointed to the formation of organozincate anions. In line with these findings, theoretical calculations by Liu et al. predicted the PhZnBr system to give a stable $\text{Li}^+\text{PhZnBrCl}^-$ zincate complex in the presence of LiCl .⁸⁵ This group also showed that the interaction of Zn/PhBr with LiCl lowered the energy of the transition structure of the Zn insertion, thus providing a rationale for the observed rate acceleration.⁸⁵ Growing evidence moreover suggests that the presence of LiX additives also changes the reactivity of the in situ formed organozinc halides and enhances their nucleophilicity.^{86–91} Organ and coworkers screened numerous simple salt additives and found LiCl and LiBr to be particularly effective in accelerating Negishi cross-coupling reactions in THF/dimethylimidazolidinone (DMI) mixtures.⁹² Based on titration experiments, these authors proposed that here the active transmetalating agent corresponds to higher-order zincates $\text{Li}_n\text{RZnBr}_3^{(2-n)-}$, $\text{R} = \text{Bu}$.⁹² Very recently Organ and collaborators also employed ESI mass spectrometry and NMR spectroscopy to support their hypothesis of higher-order zincates being present in THF/DMI mixtures.⁹³ Note that an analogous organozincate dianion was known from the structurally characterized salt $[\text{PPh}_4^+]_2[\text{EtZnBr}_3^{2-}]$.⁹⁴ Compared to the strong influence of lithium halides on organozinc halides, their effect on the reactivity of diorganylzinc compounds apparently was much smaller. As Kneisel, Dochnahl, and Knochel reported, LiCl did not activate $^i\text{Pr}_2\text{Zn}$ to undergo iodine-zinc exchange with methyl 4-iodobenzoate in diethylether/*N*-methyl-2-pyrrolidinone mixtures.⁹⁵ This reaction occurred efficiently in the presence of $\text{Li}(\text{acac})$ and $\text{Cs}(\text{acac})$, however. In these cases, the formation of $\text{Li}^+/\text{Cs}^+(\text{CH}_3\text{OOC}-\text{C}_6\text{H}_4)\text{Zn}^i\text{Pr}(\text{acac})^-$ zincate complexes was surmised.⁹⁵

To understand the effects of the LiX salts on the reactivity of organozinc halides and diorganozinc compounds, more information on the interaction of these additives with organozinc species is

required. ESI mass spectrometry has recently been established as a useful method to obtain qualitative information at a molecular level.^{28,35,36} Therefore this technique was employed for further experiments in the present study. However, ESI mass spectrometry is considered less suitable for quantitative analysis and thus offers only limited insight into the association and dissociation equilibria operative in solution. Furthermore, there is evidence that ESI mass spectrometry is incapable of detecting free zincate di-anions.⁹⁶ To check for the presence of such dianions in LiX/RZnX and LiX/R₂Zn solutions and to probe the association/dissociation equilibria in these systems, it was therefore turned to electrical conductivity measurements and NMR spectroscopy.⁹⁷ These well-established methods provide quantitative information on speciation in solution and thus lend themselves to a combination with ESI mass spectrometry.

Results and Discussion

Throughout the present work, special efforts have been made to ensure well-defined reaction conditions and to control the concentration of LiX additives carefully. For the preparation of LiX-free RZnX reagents, no transmetalation reactions were applied because the precipitation of the LiX (or MgX₂) byproducts may possibly be incomplete even in apolar solvents. Instead, rigorously salt-free solutions of RZnX were synthesized by Zn insertion into RX (in the absence of LiX) or by mixing R₂Zn with ZnX₂. Unlike Organ and co-workers,⁹³ sample solutions in THF were deliberately chosen without the addition of co-solvents, such as DMI, to keep the system as simple as possible. Solutions of RZnX·LiX and R₂Zn·LiX in pure THF, i.e., without added more polar co-solvents, also showed excellent reactivity in many synthetically valuable transformations, including Negishi cross-coupling reactions.^{19,91,98}

ESI Mass Spectrometry. RZnX/(LiCl)_n. As absolute ESI signal intensities are typically rather unstable and poorly reproducible, only relative signal intensities are considered in the present titration experiments. To the sampled solutions of organozinc compounds small amounts of NaBPh₄ ($c = 20 \mu\text{M}$) were added as internal standard and the anion ESI signal intensities were normalized to that of BPh₄⁻. However, as the concentration of NaBPh₄ was lower than that of the organozinc species by two orders of magnitude, interferences with the dissociation equilibria of the latter could be excluded. Note, that the addition of LiCl is likely to influence the concentration of free BPh₄⁻ ions in a not easily predictable manner. While this problem somewhat complicates the comparison of signal intensities within a given titration experiment (same organozinc compound with varying

LiCl concentrations), it does not affect the comparison between different systems (different organozinc compounds with the same LiCl concentration).

In the absence of LiCl, solutions of BuZnI in THF afforded only very small amounts of butylzincate anions upon anion-mode ESI mass spectrometry (Figure 6.1.1.A). Similar behavior is observed for BnZnBr (Figure 6.1.2) and PhZnBr (Figure 6.1.3). These findings indicate that spontaneous ionic disproportionation of RZnX in pure THF is not favorable.⁷⁵ In the case of BuZnI, the presence of the purely inorganic ZnI₃⁻ anion furthermore points to the occurrence of hydrolysis reactions.

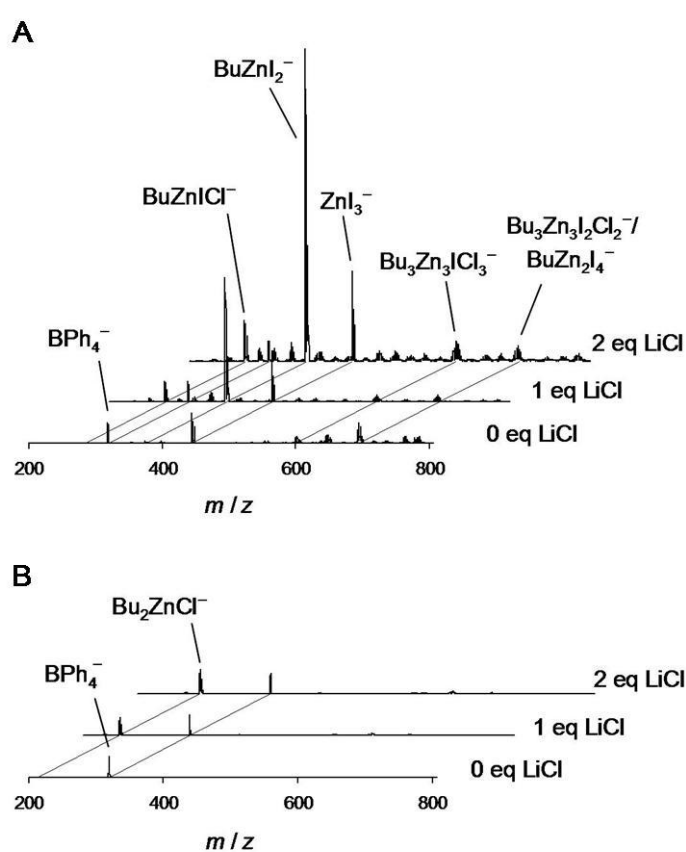


Figure 6.1.1. Anion-mode ESI mass spectra of 5 mM solutions of **A.** BuZnI/(LiCl)_n in THF ($n = 0\text{-}2$) measured with the TSQ 7000 instrument and **B.** Bu₂Zn/(LiCl)_n in THF ($n = 0\text{-}2$) measured with the HCT ion trap. The signal intensities were normalized to BPh₄⁻, whose sodium salt was added as an internal standard ($c = 20 \mu\text{M}$).

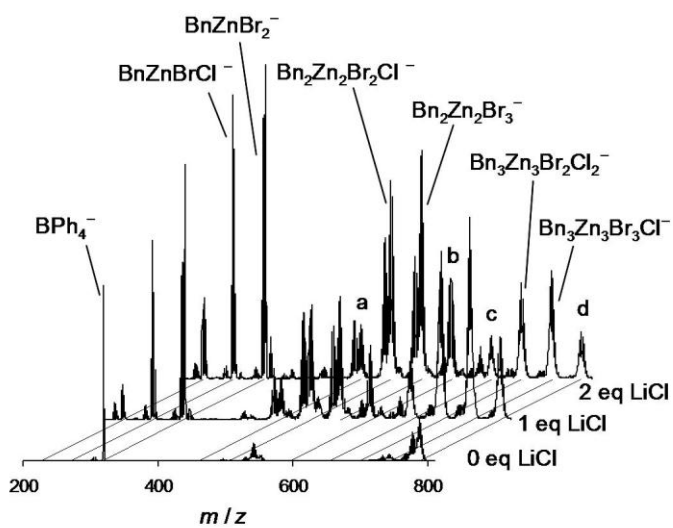


Figure 6.1.2. Anion-mode mode ESI mass spectra of 5 mM solutions of $\text{BnZnBr}/(\text{LiCl})_n$ in THF ($n = 0 - 2$) measured with the HCT ion trap, a = $\text{Bn}_2\text{Zn}_2\text{BrCl}_2^-$, b = $\text{LiBn}_2\text{Zn}_2\text{Br}_3\text{Cl}^-$, c = $\text{Bn}_3\text{Zn}_3\text{BrCl}_3^-$, and d = $\text{Bn}_3\text{Zn}_3\text{Br}_4^-$. The signals at $m/z = 535 - 551$ (0 eq LiCl) corresponded to $\text{BnZn}_2\text{Br}_4^-$. The signal intensities were normalized to BPh_4^- , whose sodium salt was added as an internal standard ($c = 20 \mu\text{M}$).

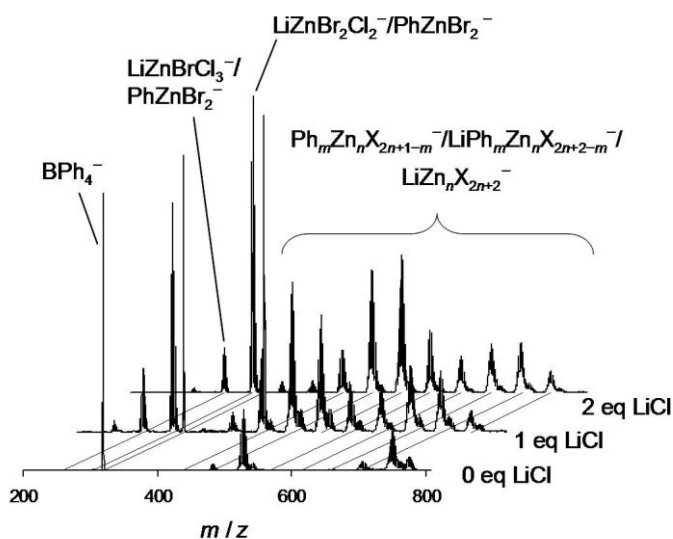
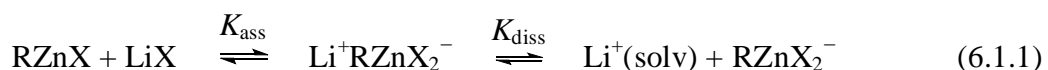


Figure 6.1.3. Anion-mode ESI mass spectra of 5 mM solutions of $\text{PhZnBr}/(\text{LiCl})_n$ in THF ($n = 0 - 2$) measured with the HCT ion trap. The signals at $m/z = 521 - 537$ and $m/z = 741 - 761$ (0 eq LiCl) corresponded to $\text{PhZn}_2\text{Br}_4^-$ and $\text{Ph}_2\text{Zn}_3\text{Br}_5^-$, respectively. The peaks at higher m/z ratios corresponded to a complex mixture of $\text{Ph}_m\text{Zn}_n\text{X}_{2n+1-m}^-/\text{LiPh}_m\text{Zn}_n\text{X}_{2n+2-m}^-/\text{LiZn}_n\text{X}_{2n+2}^-$ ($\text{X} = \text{Cl}$ and Br , $m = 1 - 3$, $n = 2$ and 3). The signal intensities were normalized to BPh_4^- , whose sodium salt was added as an internal standard ($c = 20 \mu\text{M}$).

Such hydrolysis reactions could not be completely avoided when introducing highly diluted solutions of moisture-sensitive organometallics into the ESI source of the mass spectrometer. Upon addition of one equivalent of LiCl, the butylzincate anion BuZnI_2^- appeared and further increased in intensity when a second equivalent of LiCl was added. Similarly, the presence of LiCl also resulted in increased signal intensities of organylzincate anions for BnZnBr and PhZnBr ; for the latter, the observed increase is rather small, however. For solutions of BuZnBr in DMI, Organ and collaborators also found higher ESI signal intensities of the butylzincate anion BuZnBr_2^- upon the addition of LiBr.⁹³

These experiments show that the formation of organylzincate anions directly correlated with the presence of LiCl. Thus, they are in accordance with the previous assumption that the LiCl adducts of organylzinc halides correspond to $\text{Li}^+\text{RZnX}_2^-$ complexes, which undergo heterolytic dissociation to a measurable extent (Eq. 6.1.1).



In line with this reasoning, cation-mode ESI of THF solutions of $\text{RZnX}\cdot\text{LiCl}$ afforded virtually exclusively solvated $\text{Li}(\text{THF})_n^+$ ions, $n = 2\text{--}4$.^{28a} The addition of LiCl not only leads to the formation of zincate complexes but presumably also gives rise to halide exchange reactions. Although the addition of two equivalents of LiCl resulted in a 100% excess of Cl^- compared to Br^- or I^- anions in the overall solution, respectively, the bromine- and iodine-rich complexes still predominated in the ESI mass spectra. This predominance is particularly pronounced in the case of the $\text{BuZnI}/(\text{LiCl})_2$ system, for which the signal intensity of BuZnI_2^- exceeded those of BuZnICl^- and BuZnCl_2^- ($m/z = 191/193/195$, off-scale in Figure 6.1.1.A) by factors of 5 and 50, respectively. A possible reason for these large differences might be deviating dissociation constants of the corresponding $\text{Li}^+\text{RZnX}_2^-$ complexes.^{28b}

Besides binding to Li^+ , the zincate anions can also attach to neutral RZnX , thus forming higher aggregates. Such higher aggregates of the general formula $\text{R}_n\text{Zn}_n\text{X}_{n+1}^-$, $n = 2$ and 3, were observed for all three systems $\text{BuZnI}/(\text{LiCl})_n$, $\text{BnZnBr}/(\text{LiCl})_n$, and $\text{PhZnBr}/(\text{LiCl})_n$. The identities of these polynuclear anions were confirmed by gas-phase fragmentations of the mass-selected ions (Table 6.1.1 for the most abundant species; also compare ref. 28).

Table 6.1.1. Fragmentation reactions of mass-selected organozincate anions.

parent ion ^a	<i>m/z</i>	ionic fragment ^{a,b}	<i>m/z</i>	neutral fragment ^a	Δm
$\text{Bu}_3^{64}\text{Zn}_2^{66}\text{ZnI}^{35}\text{Cl}^{37}\text{Cl}_2^-$	601	$\text{Bu}_2^{64}\text{Zn}^{66}\text{ZnI}^{37}\text{Cl}_2^-$ $\text{Bu}^{64}\text{Zn}^{66}\text{ZnI}^{35}\text{Cl}^{37}\text{Cl}_2^-$ $\text{Bu}_2^{64}\text{Zn}_2^{35}\text{Cl}^{37}\text{Cl}_2^-$ $\text{ZnI}^{35}\text{Cl}^{37}\text{Cl}_2^-$	445 423 351 263	$\text{Bu}^{64}\text{Zn}^{35}\text{Cl}$ $\text{Bu}_2^{64}\text{Zn}$ Bu^{66}ZnI $\text{Bu}_3^{66}\text{Zn}_2^{35}\text{Cl}$	156 178 250 338
$\text{Bu}_3^{64}\text{Zn}_2^{66}\text{ZnI}_2^{37}\text{Cl}_2^-$	693	$\text{Bu}^{64}\text{Zn}_2\text{I}_2^{37}\text{Cl}_2^-$ $\text{Bu}_2^{64}\text{Zn}^{66}\text{ZnI}^{37}\text{Cl}_2^-$ $^{64}\text{ZnI}_2^{37}\text{Cl}_2^-$ $^{64}\text{ZnI}^{37}\text{Cl}_2^-$	513 445 355 265	$\text{Bu}_2^{64}\text{Zn}$ Bu^{64}ZnI $\text{Bu}_3^{66}\text{Zn}_2^{37}\text{Cl}$ $\text{Bu}_3^{64}\text{Zn}^{66}\text{ZnI}$	180 248 338 428
$\text{Bn}^{64}\text{Zn}^{81}\text{Br}^{35}\text{Cl}^-$	271	$^{81}\text{Br}^-$	81	$\text{Bn}^{64}\text{Zn}^{35}\text{Cl}$	190
$\text{Bn}_2^{64}\text{Zn}^{66}\text{Zn}^{79}\text{Br}_2^{37}\text{Cl}^-$	507	$\text{Bn}^{66}\text{Zn}^{79}\text{Br}_2^-$ $^{64}\text{Zn}^{79}\text{Br}_2^{37}\text{Cl}^-$	315 259	$\text{BnZn}^{37}\text{Cl}$ $\text{Bn}_2^{66}\text{Zn}$	192 248
$\text{Bn}_2^{64}\text{Zn}^{66}\text{Zn}^{79}\text{Br}_2^{81}\text{Br}^-$	551	$^{66}\text{Zn}^{79}\text{Br}_2^{81}\text{Br}^-$	305	$\text{Bn}_2^{64}\text{Zn}$	246
$\text{Bn}_3^{64}\text{Zn}_2^{66}\text{Zn}^{81}\text{Br}_2^{35}\text{Cl}_2^-$	699	$\text{Bn}_2^{64}\text{Zn}_2^{81}\text{Br}_2^{35}\text{Cl}_2^-$ / $\text{Bn}^{64}\text{Zn}^{66}\text{Zn}^{81}\text{Br}_2^{35}\text{Cl}_2^-$ $^{64}\text{Zn}^{81}\text{Br}_2^{35}\text{Cl}_2^-$	507 453 261	$\text{Bn}^{66}\text{ZnCl}$ $\text{Bn}_2^{64}\text{Zn}$ $\text{Bn}_3^{64}\text{Zn}^{66}\text{ZnCl}$	192 246 438
$\text{Bn}_3^{64}\text{Zn}_2^{66}\text{Zn}^{79}\text{Br}^{81}\text{Br}_2^{37}\text{Cl}^-$	745	$\text{Bn}^{64}\text{Zn}_2^{79}\text{Br}^{81}\text{Br}_2^{37}\text{Cl}^-$	497	$\text{Bn}_2^{66}\text{Zn}$	248
$\text{Ph}^{64}\text{Zn}^{66}\text{Zn}^{79}\text{Br}_3^{81}\text{Br}^-$	525	$^{66}\text{Zn}^{79}\text{Br}_3^-$	303	$\text{Ph}^{64}\text{Zn}^{81}\text{Br}$	222
$\text{Ph}_2^{64}\text{Zn}^{66}\text{Zn}_2^{79}\text{Br}_3^{81}\text{Br}_2^-$	749	$^{66}\text{Zn}_2^{79}\text{Br}_3^{81}\text{Br}_2^-$	531	$\text{Ph}_2^{64}\text{Zn}^{\text{c}}$	218
$\text{Ph}_2^{64}\text{Zn}_2^{81}\text{Br}^{35}\text{Cl}_2^-/\text{Ph}^{64}\text{Zn}_2^{79}\text{Br}_2^{35}\text{Cl}_2^-/\text{Li}^{64}\text{Zn}_2^{79}\text{Br}_2^{35}\text{Cl}_3^{37}\text{Cl}^-/\text{Ph}^{64}\text{Zn}_2^{79}\text{Br}_2^{35}\text{Cl}_2^-/\text{Li}^{64}\text{Zn}_2^{79}\text{Br}_2^{35}\text{Cl}_4^-$	433	$^{64}\text{Zn}^{79}\text{Br}_2^{35}\text{Cl}^-$ $^{64}\text{Zn}^{81}\text{Br}^{35}\text{Cl}_2^-$	257 215	$\text{Ph}^{64}\text{Zn}^{35}\text{Cl}^-/\text{Li}^{64}\text{Zn}^{35}\text{Cl}_3$ $\text{Ph}_2^{64}\text{Zn}^{\text{c}}/\text{Li}^{64}\text{Zn}^{35}\text{Cl}_2^-$	176 218
$\text{Ph}_2^{64}\text{Zn}_2^{79}\text{Br}_2^{37}\text{Cl}^-/\text{Li}^{64}\text{Zn}^{66}\text{Zn}^{79}\text{Br}_2^{35}\text{Cl}_2^{37}\text{Cl}^-/\text{Li}^{64}\text{Zn}_2^{79}\text{Br}_2^{35}\text{Cl}_2^{37}\text{Cl}^-/\text{Li}^{64}\text{Zn}_2^{79}\text{Br}_2^{35}\text{Cl}_3^{37}\text{Cl}^-/\text{Ph}^{64}\text{Zn}^{66}\text{Zn}^{79}\text{Br}_2^{35}\text{Cl}^-$	477	$\text{Ph}^{64}\text{Zn}^{79}\text{Br}^{81}\text{Br}^-/\text{Li}^{64}\text{Zn}^{79}\text{Br}^{81}\text{Br}^{35}\text{Cl}_2^-/\text{Zn}^{79}\text{Br}_3^-$ $^{64}\text{Zn}^{79}\text{Br}_2^{37}\text{Cl}^-/\text{Li}^{64}\text{Zn}^{79}\text{Br}^{35}\text{Cl}_2^{37}\text{Cl}^-$ $^{64}\text{Zn}^{79}\text{Br}_2^{35}\text{Cl}_2^-$	301 259 213	$\text{Ph}^{64}\text{Zn}^{35}\text{Cl}^-/\text{Li}^{64}\text{Zn}^{35}\text{Cl}_3$ $\text{Ph}_2^{64}\text{Zn}^{\text{c}}/\text{Li}^{64}\text{Zn}^{35}\text{Cl}_2^-$ $^{7}\text{Li}^{64}\text{Zn}^{79}\text{Br}_2^{35}\text{Cl}^-$	176 218 264

^a Only one major isotopologue is given. In several cases, additional isotopologues will significantly contribute to the signal intensity of the observed ion. ^b For isotopic or isotopologue fragment ions, respectively, observed at neighboring *m/z* ratios only one major component is listed. ^c The complex mixtures generate the neutral fragment $\Delta m = 218$ amu, which largely corresponds to Ph_2Zn and thus is indicative of the presence of $\text{Ph}_2\text{Zn}_2\text{X}_3^-/\text{LiPh}_2\text{Zn}_2\text{X}_4^-$ ($\text{X} = \text{Cl}, \text{Br}$) in the mixture of isobaric parent ions.

While the relative signal intensities of the larger aggregates were rather low in the case of $\text{BuZnI}/(\text{LiCl})_n$, they were higher for $\text{BnZnBr}/(\text{LiCl})_n$ and $\text{PhZnBr}/(\text{LiCl})_n$. The present experiments alone could not clearly distinguish whether these different tendencies toward aggregation are caused by the organyl or the halide substituents. Previous studies comparing BuZnI/LiCl and $\text{BuZnCl}/\text{LiCl}$ as well as $\text{BnZnBr}/\text{LiCl}$ and $\text{BnZnCl}/\text{LiCl}$, however, suggested that the halide had the bigger effect on the aggregation behavior.²⁸

ESI Mass Spectrometry. $\text{Bu}_2\text{Zn}/(\text{LiCl})_n$. Next, $\text{Bu}_2\text{Zn}/(\text{LiCl})_n$ solutions in THF were analyzed by ESI mass spectrometry, which were prepared by adding n equivalents of a LiCl solution in THF and extra THF to Bu_2Zn . Without added LiCl, no zincate complexes were detected for solutions of Bu_2Zn in THF (Figure 6.1.1.B), indicating that, like in the case of BuZnI , spontaneous ionic disproportionation does not occur to a significant extent. In the presence of LiCl, the Bu_2ZnCl^- anion appeared but had a much lower normalized signal intensity than its $\text{BuZnI}_2^-/\text{BuZnICl}^-$ analogs observed for the $\text{BuZnI}/(\text{LiCl})_n$ system. This finding may be taken as a first indication that diorganylzinc compounds R_2Zn have lower tendencies to add halide anions and form ate complexes than the corresponding organylzinc halides RZnX . Another difference between $\text{Bu}_2\text{Zn}/(\text{LiCl})_n$ and $\text{BuZnI}/(\text{LiCl})_n$ refers to their aggregation tendencies. Whereas several polynuclear anions were detected for the latter (although in relatively low signal intensities), no analogous aggregates were visible for the former. This observation fully agrees with previous experiments on $\text{Bu}_2\text{Zn}/\text{LiCl}$ that was produced by transmetalation of ZnCl with two equivalents of BuLi ,^{28a} and shows that the obtained reagent was the same, irrespective of the way it was prepared. In the previous study, it is reasoned that a minimum number of halide substituents were needed for stabilizing polynuclear complexes by adopting bridging binding modes between different zinc centers.^{28b} In the meantime, Clyburne and coworkers had reported the crystal structure of $(\text{Ph}_4\text{P}^+)_2\text{Et}(\text{Cl})\text{Zn}(\mu\text{-Cl})_2\text{Zn}(\text{Cl})\text{Et}^{2-}$ and thus provided direct evidence for the inferred bridging binding geometry in polynuclear zincates.⁹⁴

ESI Mass Spectrometry. $\text{ZnX}_2/(\text{LiCl})_n$. For comparison, the purely inorganic systems $\text{ZnCl}_2/(\text{LiCl})_n$ and $\text{ZnBr}_2/(\text{LiCl})_n$ in THF were briefly considered. In the absence of LiCl, not much of the mononuclear zincates ZnCl_3^- and ZnBr_3^- were observed, but polynuclear complexes, $\text{Zn}_n\text{Cl}_{2n+1}^-$, $n = 2 - 5$, and $\text{Zn}_n\text{Br}_{2n+1}^-$, $n = 2$ and 3 (Figure 6.1.4.A and 6.1.4.B) were abundant. This predominance of higher aggregation states once more points to the effectiveness of chloride and bromide in bridging multiple zinc centers. Upon the addition of LiCl, the size distributions of the

zincates strongly shifted to smaller aggregates, with the mononuclear species becoming more prominent. Here, the added chloride ions apparently helps in breaking up the higher aggregates.⁹⁹ Therefore, it is somewhat surprising that with added LiCl the overall ESI signal intensities of the zincate ions seemed to decrease, thus being in marked contrast to the behavior observed for $\text{RZnX}/(\text{LiCl})_n$ and $\text{Bu}_2\text{ZnCl}/(\text{LiCl})_n$.

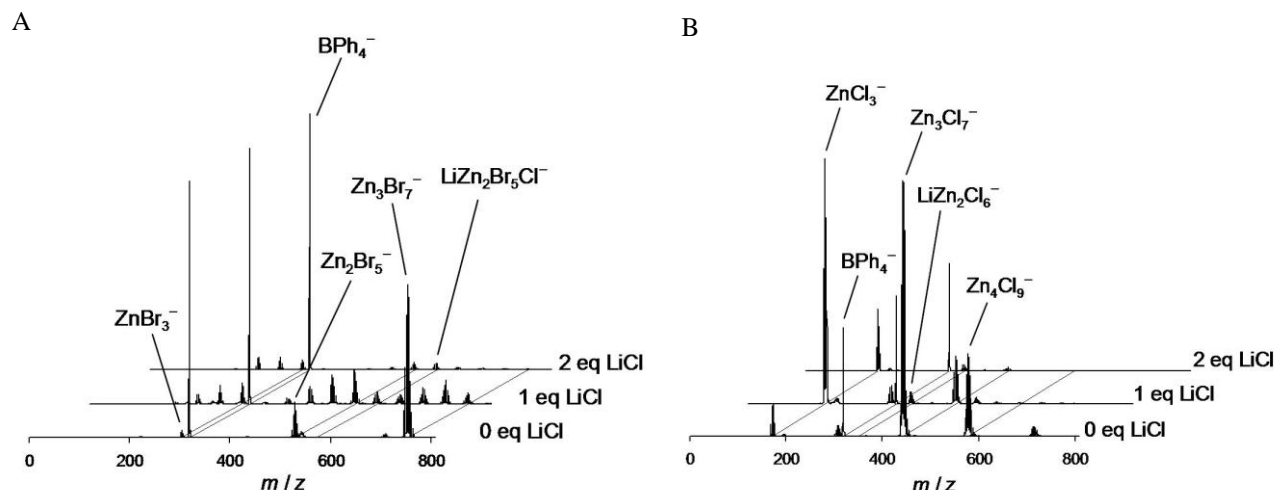


Figure 6.1.4.A: Anion-mode ESI mass spectra of 5 mM solutions of $\text{ZnBr}_2/(\text{LiCl})_n$ in THF ($n = 0 - 2$) measured with the HCT ion trap. The ions at $340 \leq m/z \leq 770$ (particularly prominent for 1 eq LiCl) corresponded to $\text{Zn}_m\text{Br}_n\text{Cl}_{2m+1-n}^-$, $m = 2$ and 3, $n = 2$ and 3. The signal intensities were normalized to BPh_4^- , whose sodium salt was added as an internal standard ($c = 20 \mu\text{M}$). **B:** Anion-mode ESI mass spectra of 5 mM solutions of $\text{ZnCl}_2/(\text{LiCl})_n$ in THF ($n = 0 - 2$) measured with the HCT ion trap. The signal intensities were normalized to BPh_4^- , whose sodium salt was added as an internal standard ($c = 20 \mu\text{M}$).

ESI Mass Spectrometry. Zincate Di-anions. As mentioned above, zinc(II) compounds may not only form mono-anionic, tricoordinated ate complexes, but also di-anionic, tetracoordinated zincates. In none of the present experiments, such di-anionic species were observed. This result does not exclude the presence of di-anionic zincates in solution, however. Estager et al. demonstrated that ESI mass spectrometry did not detect $\text{Zn}_n\text{Cl}_{2n+2}^{2-}$ anions present in ionic liquids.⁹⁶ This incapability is not surprising, as small di-anions were prone to undergo Coulomb fission in the gas-phase. While it therefore cannot be relied on ESI mass spectrometry for probing free zincate di-anions, this method can be used for detecting the corresponding Li^+ -paired

complexes. Indeed these species were observed, such as $\text{LiZn}_2\text{X}_6^-$ and $\text{LiPh}_2\text{Zn}_2\text{X}_4^-$ ($\text{X} = \text{Cl}$ and Br) in some cases (Figures 6.1.3, Table 6.1.1 entry 11, 6.1.4.A, and 6.1.4.B). Similarly, Organ and collaborators found related LiBuZnBr_3^- and LiZnBr_4^- complexes in THF/DMI solutions of $\text{BuZnBr}/(\text{LiBr})_2$.⁹³ These results suggest that $(\text{Li}^+)_2\text{ZnX}_4^{2-}$, $(\text{Li}^+)_2\text{PhZnX}_3^{2-}$, $(\text{Li}^+)_2\text{BuZnX}_3^{2-}$, and analogous higher aggregates can form as intermediates in THF or THF/DMI solutions. However, the rather low signal intensities of Li^+ -paired dianions⁹³ indicate that tetracoordinated zincates presumably constitute only relatively minor components of the equilibria operative under the given conditions.

Conductivity Measurements. $\text{RZnX}/(\text{LiCl})_n$. Measurements of the electrical conductivity ideally complement ESI mass-spectrometric experiments because both methods probe the charged components present in solution. Solutions of pure BuZnX ($\text{X} = \text{Cl}, \text{Br}, \text{I}$) as well as BnZnBr and PhZnBr in THF, prepared as mentioned above, were diluted to a concentration of $c \approx 157 \text{ mM}$ and showed only very low specific conductivities at 258 K (Figures 6.1.5 and 6.1.6, respectively). This finding is in full accordance with the low ion yields observed in the ESI mass-spectrometric experiments of solutions of these reagents (see above). Note that for the case of BuZnI similarly low specific conductivities were measured irrespective of the way how it was prepared (by mixing Bu_2Zn with ZnI_2 or by Zn insertion into BuI). In the presence of n equivalents of LiCl ($n = 0.5, 1, 2$), the specific conductivities of the RZnX reagents drastically increased. This increase again fully matches the behavior observed by ESI mass spectrometry and the inferred formation of lithium butylzincate complexes, which undergo partial heterolytic dissociation according to Eq. 6.1.1. Control experiments, in agreement with the literature,¹⁰⁰ showed that solutions of pure LiCl and LiBr in THF displayed only very low specific conductivities; the conductivity of LiI was higher but still well below that of $\text{BuZnI}\cdot\text{LiCl}$ (Figure 6.1.5). Thus, the steep increase in conductivity observed upon addition of LiCl apparently indeed reflects the formation of lithium organylzincate complexes.

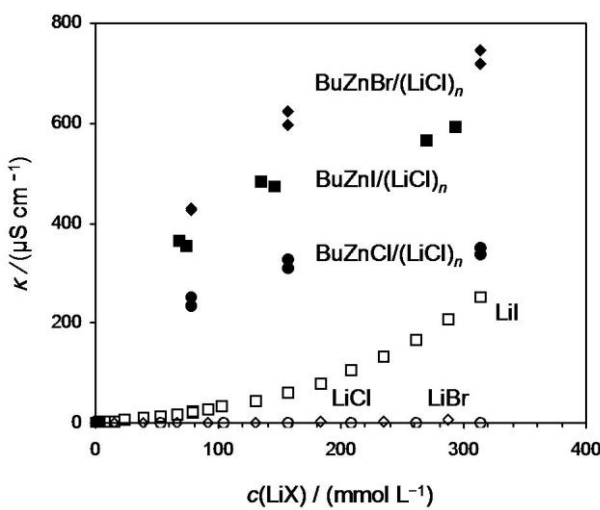


Figure 6.1.5. Specific conductivities of $\text{BuZnX}/(\text{LiCl})_n$ (filled symbols, X = Cl (circles), Br (diamonds), I (squares), $c \approx 157 \text{ mM}$, $T = 258 \text{ K}$) in THF as functions of $c(\text{LiX})$, X = Cl. In the absence of LiCl, specific conductivities $\kappa < 7 \mu\text{S cm}^{-1}$ of BuZnX were measured. The open symbols represent the specific conductivities of pure LiX (X = Cl (circles), Br (diamonds), I (squares)), shown for comparison.

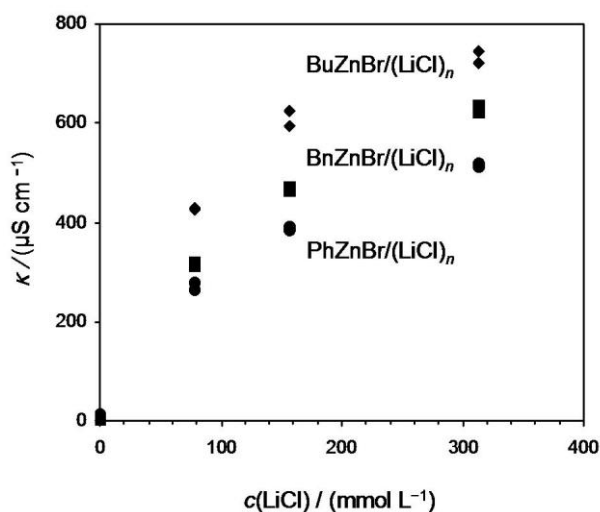


Figure 6.1.6. Specific conductivities of $\text{RZnBr}/(\text{LiCl})_n$ ($\text{R} = \text{Bn}$ (squares), Ph (circle), $c \approx 157 \text{ mM}$, $T = 258 \text{ K}$) in THF as functions of $c(\text{LiCl})$. In the absence of LiCl, specific conductivities $\kappa < 14 \mu\text{S cm}^{-1}$ were measured. For comparison, the specific conductivity of $\text{BuZnBr}/(\text{LiCl})_n$ (diamonds) in THF is also shown.

While the individual systems $RZnX/(LiCl)_n$, $X = Br$ and I , all exhibited very similar trends, their $BuZnCl/(LiCl)_n$ counterpart showed somewhat lower specific conductivities. As already inferred from the ESI mass spectrometry experiments, the $Li^+BuZnCl_2^-$ complex appears to have a lower dissociation constant. Presumably, the hard Li^+ cation interacts more strongly with the relatively small Cl atoms in the $BuZnCl_2^-$ anion than with the larger Br or I atoms of the other zincate anions.^{28b,101} The $BuZnCl/(LiCl)_n$ system is also special in that here no complicating halide exchange reactions could occur. Thus, it offers itself to a more detailed analysis. The measured specific conductivity clearly leveled off after the addition of one equivalent of LiCl, indicating that almost all of the $BuZnCl$ was transformed to $Li^+BuZnCl_2^-$. This finding suggests an appreciable association constant K_{ass} . The fact that the conductivity hardly further increased when a second equivalent of LiCl was added moreover contradicts the formation of significant amounts of $BuZnCl_3^{2-}$ di-anions. For fitting the experimental data, the dependence of the conductivity on the concentration of the electrolyte must be known. This relation would be straightforward if only simple dissociation processes according to Eq. 6.1.1 occurred, but become much more complex if the ions form higher aggregates. In the case of the organozincates, both the ESI mass spectrometric experiments and the conductivity measurements point to the occurrence of such processes to a certain, yet unknown extent. A reliable quantitative analysis of the measured data for the $BuZnCl/(LiCl)_n$ system thus seems impossible.

For the $Li^+BuZnICl^-$ system, the concentration dependence of the molar conductivity Λ was also studied. Starting at very low concentrations, the molar conductivity first declined with increasing concentration because ion pairing became more important (Figure 6.1.7). Interestingly, the molar conductivity then passed through a minimum and increased at higher concentrations. Two factors may cause this increase: (i) At higher concentration, the law of mass action favors the association of $BuZnI$ and $LiCl$ to produce the active electrolyte $Li^+BuZnICl^-$. (ii) With increasing concentration, the $BuZnICl^-$ ions can form so-called triple ions, i.e., larger ionic aggregates, which then contribute to the molar conductivity.¹⁰²

To separate these two factors, an effective molar conductivity Λ_{eff} is considered based on the concentration of the active electrolyte $Li^+BuZnICl^-$, Eq. 6.1.2.

$$\Lambda_{eff} = \kappa / [Li^+BuZnICl^-] \quad (6.1.2)$$

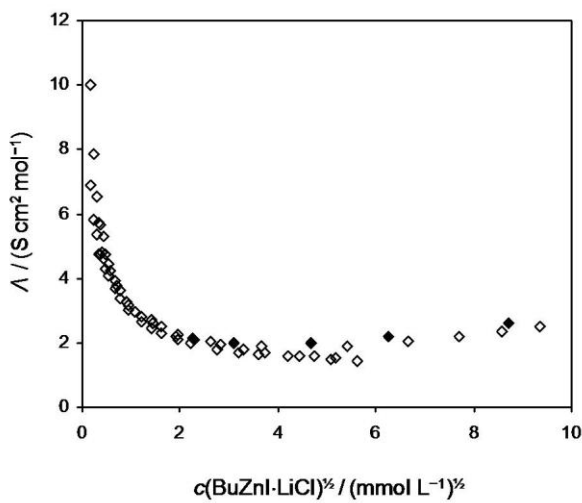
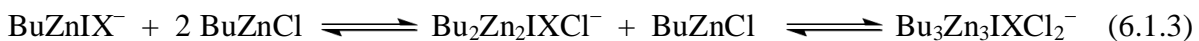


Figure 6.1.7. Concentration dependence of the molar conductivity of $\text{BuZnI}\cdot\text{LiCl}$ ($T = 258$ K) in THF. The open symbols represented data points obtained from titration experiments, for which the extent of hydrolysis could not be rigorously controlled. The filled symbols represented data points obtained from measurements at fixed concentrations, for which hydrolysis could be almost completely excluded (see Experimental Section for details). Activity coefficients were neglected.

For calculating the actual concentration of $\text{Li}^+\text{BuZnCl}_2^-$, its formation constant K_{ass} was approximated by that of $\text{Li}^+\text{BuZnCl}_2^-$, for which a value of $K_{\text{ass}}(\text{Li}^+\text{BuZnCl}_2^-) \approx 100 \text{ L mol}^{-1}$ was derived from the ^1H NMR spectroscopic studies (see below). The resulting Λ_{eff} curve still shows a minimum, which is very shallow, though. This minimum is interpreted as evidence for the formation of zincate ions in higher aggregation states. Independent support for the presence of such complexes is provided by the ESI MS experiments, which detected $\text{Bu}_3\text{Zn}_3\text{I}_n\text{Cl}_{4-n}^-$ complexes, $n = 1$ and 2 (see above). These species could be formed by the successive reaction of BuZnIX^- with two molecules of BuZnCl , Eq. 6.1.3 with $\text{X} = \text{Cl}$ and I .



Conductivity Measurements. $\text{Bu}_2\text{Zn}/(\text{LiCl})_n$. Furthermore solutions of Bu_2Zn in THF exhibited very low specific conductivities at 258 K (Figure 6.1.8.A). Upon the addition of LiCl, the conductivity increased, but much less than for the BuZnCl system. Three different factors may account for this deviating behavior: (i) The limiting molar conductivity of Bu_2ZnCl^- might be lower than that of BuZnCl_2^- . However, it seems very unlikely that this difference can be sufficiently large

to cause the observed effect. (ii) The dissociation constant of $\text{Li}^+\text{Bu}_2\text{ZnCl}^-$ may be lower than that of $\text{Li}^+\text{BuZnCl}_2^-$. Given that the ESI mass-spectrometric experiments point to a reduced aggregation tendency of the Bu_2ZnCl^- ion (see above), this rationalization does not seem plausible either. (iii) The equilibrium constant for the association of Bu_2Zn and LiCl could be lower than that for the association of BuZnCl and LiCl . In line with this explanation, the specific conductivity of the $\text{Bu}_2\text{Zn}/(\text{LiCl})_n$ system did not level off after the addition of the first equivalent of LiCl but instead continued to rise almost linearly (Figure 6.1.8.A). This behavior provides clear evidence for the relatively low affinity of Bu_2Zn toward chloride ions and thus supports the interpretation of the ESI mass-spectrometric results.

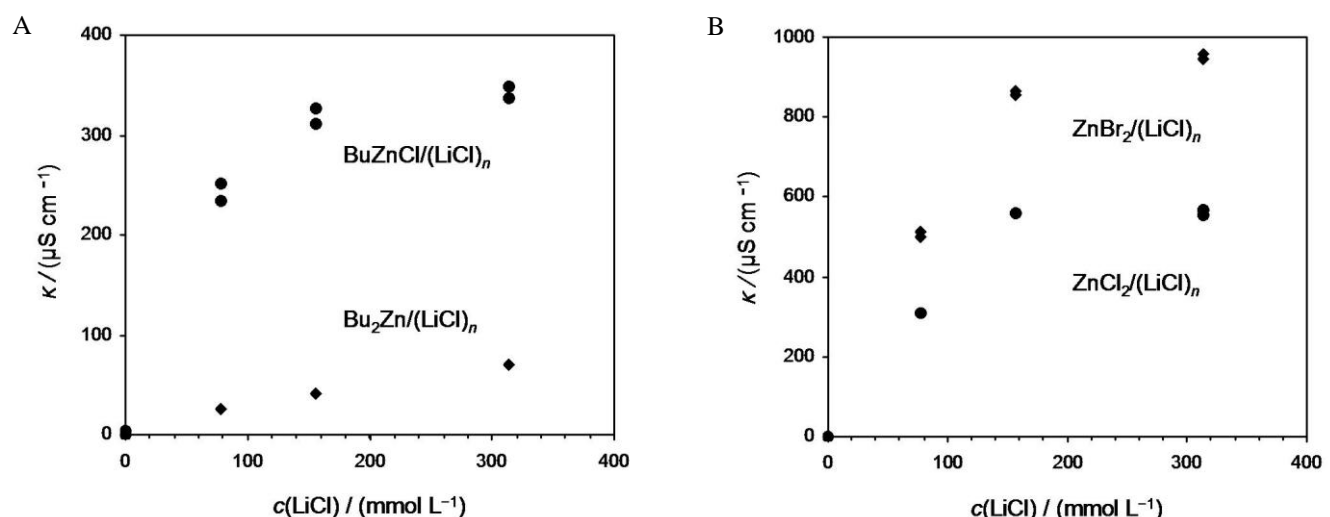


Figure 6.1.8.A. Specific conductivities of $\text{Bu}_2\text{Zn}/(\text{LiCl})_n$ ($c \approx 157 \text{ mM}$, $T = 258 \text{ K}$) in THF as functions of $c(\text{LiCl})$. For comparison, the specific conductivity of $\text{BuZnCl}/(\text{LiCl})_n$ in THF was also shown. **B.** Specific conductivities of $\text{ZnBr}_2/(\text{LiCl})_n$ and $\text{ZnCl}_2/(\text{LiCl})_n$ ($c \approx 157 \text{ mM}$, $T = 258 \text{ K}$) in THF as function of $c(\text{LiCl})$.

Conductivity Measurements. $\text{ZnX}_2/(\text{LiCl})_n$. The specific conductivities of ZnCl_2 and ZnBr_2 in THF at 258 K were scanned and were again very low but strongly increased upon the addition of LiCl and then leveled off (Figures 6.1.8.B). In the case of $\text{ZnCl}_2/(\text{LiCl})_n$, a plateau was already reached when exactly one equivalent of LiCl was added. This finding indicates a particularly high association constant for $\text{Li}^+\text{ZnCl}_3^-$ (higher than for $\text{Li}^+\text{ZnBr}_3^-$ and $\text{Li}^+\text{RZnX}_2^-$). Moreover, the observed saturation after the addition of one equivalent of LiCl strongly suggests the absence of ZnCl_4^{2-} dianions, in contrast to the situation found for ZnCl_2 -containing ionic liquids.⁹⁶

In the present experiments, the abundant Lewis-basic THF molecules presumably prevent further chloride anions from binding to the ZnCl_3^- complexes.¹⁰³ With respect to the heterolytic dissociation of the inorganic lithium zincates, the higher conductivities measured for the $\text{ZnBr}_2/(\text{LiCl})_n$ system point to a more facile dissociation of the bromide-containing species. Thus, the inorganic $\text{Li}^+\text{ZnX}_3^-$ complexes mimic the behavior of their $\text{Li}^+\text{BuZnX}_2^-$ counterparts.

NMR Spectroscopy. $\text{BuZnX}/(\text{LiCl})_n$. In a careful study on lithium tri- and tetramethylzincate complexes, Uchiyama et al.¹⁰⁴ found the ^1H NMR signals of these species to display large upfield shifts in comparison to simple $(\text{CH}_3)_2\text{Zn}$. These upfield shifts correlated with the enhanced nucleophilic reactivity of $\text{LiZn}(\text{CH}_3)_3$ and, particularly, $\text{Li}_2\text{Zn}(\text{CH}_3)_4$ relative to $(\text{CH}_3)_2\text{Zn}$.¹⁰⁴ The chemical shift of the α -H atoms thus apparently formed a sensitive probe of the electronic character of organozinc compounds and should also provide insight into the interaction of BuZnX with LiCl (for experimental details see Chapter 3). In the absence of LiCl , the α -H atoms in BuZnCl , BuZnBr , and BuZnI exhibited quite similar chemical shifts (Table 6.1.2). For the latter, it did not make any difference whether it was prepared by mixing Bu_2Zn with ZnI_2 or by Zn insertion into BuI , indicating that both samples are identical.

Table 6.1.2. ^1H NMR shifts of the α -H atoms of butylzinc reagents in $\text{THF}-\text{D}_8$ at 296 K.

Butylzinc species	$\delta(\alpha\text{-H})$ in ppm
BuZnCl	0.21
BuZnBr	0.23
BuZnI^a	0.24
BuZnI^b	0.24
Bu_2Zn	0.14
$\text{Li}^+\text{BuZnCl}_2^-$	0.08 ± 0.01^c

^aPrepared from $\text{Bu}_2\text{Zn}/\text{ZnI}_2$. ^bPrepared by Zn insertion. ^cDerived from fit.

Upon the addition of one equivalent of LiCl , the absorption of the α -H atoms in BuZnCl shifted upfield while the absorptions of the H atoms further away from the Zn center hardly changed (Figure 6.1.9). This behavior points to a specific interaction of LiCl with the Zn center and thus is fully in line with the inferred formation of a $\text{Li}^+\text{BuZnCl}_2^-$ complex.

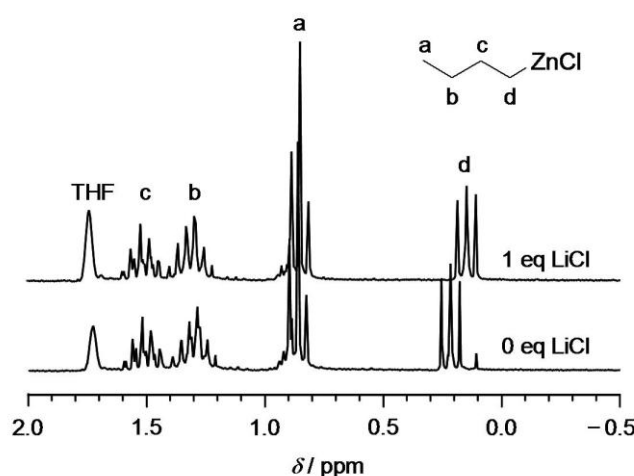


Figure 6.1.9. ¹H NMR spectrum of a solution of BuZnCl ($c \approx 40$ mM) in THF-D₈ with and without the addition of 1 equivalent of LiCl ($T = 296$ K). The signal at $\delta 0.10$ ppm (0 eq LiCl) resulted from a contamination with silicon grease.

The upfield shift observed for the α -H atoms demonstrates that the zincate species indeed exhibited a higher electron density than simple BuZnCl. Solutions of BuZnBr/(LiCl)_n and BuZnI/(LiCl)_n behaved in a completely analogous fashion. Organ and collaborators also found a very similar behavior for BuZnBr/(LiBr)_n in THF/DMI.⁹³

At higher LiCl concentrations, the chemical shifts of the α -H atoms moved further upfield and finally levelled off (Figure 6.1.10). This behavior fully matches the results from the conductivity measurements and confirmed the hypothesis that exactly one equivalent of LiCl reacts with BuZnX to produce $\text{Li}^+\text{BuZnXCl}^-$; higher adducts, such as $(\text{Li}^+)_2\text{BuZnXCl}_2^-$, apparently did not form to a significant extent in the sampled concentration range. The fact that only one averaged signal was observed for the α -H atoms furthermore indicates that the interconversion between BuZnX and $\text{Li}^+\text{BuZnXCl}^-$ occurred fast on the NMR time scale. Lowering the temperature to 193 K did not resolve the individual NMR shifts of the two components either.

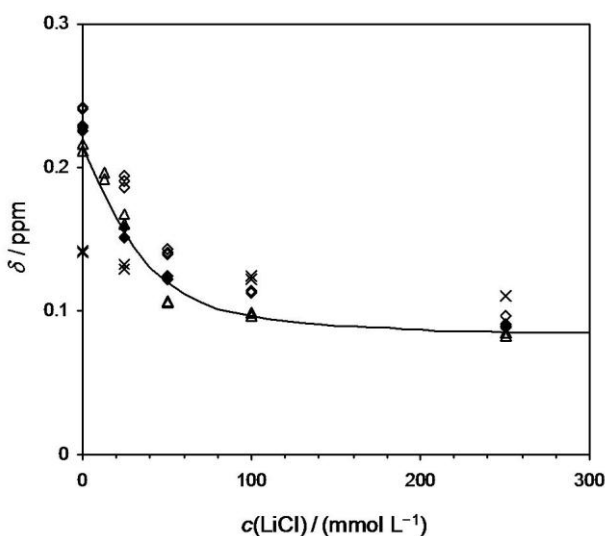


Figure 6.1.10. ^1H NMR shifts of the α -protons of $\text{BuZnX}/(\text{LiCl})_n$ ($\text{X} = \text{Cl}$ (open triangles), Br (filled diamonds), I (open diamonds), $c \approx 40 \text{ mM}$, $T = 296 \text{ K}$) and of $\text{BuZn}_2/(\text{LiCl})_n$ (crosses), $c \approx 40 \text{ mM}$, $T = 296 \text{ K}$) in THF-D_8 as functions of $c(\text{LiCl})$. The solid line represented a fit of the $\text{BuZnCl}/(\text{LiCl})_n$ shifts based on an association constant of $K_{\text{ass}} = 113 \text{ L mol}^{-1}$.

For a quantitative analysis, it is focused on the $\text{BuZnCl}/(\text{LiCl})_n$ system to avoid complications by X/Cl exchange processes. The simplified model only takes into account the reaction of LiCl with BuZnCl according to Eq. 6.1.1 with $\text{X} = \text{Cl}$ and neglects the formation of higher aggregates.¹⁰⁵ Thus it is assumed that the measured chemical shift corresponds to the average of the shifts of BuZnCl and $\text{Li}^+\text{BuZnCl}_2^-$ weighted according to their concentrations. The shift of the former was directly observable (Table 6.1.2) whereas that of the latter could be obtained by fitting the experimental data on the basis of the law of mass action as well as the association constant K_{ass} . The best fit obtained reproduced the experiment reasonably well (Figure 6.1.10) and afforded an association constant of $K_{\text{ass}} = 113^{+90}_{-40} \text{ L mol}^{-1}$. This finding implies that at synthetically relevant concentrations the equilibrium favors the formation of the $\text{Li}^+\text{BuZnXCl}_2^-$ complex. The analogous trends observed for $\text{BuZnBr}/(\text{LiCl})_n$ and $\text{BuZnI}/(\text{LiCl})_n$ suggest a very similar behavior of these systems. In the case of $\text{BuZnI}/(\text{LiCl})_n$ the effect of varying BuZnI concentrations was also investigated and it was found that the more concentrated samples required higher amounts of LiCl to reach the full upfield shift of the α -H atoms (Figure 6.1.11). This observation provides further evidence for the formation of specific 1:1 adducts of BuZnX and LiCl ($\text{X} = \text{I}, \text{Cl}$).

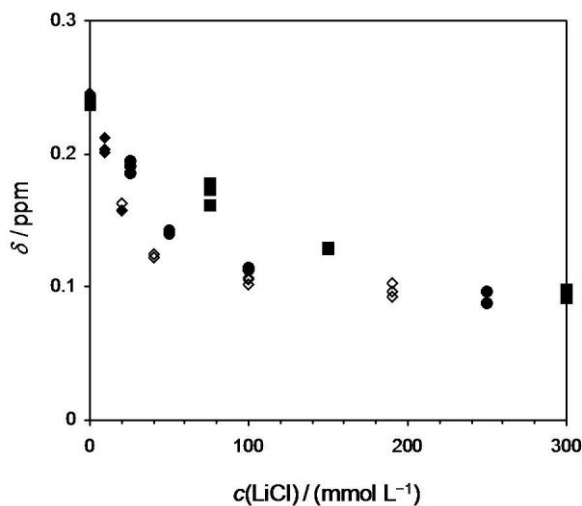


Figure 6.1.11. ^1H -NMR shift of the α -H atoms of $\text{BuZnI}/(\text{LiCl})_n$ in THF-D_8 as functions of $c(\text{LiCl})$. Data for three different concentrations of BuZnI ($c \approx 120 \text{ mM}$ (squares), $c \approx 35 \text{ mM}$ (circles), $c \approx 12 \text{ mM}$ (diamond symbols) $T = 296 \text{ K}$) were shown. Open symbols represented chemical shifts measured for samples with $> 25\%$ hydrolysis and were considered less reliable.

Further ^1H -NMR experiments were employed to probe the active BuZnX ($X = \text{Cl}, \text{I}$) in the presence of MgCl_2 salts. For $\text{BuZnX}/(\text{MgX}_2)_{0.5}$, $X = \text{Cl}$ and Cl/I upfield shifts of $\Delta\delta \leq 0.03 \text{ ppm}$ relative to simple BuZnCl and BuZnI were observed. It thus appears that MgCl_2 salts, though forming adducts with alkylzinc halides in some cases,¹⁰⁶ influence the electronic properties less strongly than the LiX salts.

In addition to ^1H NMR spectroscopy, ^{13}C and ^7Li NMR spectroscopy were also considered as possible tools to characterize the complexation of BuZnX by LiCl . With increasing LiCl concentration, the shifts of the α -C atoms of BuZnCl and BuZnBr moved slightly downfield, thus opposing the behavior of the α -H atoms (Table 6.1.3). This results may at first sight appear surprising because both the α -C and the α -H atoms supposedly experienced similar local electronic environments and might therefore be expected to display parallel trends in their NMR absorbances. However, an analysis of the relatively few available NMR data of organozinc compounds reported in the literature showed that opposing trends for ^1H and ^{13}C NMR shifts are actually the rule rather than the exception for these species.^{107,108} ^7Li NMR spectroscopy of solutions of LiCl in THF-D_8 at room temperature found a rather small upfield shift of the ^7Li signal from 0.38 to -0.05 ppm upon the addition of one equivalent of BuZnCl .

Table 6.1.3. ^{13}C NMR shifts of the α -C atoms of organozinc reagents in THF–D₈.

organozinc species	<i>n</i> equivalents of LiCl	$\delta(\alpha\text{-C})/\text{ppm}$	$\delta(\alpha\text{-C})/\text{ppm}$
		at 296 K	at 193 K
BuZnCl	0	8.38	8.30
	1	10.31	9.89
	5	10.94	11.43
BuZnBr	0	9.71	-
	1	11.35	-
Bu ₂ Zn	0	13.33	-
	1	13.85	-

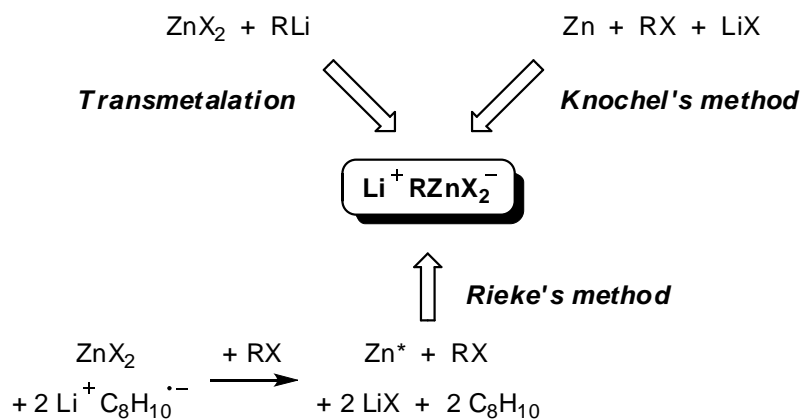
NMR Spectroscopy. Bu₂Zn/(LiCl)_n. Compared to BuZnX, Bu₂Zn showed an upfield shift of its α -H atoms (Table 6.1.2), which reflects the enhanced electron density at the metal center and agrees with the well-known higher nucleophilic reactivity of diorganozinc compounds.⁵⁵ Upon treatment with LiCl, the signal of the α -H atoms of Bu₂Zn very slightly moved upfield. Unlike the case of BuZnX/(LiCl)_n, a saturation at a high excess of LiCl was not observed (Figure 6.1.10). Instead a continuous, though very small upfield shift was found. This behavior indicates a lower tendency of Bu₂Zn to add LiCl and form an ate complex, thus being fully in line with the ESI mass-spectrometric and conductometric findings.

^{13}C NMR spectroscopy of Bu₂Zn measured an absorption of the α -C atom that was shifted downfield relative to BuZnX (Table 6.1.3), thus contrasting the trend in the corresponding ^1H NMR spectra. Organ and collaborators reported analogous opposing shifts of the ^1H and ^{13}C signals of BuZnBr and Bu₂Zn in THF/DMI.⁹³ Obviously, this finding is another example of the above discussed contrasting trends in ^1H and ^{13}C NMR spectroscopy of organozinc compounds. The addition of one equivalent of LiCl resulted in a further downfield shift of the α -C atom of Bu₂Zn. This behavior resembles that of BuZnX/(LiCl)_n, but the magnitude of the effect is smaller. This finding is interpreted as additional evidence of the lower tendency of Bu₂Zn toward complexation by LiCl.

Conclusion

Using a combination of ESI mass spectrometry, electrical conductivity measurements, and NMR spectroscopy, consistent evidence has been obtained that the action of LiCl on organylzinc halides $RZnX$ ($X = Cl, Br, I$) in THF leads to the formation of lithium organozincate complexes $Li^+RZnXCl^-$ and the corresponding $Li^+RZnX_2^-$ species resulting from halide-exchange. These complexes can further undergo heterolytic dissociation to afford free $Li^+(solv)$ and $RZnXCl^-/RZnX_2^-$ ions. At higher concentrations, evidence was found for the presence of polynuclear organozincate ions $R_nZn_nX_{n+1}^-$. In the case of $R = Ph$, ESI mass spectrometry furthermore detected small amounts of $LiR_2Zn_2X_4^-$, which can be considered as the Li^+ adduct of an $R_2Zn_2X_4^{2-}$ di-anion. This observation indicates that the formation of Li^+ -paired organozincate dianions in THF solutions in principle may be feasible. The conductometric and NMR spectroscopic results showed that such reactions only occur to a very low extent, however, if ≤ 2 equivalents of LiX are added.

Analogous experiments on $Bu_2Zn/(LiCl)_n$ point to a significantly decreased tendency of diorganylzinc compounds to add halide anions and form the corresponding zincate complexes. This finding fully explains why LiCl does not activate iPr_2Zn in iodine-zinc exchange reactions.⁹⁵ In contrast, the inorganic zinc halides $ZnCl_2$ and $ZnBr_2$ very readily formed zincate anions in the presence of LiCl. As the ESI mass-spectrometric measurements demonstrate, these species also easily gave polynuclear aggregates, unlike Bu_2Zn . The different behavior of ZnX_2 , $RZnX$, and R_2Zn directly correlates with their Lewis acidities. Due to the electronegativity of the halogen atoms, ZnX_2 has an enhanced Lewis acidity and very easily adds X^- and ZnX_3^- anions to form mono- and polynuclear zincate complexes, respectively. Substitution of one halogen by a less electronegative organyl group reduces the Lewis acidity of the resulting $RZnX$. Therefore, these species show a somewhat decreased affinity toward X^- and $ZnRX_2^-$ anions. Finally, the Lewis acidity of R_2Zn was lowered to such an extent that complexation reactions became unfavorable. Note again that these findings are supported by three different, independent analytical methods. The good agreement between ESI mass spectrometry and electrical conductivity measurements as well as NMR spectroscopy suggests that the former technique indeed is well suitable for probing ion speciation in solution. The inferred facile complexation of $RZnX$ with LiX has far-reaching implications for organozinc chemistry.



Scheme 6.1.1. Common methods for the synthesis of organozinc halides RZnX involving LiX and thus giving rise to the in situ formation of lithium organozincates.

The association constant of $K_{\text{ass}} \approx 100 \text{ L mol}^{-1}$ derived for $\text{Li}^+ \text{BuZnCl}_2^-$ suggests that at synthetically relevant concentrations the lithium organozincate complex predominat.

The most common synthetic routes to organylzinc halides, i.e., transmetalation of ZnX_2 with RLi , Knochel's LiCl -mediated Zn insertion into RX as well as the insertion of Rieke Zn into RX, all involve stoichiometric amounts of LiX . It is therefore concluded that the supposedly formed RZnX species in reality largely correspond to lithium organozincates $\text{Li}^+ \text{RZnX}_2^-$ (Scheme 6.1.1). The reactivities of the latter most likely differed from those of simple RZnX species and thus explained the pronounced effects of LiX in organozinc chemistry. The described effect of LiX salts plays an important role not only in organozinc chemistry, but in magnesium chemistry, too.^{109,110}

6.2 Comparison of Lithium Organozincate Complexes with $i\text{PrMgCl}/(\text{LiCl})_n$

Introduction

In Chapter 6.1 the importance of investigations of LiX salts effects on the reactivity of organozinc halides and diorganozinc compounds is shown. Combined analytical methods, such as ESI mass spectrometry, electrical conductivity and NMR spectroscopy were applied and the achieved results consistently pointed to the formation of lithium organozincates $\text{Li}^+\text{RZnX}_2^-$. Recently, Knochel and co-workers reported that the halogen-magnesium exchange reactions using Mg and stoichiometric amounts of LiCl allowed an efficient preparation of organomagnesium reagents.¹⁰⁹ With the development of $i\text{PrMgCl}/\text{LiCl}$ the general preparation of organomagnesium reagents starting from aromatic and heteroaromatic bromides was possible.¹¹⁰ The group demonstrated with these results the promoter effect of LiCl in the Br/Mg exchange reaction.^{109,110} The promoting influence of LiCl on the latter reaction is comparable with the one of LiCl on organozinc species discussed in Chapter 6.1. To make a comparison between the behavior of organozinc halides and organomagnesium halides in the presence of LiCl , the investigation of the $i\text{PrMgCl}/\text{LiCl}$ system via ESI mass spectroscopy, electrical conductivity and NMR spectroscopy was started.

Results and Discussion

Conductivity Measurements. Measurements of the electrical conductivity of solutions of pure $i\text{PrMgCl}$ in THF showed only very low specific conductivities at 258 K (Figure 6.2.1).¹¹¹ In the presence of LiCl , the specific conductivities of the $i\text{PrMgCl}$ reagents drastically increased. Control experiments, in agreement with the literature,¹⁰⁰ showed that solutions of LiCl in THF displayed only very low specific conductivities (Figure 6.1.5). Thus, the increase in conductivity observed upon addition of LiCl apparently reflects the formation of ionized complexes. The conductivity of the $i\text{PrMgCl}/(\text{LiCl})_n$ reagents increased almost linearly in comparison to the $\text{BuZnCl}/(\text{LiCl})_n$ system, whose measured conductivity clearly levelled off after the addition of one equivalent of LiCl , indicating that almost all of the BuZnCl was transformed to $\text{Li}^+\text{BuZnCl}_2^-$. Experiments on the $i\text{PrMgCl}/(\text{LiCl})_n$ system at elevated temperatures (298 K) showed the expected increase of the conductivity (Figure 6.1.5). The general increase of the measured conductivities upon addition of LiCl probably points to the formation of magnesate complexes.

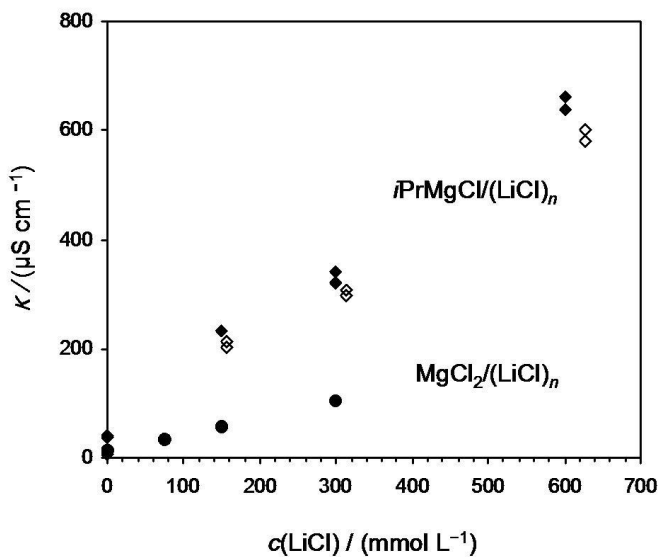
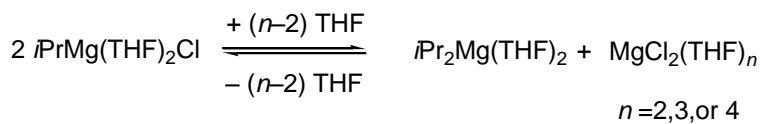


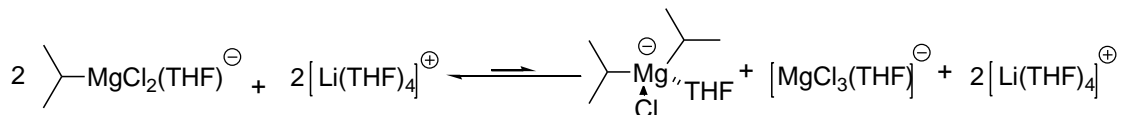
Figure 6.2.1. Specific conductivities of $i\text{PrMgCl}/(\text{LiCl})_n$ ($c \approx 300 \text{ mM}$, $T = 298 \text{ K}$ (filled diamonds) and $c \approx 313 \text{ mM}$, $T = 258 \text{ K}$ (open diamonds) in THF as functions of $c(\text{LiCl})$. In the absence of LiCl, specific conductivities $\kappa < 12 \mu\text{S cm}^{-1}$ at 258 K were measured. For comparison, the specific conductivity of $\text{MgCl}_2/(\text{LiCl})_n$ in THF ($c \approx 150 \text{ mM}$, $T = 298 \text{ K}$ (circles) is also shown.

This observation confirms the suggestions of the Knochel group that the $i\text{PrMgCl}/\text{LiCl}$ complex exhibited an ionic structure.¹¹² They speculated that the high reactivity of this reagent, in comparison to $i\text{PrMgCl}$ (see basic Schlenk equilibrium of $i\text{PrMgCl}$, Scheme 6.2.1.A), was due to the magnesate character of $i\text{PrMgCl}/\text{LiCl}$ in THF (see anionic Schlenk equilibrium of $i\text{PrMgCl}$, Scheme 6.2.1.B).^{110b} Their quantum chemical model calculations of halogen-metal exchange reactions predicted that the energy of the reaction barrier decreased with increased electronic saturation at the magnesium center. To increase the effective negative charge at the magnesium center through separation of the lithium cation from the magnesate anion they used chelating ethers. The employed Li^+ selective 12-crown-4 ether had no strong effect and therefore only a small rate enhancement was observed, but this result indicated that $i\text{PrMgCl}/\text{LiCl}$ was already an ionic reagent, presumably with the formula $[\text{Li}(\text{THF})_4]^+ [\text{Mg}(\text{THF})-(i\text{Pr})\text{Cl}_2]^-$. The anionic Schlenk equilibrium (Scheme 6.2.1.B) lies on the left side, but can be shifted to the right side by addition of 1,4-dioxane and 15-crown-5 ether.^{110b}

A Schlenk equilibrium of $i\text{PrMgCl}$ in the absence of LiCl



B Anionic Schlenk equilibrium/Magnesate equilibrium of $i\text{PrMgCl}$ in the presence of LiCl



Scheme 6.2.1.A. Schlenk equilibrium of $i\text{PrMgCl}$ in the absence of LiCl . **B.** Proposed anionic Schlenk equilibrium of $i\text{PrMgCl}$ in the presence of LiCl .^{110b}

In addition, the specific conductivities of MgCl_2 in THF at 298 K were measured. The observed specific conductivities were very low but increased almost linearly upon the addition of LiCl (Figure 6.2.1). Again, no constant plateau was reached which was the case for the $\text{ZnCl}_2/\text{LiCl}$ system, but the $\text{MgCl}_2/(\text{LiCl})_n$ complexes mimic the behavior of their $i\text{PrMgCl}/(\text{LiCl})_n$ counterparts. Because of the low solubility of MgCl_2 in THF no experiments at 258 K could be performed.

NMR Spectroscopy. $^1\text{H-NMR}$ spectra of $i\text{PrMgCl}$ ($c = 0.300 \text{ M}$) displayed a single set of signals at room temperature, which is in good agreement with the literature.¹¹³ The $i\text{PrMgCl}$ reagents obey the basic Schlenk equilibrium (Scheme 6.2.1.A) and therefore monomeric $i\text{PrMgCl}$ and $i\text{Pr}_2\text{Mg}$ co-exist over a wide concentration range.¹¹⁴ The observation of just a single set of $i\text{PrMgCl}$ signals in the $^1\text{H-NMR}$ spectrum indicates a rapid exchange between these two species. Upon the addition of one or five equivalents of LiCl , the signals of the α -H atoms in $i\text{PrMgCl}$ shifted slightly upfield (Table 6.2.1). However, the signals of the H atoms of the methyl groups shifted as well. Consequently the absorption of all H atoms shifted upfield and the upfield shifts only derived from the addition of LiCl was $\Delta\delta \leq 0.02 \text{ ppm}$ relative to simple $i\text{PrMgCl}$. It seems that the electronic properties of the organomagnesium halides are less affected by the addition of LiX salts than the organozinc species. The situation is far more complex in comparison to the zincates, as the basic Schlenk equilibrium (Scheme 6.2.1.A) and the “magnesate” equilibrium (Scheme 6.2.1.B) have to be considered as well.

Table 6.2.1. ^1H NMR shifts of the α -H atoms of $i\text{PrMgCl}/(\text{LiCl})_n$ in THF–D₈.

entry	n equivalents of LiCl	δ (–CH–)/ppm	δ (–CH ₃ –)/ppm
1	0	−0.417	1.22
2	1	−0.471	1.17
3	5	−0.495	1.16

ESI Mass Spectrometry.

Several extensive attempts were endeavored to detect organomagnesium reagents employing ESI mass spectrometry, but only inorganic compounds such as MgX₃[−], LiMgX₄[−] complexes, or related inorganic zinc compounds could be detected for $i\text{PrMgCl}/\text{LiCl}$ and $\text{BuZnCl}/(\text{MgCl}_2)_{0.5}$ solutions in THF.

Conclusion

The interpretation of the obtained results is problematic. Upon addition of LiCl to $i\text{PrMgCl}$ solutions the electrical conductivity increased and the formation of lithium isopropylmagnesium complexes Li⁺ $i\text{PrMgCl}_2^-$ was assumed. However, the NMR results do not support formation of magnesates clearly. Besides, Koszinowski and co-workers were not able to detect any organylmagnesium species by ESI mass spectrometry.¹¹⁵ Hence, no clear statement about the picture of the magnesate can be made in this case.

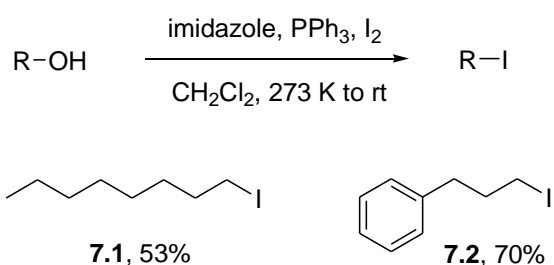
7 Characterization of the Simmons-Smith Reagent

Introduction

Over the past 50 years the Simmons-Smith cyclopropanation reaction has been the subject of considerable synthetic investigations.^{7b,116,117} The classical procedure involves treatment of an olefin with Zn/Cu couple and CH₂I₂ to produce the corresponding cyclopropane.^{7,118} In 1966, Furukawa and coworkers reported on a more reactive reagent which could be prepared by replacing the Zn/Cu couple/CH₂I₂ system with ZnEt₂/CH₂I₂.^{7c,119} A great deal of work has been accomplished to determine the exact nature of the reagents formed in the Simmons-Smith cyclopropanation reactions¹²⁰ and several controversies have then reported in literature, although, the formation of zinc carbenoids RZnCH₂I has been suggested in most cases. In 1996 Charette and co-workers characterized the so called Simmons-Smith reagent CH₂IZnI by NMR Spectroscopy¹²¹ and X-ray crystallography¹²². In this work the reaction of geminal diiodides with zinc was analyzed by ESI mass spectrometry to gain more information about the nature of the Simmons-Smith reagent.

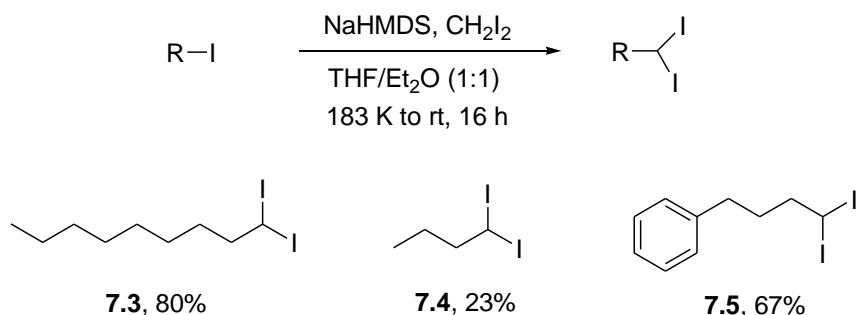
Results and Discussion

Preparation of Geminal Diiiodides.¹²³ The precursors 1-iodooctane (**7.1**) and 3-iodopropylbenzene (**7.2**) were prepared from the adequate alcohol via the redox condensation of Mukaiyama.⁴⁷ The alcohol reacted with imidazole, triphenylphosphine and iodine to the expected products **7.1** and **7.2** and could be isolated in 53 and 70% yield, respectively (Scheme 7.1).



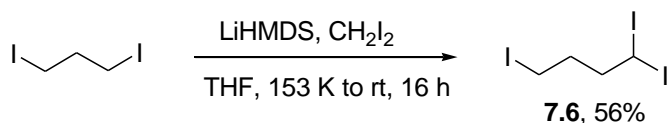
Scheme 7.1. Iodination⁴⁷ via the redox condensation of Mukaiyama.

The geminal diiodides were generated from the iodides **7.1** and **7.2** in a nucleophilic substitution reaction. At first the base NaHMDS reacts with the diiodomethane to a diiodo anion and after the addition of the corresponding iodides the substitution reaction takes place. The gained yields of the products **7.3** and **7.5** were acceptable (Scheme 7.2).⁴⁸



Scheme 7.2. Preparation of *gem*-diiodides using NaHMDS = sodium hexamethyldisilazide.⁴⁸

However, the yield of 1,1,4-triiodobutane (**7.4**) was quite low and compound **7.6** could not be prepared at all with the method of Bull and Charette.⁴⁸ Therefore, reagent **7.6** was synthesized according to Hoffmann using LiHMDS at 153 K (Scheme 7.3).⁴⁹



Scheme 7.3. Preparation of *gem*-diiodides using LiHMDS = lithium hexamethyldisilazide.⁴⁹

ESI Mass Spectrometry Analysis of the Zinc Insertion Reaction into 1,1-Diiodononane (7.3). Preliminary studies started with the zinc insertion reaction of the gem-diiodides **7.3-7.5** with and without the addition of LiCl in THF ($c = 5 \text{ mM}$). Anion-mode mass spectrometry of these solutions showed only the formation of inorganic zinc species in all cases. The absence of organozinc species points to the occurrence of hydrolysis and/or oxidation reactions in the highly diluted solutions. At the low concentrations of the organometallic reagent employed, even very small residual contaminations of water and/or oxygen may become significant. Similar observations had previously been made for other organozincate species as well.^{28,35,36} As former studies showed that DMF is a good solvent to ionize and stabilize the zinc species (see Chapter 4), the reaction of zinc with 1,1-diiodononane (**7.3**) was performed in DMF. Upon cation-mode ESI solutions of α -

iodononyl zinc iodide in DMF afforded $\text{ZnC}_9\text{H}_{18}\text{I}(\text{DMF})_3^+$ and $\text{ZnI}(\text{DMF})_3^-$. Besides, the inorganic compounds $\text{Na}(\text{DMF})_3^+$, $\text{K}(\text{DMF})_n^+$ ($n = 2$ and 3) and $(\text{CH}_3)_2\text{NH}_2(\text{DMF})_2^+$ were detected as well (Scheme 7.1.A); whereas the latter resulted from the decomposition of DMF. The solvated sodium and potassium cations originated from a contamination in the inlet system and/or ESI source and from the drying of the THF solvent over sodium and benzophenone.

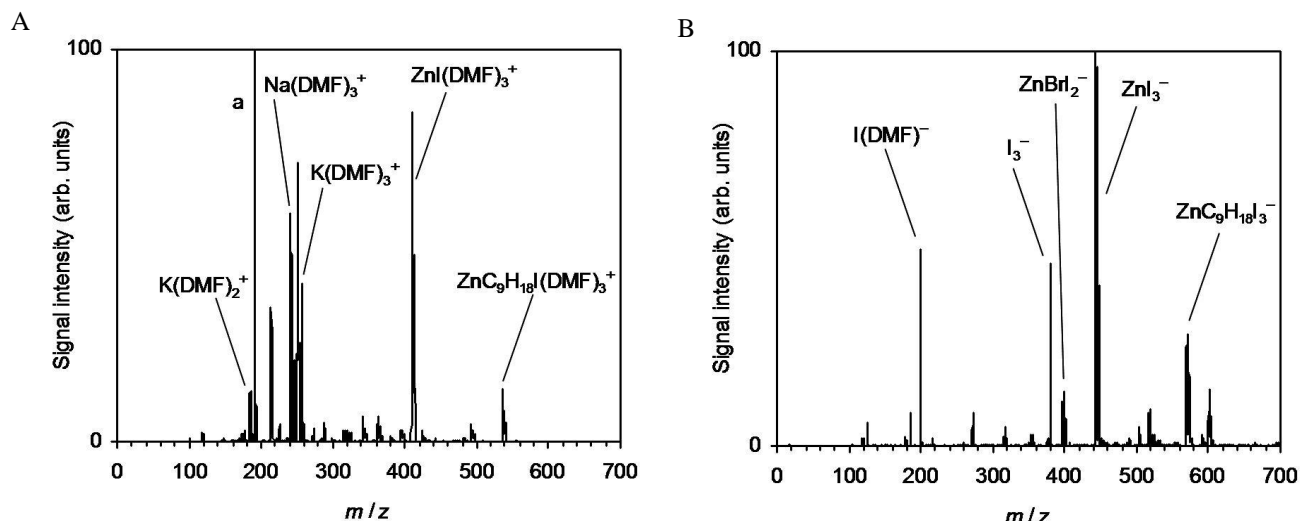
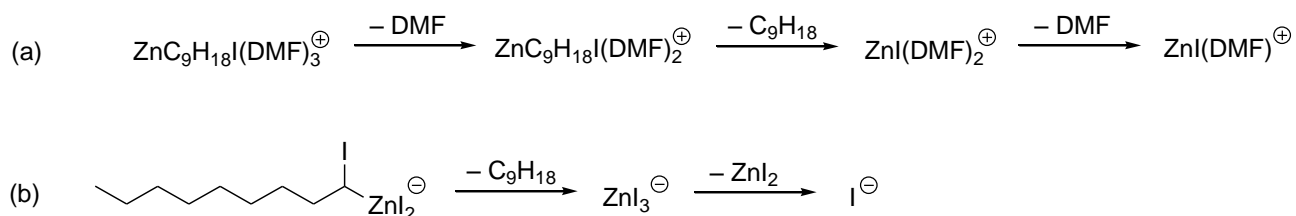


Figure 7.1.A. Cation-mode ESI mass spectrum of an approx. 5 mM solution of the products formed upon reaction of Zn with 1,1-diiodononane (**7.3**) in DMF measured with the TSQ 7000 instrument, $a = (\text{CH}_3)_2\text{NH}_2(\text{DMF})_2^+$. **B.** Anion-mode ESI mass spectrum of an approx. 5 mM solution of the products formed upon reaction of Zn with 1,1-diiodononane (**7.3**) in DMF measured with the TSQ 7000 instrument.

The assignment as $\text{ZnC}_9\text{H}_{18}\text{I}(\text{DMF})_3^+$ was based on the pronounced isotopic pattern characteristic of mononuclear zinc and the fragmentation behavior. Upon CID, the cation $\text{ZnC}_9\text{H}_{18}\text{I}(\text{DMF})_3^+$ lost two DMF solvent molecules and a neutral fragment corresponding to a formal carbene to yield $\text{ZnI}(\text{DMF})^+$ (Scheme 7.4.a). The formal carbene may rearrange in a consecutive reaction to an olefin or a cyclic alkane. The formation of a carbene would support the carbenoid character of the organozinc compounds, which was already assumed for the Simmons-Smith reagents.¹²⁴ Via ESI mass spectrometry the structure of the neutral C_9H_{18} cannot be further elucidated.

Anion-mode ESI of solutions of α -iodononylzinc iodide produced only relatively small amounts of the organozincate $\text{ZnC}_9\text{H}_{18}\text{I}_3^-$ (Scheme 7.1.B). Intense signals were detected for the inorganic anions $\text{ZnI}_n\text{Br}_{3-n}^-$, $n = 2$ and 3, $\text{I}(\text{DMF})_3^-$ and I_3^- .



Scheme 7.4. (a) Fragmentation reaction of mass-selected $\text{ZnC}_9\text{H}_{18}\text{I}(\text{DMF})_3^+$ ($m/z = 563$). (b) Fragmentation reaction of mass-selected $\text{ZnC}_9\text{H}_{18}\text{I}_3^-$ ($m/z = 571$).

CID experiments of the organozinc anion $\text{ZnC}_9\text{H}_{18}\text{I}_3^-$ showed the fragmentation into inorganic ZnI_3^- and a neutral fragment corresponding to a formal carbene (Scheme 7.4.b).

ESI Mass Spectrometry Analysis of the Zinc Insertion Reaction into 1,1,4-Triiodobutane (7.6). Cation-mode mass spectrometry of solutions of 1,1,4-triiodobutane (7.6) and its reaction with zinc in DMF displayed not only inorganic compounds such as $\text{Na}(\text{DMF})_3^+$, $\text{K}(\text{DMF})_n^+$ ($n = 2$ and 3) and $(\text{CH}_3)_2\text{NH}_2(\text{DMF})_2^+$, but also small amounts of organozinc species $\text{ZnC}_4\text{H}_7\text{I}_2(\text{DMF})_3^+$ and $\text{ZnC}_4\text{H}_8\text{I}(\text{DMF})_3^+$ (Scheme 7.2.A). Again, the solvated cations resulted from a contamination in the inlet system and/or ESI source, from the drying of the THF solvent over sodium benzophenone ketyl and $(\text{CH}_3)_2\text{NH}_2(\text{DMF})_2^+$ originated from the decomposition of DMF. Upon CID, the cation $\text{ZnC}_4\text{H}_7\text{I}_2(\text{DMF})_3^+$ lost a DMF molecule to yield $\text{ZnC}_4\text{H}_7\text{I}_2(\text{DMF})_2^+$, which could dissociate into $\text{ZnC}_4\text{H}_7\text{I}_2(\text{DMF})^+$ and DMF or $\text{ZnI}(\text{DMF})_2^+$ and $\text{C}_4\text{H}_7\text{I}$ (Scheme 7.5). The neutral fragment of the latter corresponded to a formal carbene $\text{C}_4\text{H}_7\text{I}$. The cation $\text{ZnC}_4\text{H}_7\text{I}_2(\text{DMF})^+$ lost $\text{C}_4\text{H}_7\text{I}$ as a neutral fragment to yield $\text{ZnI}(\text{DMF})^+$, which could also be generated by the dissociation of $\text{ZnI}(\text{DMF})_2^+$.

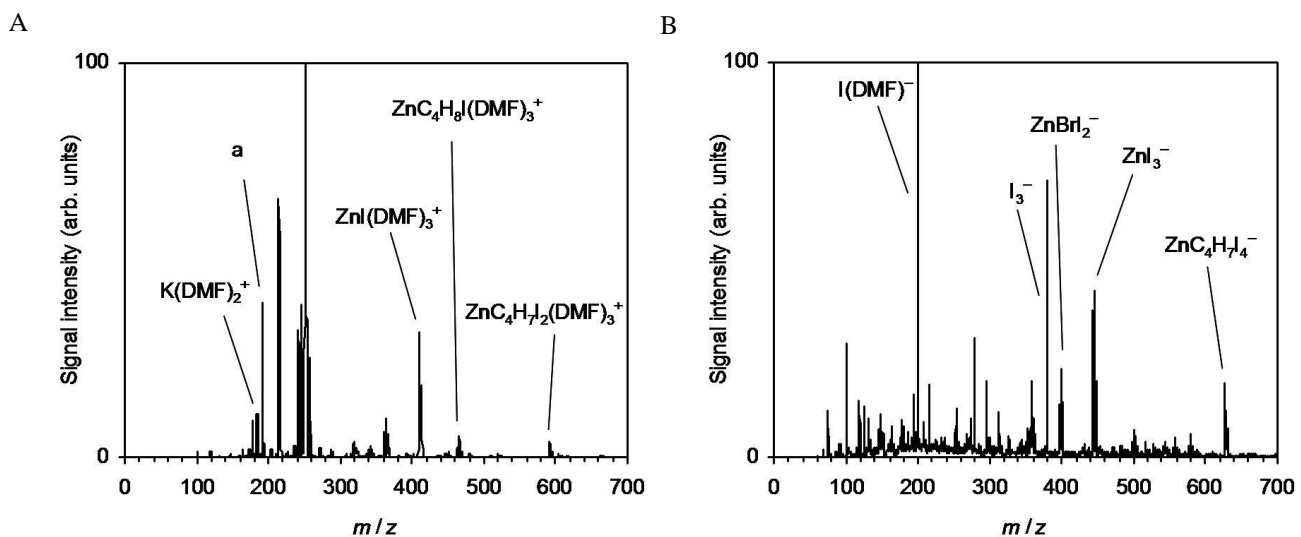
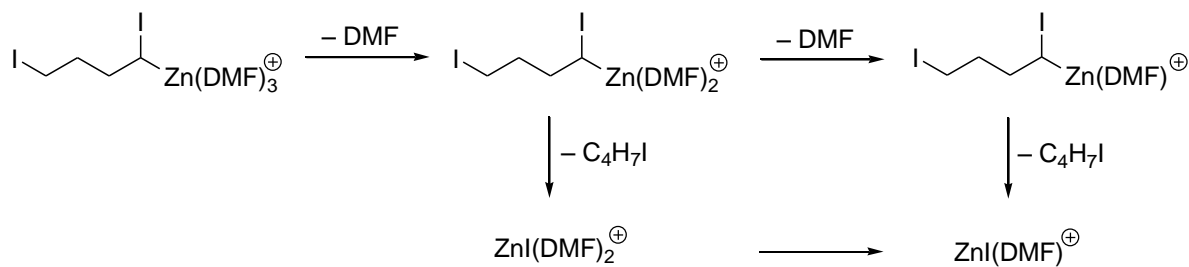


Figure 7.2.A. Cation-mode ESI mass spectrum of an approx. 5 mM solution the products formed upon reaction of Zn with 1,1,4-triiodobutane (**7.6**) in DMF measured with the TSQ 7000 instrument, a = $(\text{CH}_3)_2\text{NH}_2(\text{DMF})_2^+$. **B.** Anion-mode ESI mass spectrum of an approx. 5 mM solution the products formed upon reaction of Zn with 1,1,4-triiodobutane (**7.6**) in DMF measured with the TSQ 7000 instrument.



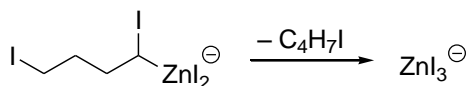
Scheme 7.5. Fragmentation reaction of mass-selected $\text{ZnC}_4\text{H}_7\text{I}_2(\text{DMF})_3^+$ ($m/z = 592$).

Two different structures were conceivable for the cation $\text{ZnC}_4\text{H}_8\text{I}(\text{DMF})_3^+$ (Scheme 7.6.a). CID experiments of this cation showed the loss of two DMF molecules and the neutral fragment corresponding to a formal carbene C_4H_8 (Scheme 7.6.b). This behavior is comparable to the fragmentation pattern of $\text{ZnC}_4\text{H}_7\text{I}_2(\text{DMF})_3^+$ and $\text{ZnC}_9\text{H}_{18}\text{I}(\text{DMF})_3^+$. The fragmentation pattern of BuZn^+ (**7.8**) was discussed in Chapter 4 and the latter dissociated into the C_4H_9^+ cation and neutral zinc. Therefore, the cation $\text{ZnC}_4\text{H}_8\text{I}(\text{DMF})_3^+$ can be assigned to compound **7.7**.



Scheme 7.6. (a) Possible structures of compound $\text{ZnC}_4\text{H}_8\text{I}(\text{DMF})_3^+$ (b) Fragmentation reaction of mass-selected $\text{ZnC}_4\text{H}_7\text{I}_2(\text{DMF})_3^+$ ($m/z = 592$).

The direct zinc insertion reaction analyzed by anion-mode ESI mass spectrometry showed small amounts of the zincate $\text{ZnC}_4\text{H}_7\text{I}_4^-$ and higher amounts of inorganic anions $\text{ZnI}_n\text{Br}_{3-n}^-$, $n = 2$ and 3 , $\text{I}(\text{DMF})_3^-$ and I_3^- (Scheme 7.2.B). The overall signal intensity was quite low. Upon CID the fragmentation of $\text{ZnC}_4\text{H}_7\text{I}_4^-$ into inorganic ZnI_3^- and a neutral fragment corresponding to a formal carbene was observed (Scheme 7.7).



Scheme 7.7. Fragmentation reaction of mass-selected $\text{ZnC}_4\text{H}_7\text{I}_4^-$ ($m/z = 627$).

Conclusion

The preparation of the geminal diiodides worked quite well and their reaction with zinc could be analyzed by ESI mass spectrometry. ESI mass spectra of the zinc insertion reactions into 1,1-diiodononane (**7.3**) and 1,1,4-triiodobutane (**7.6**) displayed the detection of organozinc cations and anions in DMF. CID experiments showed the formation of a neutral compound corresponding to a formal carbene derived from mass-selected organozinc cations and anions. The structure of this formal carbene cannot be further elucidated by mass spectrometry. However, the formation of a carbene could support the assumption of a carbenoid character of organozinc Simmons-Smith reagents.

8 Charged Tags as Probes for Monitoring Cross-Coupling Reactions by ESI-MS

Introduction

In the Chapters 4-7 the characterization of organozinc halides in solution analyzed by ESI mass spectrometry is described. These experiments resulted in the detection of organozinc cations and organozinc anions, whose formal charge is located on the zinc center. As mentioned above, ESI mass spectrometry exclusively detects charged species and this feature could be advantageous if ionic systems are to be probed selectively. In the case of chapter 4-7, the restriction to charged species formed a minor drawback, because neutral organometallics usually prevailed over their ionized counterparts. While the fraction of ionized species may be increased by additives that led to protonation, deprotonation, or complexation,¹²⁵ these reactions could possibly change the nature of the organometallic system under investigation. For instance, protonation will obviously adversely affect organometallics sensitive to hydrolysis. In other cases, the use of additives may have more subtle effects and could thus lead to less conspicuous artifacts.

A potentially better approach, pioneered by Colton and Traeger¹²⁶ and the groups of Dyson¹²⁷ and Chen^{25b,128}, used covalently attached charged tags to make neutral organometallics amenable to ESI mass spectrometry. Provided that the charged tags had only low tendencies to form ion pairs with the counterions in the chosen solvent, almost the complete population of neutral organometallics could thus be ionized.

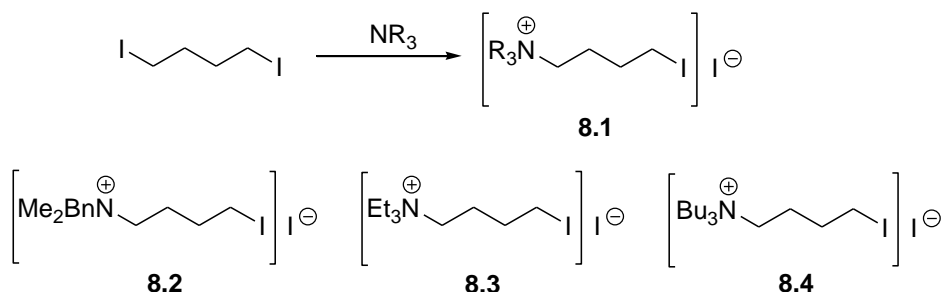
Commonly employed tags are quaternary ammonium cation^{25,126,128,129,130} and sulfonate anions.^{142,131} In these ions, the charge was spread over several atoms, which not only reduced their propensity to ion pairing but also minimized possible interactions with the metal center and unwanted changes in reactivity. Most of the examples reported so far bear a charged tag linked to coordinating ligands,¹³² such as phosphines^{127,128a,128c,130} or carbenes.^{128d} Obviously, this strategy was particularly suited for probing transition metal complexes, whereas it could not be applied to the detection of main-group organometallics that do not bear coordinating ligands.

Alternatively, the charged tag could be directly incorporated into an organyl moiety covalently bound to the metal center.^{35,128b,128c,133} This tagging scheme not only enabled the analysis of systems lacking coordinating ligands but also lent itself to the analysis of coupling reactions that transferred

the organyl moiety with the charged tag and thus ensured straightforward product identification. In this chapter it will be shown that organometallics with covalently bound charged tags could be accessed by insertion of zinc into charge-tagged organic iodides. The solutions of the reaction products were analyzed by ESI mass spectrometry and the obtained results were compared with available data for the related untagged systems. Moreover, ESI mass spectrometry was used for monitoring cross-coupling reactions of charge-tagged substrates and analyzing their kinetics.

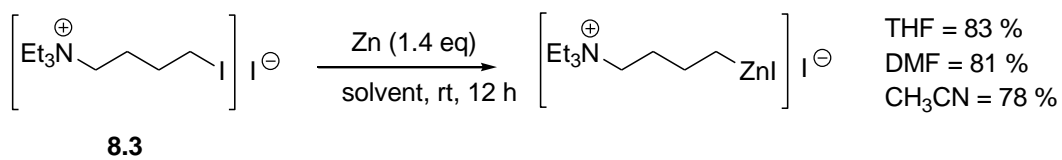
Results and Discussion

Preparation of Charge-Tagged Organozinc Reagents. The extraordinary functional group tolerance and unique reactivity of organozinc reagents made the synthesis of charge-tagged organozinc reagents possible. Starting from α,ω -diiodoalkanes, a substitution reaction using a tertiary amine led to the corresponding charge-tagged alkyl iodide of type **8.1** (Scheme 8.1).⁵⁰



Scheme 8.1. Synthesis of charge-tagged alkyl iodides.⁵⁰

According to the general zinc insertion procedure, compound **8.3** could be converted into the corresponding zinc reagent in three different solvents (THF, DMF and CH₃CN) (Scheme 8.2).



Scheme 8.2. Synthesis of charge-tagged organozinc reagents in different solvents.

As the solubility of the triethyl-(4-iodobutyl)-ammonium iodide (**8.3**) in THF was marginal, although the yield was quite acceptable (83%), zinc insertion reactions in DMF and CH₃CN were carried out. These solvents turned out to be suitable as they completely dissolved the quaternary ammonium salts and allowed an efficient insertion reaction. Thus, the reactions of **8.3** in DMF and CH₃CN prepared according to the general procedure, afforded the charge-tagged organozinc reagent in 81% and 78% yield, respectively.

ESI Mass Spectrometry of Charge-Tagged Organozinc Reagents. Cation-mode ESI mass spectrometry of solutions of triethyl-(4-iodobutyl)-ammonium iodide (**8.3**) in DMF displayed C₁₀H₂₃NI⁺ as the major ion (Figure 8.1.A).

The cationic charged tags employed here were obviously designed for the detection of organometallic intermediates by cation-mode ESI mass spectrometry. Nevertheless, analysis of a solution of pure reactant RI⁺I⁻ in DMF by anion-mode mass spectrometry showed not only inorganic compounds such as I(DMF)_n⁻ (*n* = 1-3) and I_x⁻ (*x* = 1 and 3), but also small amounts of RI₃⁻, which indicate that coordination of two I⁻ ions to the quaternary ammonium group can occur (Figure 8.1.B)

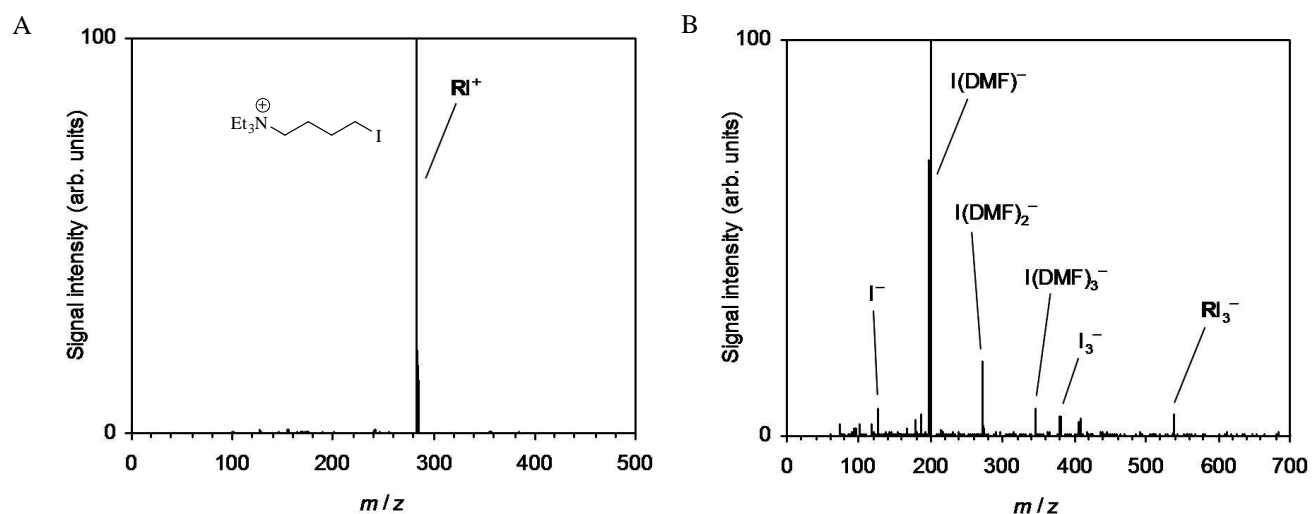


Figure 8.1.A. Cation-mode ESI mass spectrum of an approx. 5 mM solution triethyl-(4-iodobutyl)-ammonium iodide (**8.3**, RI⁺I⁻) in DMF measured with the TSQ 7000 instrument. **B.** Anion-mode ESI mass spectrum of an approx. 5 mM solution triethyl-(4-iodobutyl)-ammonium iodide (**8.3**, RI⁺I⁻) in DMF measured with the TSQ 7000 instrument.

As test systems for the ESI-analysis of organozinc reagents the charge-tagged triethyl-(4-iodobutyl)-ammonium iodide (**8.3**, RI^+I^-) and (*p*-iodophenyl)-trimethylammonium iodide^{50,134} (**8.5**, ArI^+I^-) were chosen. The reaction of zinc dust with the charge-tagged organic iodides **8.3** and **8.5** in THF and ESI mass spectrometric analysis of the resulting solutions afforded RH^+ (Figure 8.2.A) and ArH^+ (Figure 8.2.B), thus indicating conversion of both RI^+ and ArI^+ , but also complete hydrolysis of the charge-tagged organozinc intermediates.

A comparison of the two reactions shows complete consumption of the alkyl iodide RI^+ at room temperature overnight whereas its aryl counterpart ArI^+ did not react to completion even at 323 K. This lower reactivity of the aryl iodide toward Zn fully agrees with reports in the literature.¹⁷

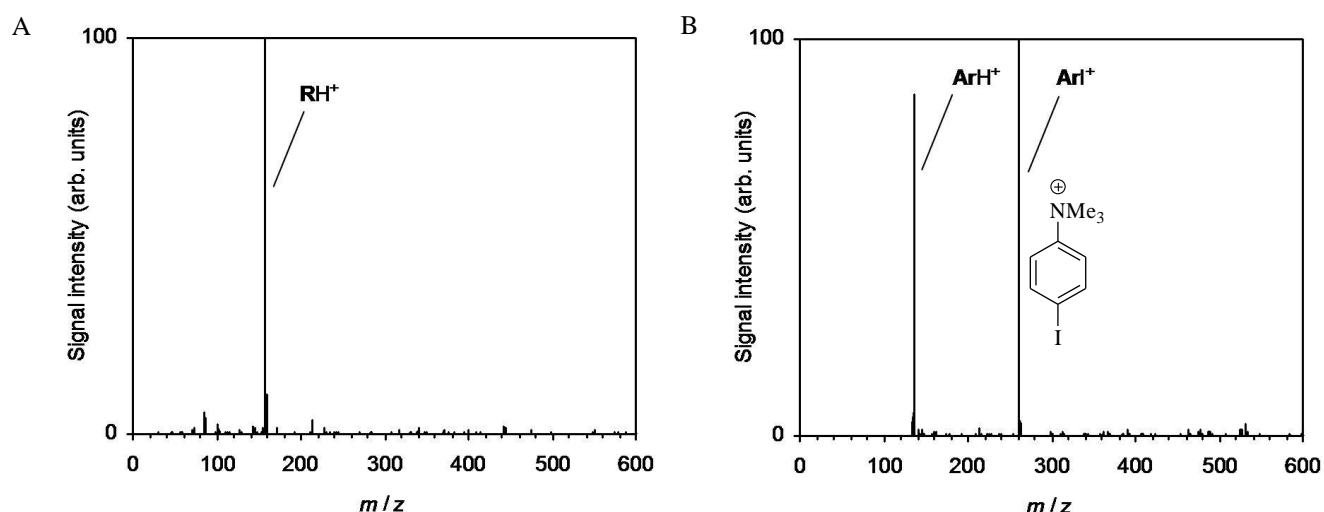


Figure 8.2.A. Cation-mode ESI mass spectrum of an approx. 1 mM solution of the products formed upon reaction of Zn with triethyl-(4-iodobutyl)-ammonium iodide (**8.3**, RI^+I^-) in THF measured with the TSQ 7000 instrument. **B.** Cation-mode ESI mass spectrum of an approx. 2 mM solution of the products formed upon reaction of Zn with (*p*-iodophenyl)-trimethylammonium iodide (**8.5**, ArI^+I^-) in THF at 323 K measured with the TSQ 7000 instrument.

The extreme hydrolysis sensitivity of the charge-tagged organozinc intermediates is surprising because previous studies observed related intact zinc species with simple neutral alkyl substituents, such as $\text{ZnR}(\text{THF})_n^+$ and ZnRHal_2^- (R = benzyl and butyl, Hal = Br and I, n = 1-3), under very similar experimental conditions (see Chapter 4).^{28,75,135} The stability of these ions was further enhanced by DMF.⁷⁵ Therefore this solvent was also tested in the reaction of Zn with RI^+I^- and now indeed the charge-tagged organozinc species $\text{RZnI}(\text{DMF})_n^+$, n = 1 and 2 could be detected, along with some hydrolysis product RH^+ and a small amount of remaining reactant RI^+ (Figure 8.3). The

organozinc species observed display the stoichiometry expected for Zn(II) compounds and moreover provide insight into their solvation behavior. The fact that abundant DMF adducts were only found for Zn-containing species but not for RH^+ or RI^+ strongly suggest coordination of the solvent molecules to the Zn center and not to the quaternary ammonium group.

The inferred coordination numbers of 3 and 4 agree with results obtained for microsolvated alkylzinc cations $\text{ZnR}(\text{solv})_n^+$ (solv = THF, CH_3CN , and DMF), for which coordination numbers ≤ 4 were observed.^{75,62,136} Presumably, these organozinc species adopt tetrahedral coordination geometries in solution but are prone to lose one solvent molecule during the ESI process.

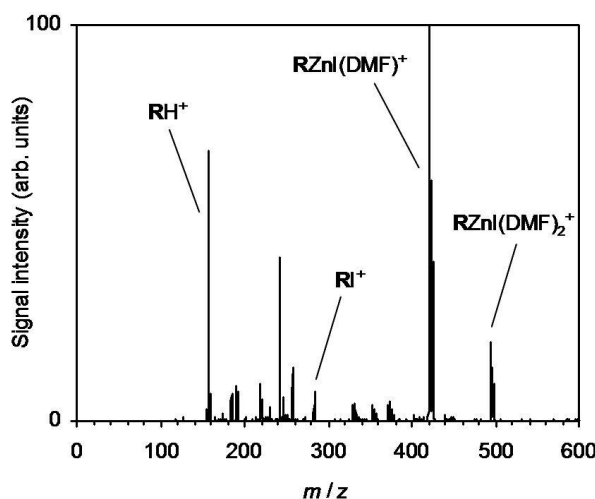
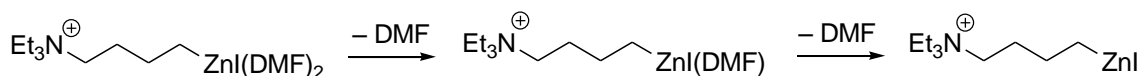


Figure 8.3. Cation-mode ESI mass spectrum of an approx. 1 mM solution of the products formed upon reaction of Zn dust with triethyl-(4-iodobutyl)-ammonium iodide (**8.3**, RI^+I^-) in DMF measured with the TSQ 7000 instrument. The ion at $m/z = 242$ corresponded to $\text{Na}(\text{DMF})_3^+$, which presumably originates from a contamination of the ESI source.

In line with this conjecture, mass-selected $\text{RZnI}(\text{DMF})_2^+$ ($\text{R} =$ 4-triethylammonium-butyl, $\text{C}_{10}\text{H}_{23}\text{N}^+\text{ZnI}(\text{DMF})_2^+$) lost the attached solvent molecules quite easily when subjected to gas-phase fragmentation (Scheme 8.3).



Scheme 8.3. Fragmentation reaction of mass-selected $\text{C}_{10}\text{H}_{23}\text{N}^+\text{ZnI}(\text{DMF})_2^+$ ($m/z = 494$, $\text{R}^{64}\text{ZnI}(\text{DMF})_2^+$, $\text{R} =$ 4-triethylammonium-butyl).

Although the used charged tags were designed for the detection of organometallic intermediates by cation-mode ESI mass spectrometry, analysis of the products formed upon reaction of Zn with RI^+I^- in DMF by anion-mode ESI mass spectrometry (Figure 8.4) not only resulted in the detection of $\text{I}(\text{DMF})_n^-$ ($n = 0$ and 1), I_3^- , and ZnI_3^- , but also of small quantities of RZnI_3^- .

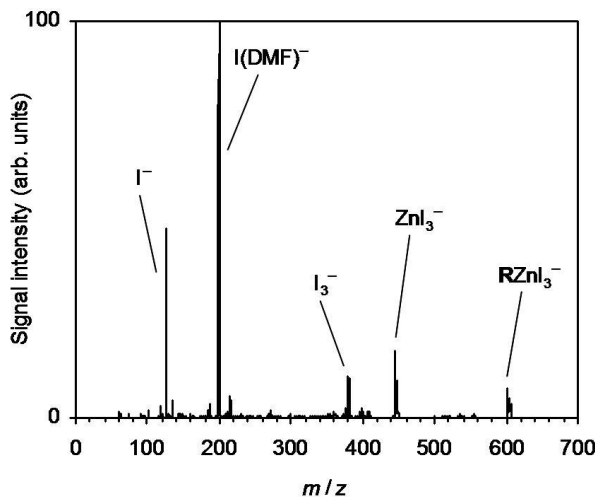
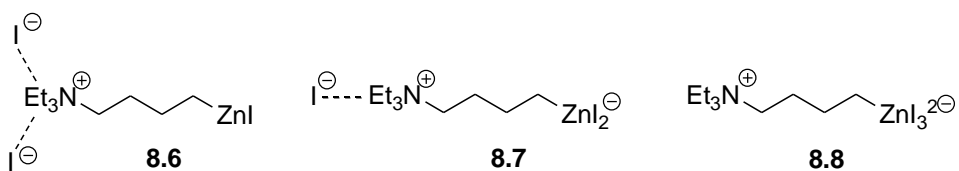


Figure 8.4. Anion-mode ESI mass spectrum of an approx. 1 mM solution of the products formed upon reaction of Zn with triethyl-(4-iodobutyl)-ammonium iodide (**8.3**, RI^+I^-) in DMF measured with the TSQ 7000 instrument.

For RZnI_3^- , three different structures seem conceivable (Scheme 8.4).

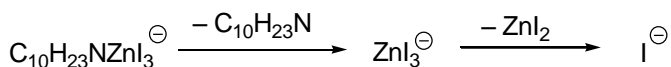


Scheme 8.4. Conceivable structures of the observed anion RZnI_3^- .

In structure **8.6**, two I^- anions are bound electrostatically to the ammonium group. This type of complex is considered less likely because the absence of the analogous ions $(\text{RH})\text{I}_2^-$ and $(\text{RI})\text{I}_2^-$ in the mass spectrum indicates a low stability of this binding motif under the ESI conditions applied. For the specific experiment shown (Figure 8.5), analysis of the same sample by positive ion mode ESI mass spectrometry proves the presence of the hydrolysis product RH^+ (55% signal intensity relative to that of the base peak $\text{RZnI}(\text{DMF})^+$) and RI^+ (10% relative signal intensity). Note that the anion-mode mass spectrum of a solution of pure RI^+I^- **8.3** in DMF showed small amounts of RI^-

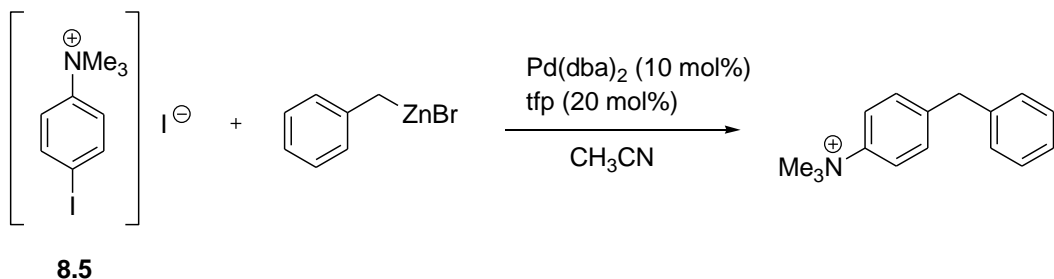
(Figure 8.1.B), which indicates that coordination of two I^- ions to the quaternary ammonium group can occur.

Structure **8.7** contains an organozincate moiety, which closely resembles previously observed alkylzincates RZnHal_2^- .^{28,75,97} In structure **8.8**, coordination of all three I^- anions to the Zn atom build up a twofold negative charge at the metal center, which would be energetically unfavorable for a linear conformation. However, adoption of a cyclic conformation can permit a stabilizing electrostatic interaction between the dianionic ZnI_3^{2-} moiety and the cationic ammonium group. Fragmentation of mass-selected RZnI_3^- ($\text{C}_{10}\text{H}_{23}\text{NZnI}_3^-$) yielded I^- and ZnI_3^- as ionic products (Scheme 8.5), which was of limited significance only because the involvement of rearrangement reactions seem quite likely. Hence, the experimental results do not suffice for an unambiguous structural assignment.



Scheme 8.5. Fragmentation reaction of mass-selected $\text{C}_{10}\text{H}_{23}\text{NZnI}_3^-$ ($m/z = 602$, $\text{R}^{64}\text{ZnI}_3^-$, $\text{R} = 4$ -triethylammonium-butyl).

Monitoring of Coupling Reactions. As shown above, ESI mass spectrometry has permitted the tracking of degradation and hydrolysis of organometallics bearing organic substituents with charged tags. Obviously, it would be even more interesting to use this approach for analyzing synthetically valuable reactions of these species. Therefore, the potential of this analytical method is demonstrated by studying the Pd-catalyzed Negishi cross-coupling of **ArI⁺** (**8.5**) with benzylzinc bromide (Scheme 8.6).



Scheme 8.6. Pd-catalyzed cross-coupling of **8.5** with benzylzinc bromide. $\text{Pd}(\text{dba})_2 =$ bis(dibenzylideneacetone)palladium, tfp = tri-2-furylphosphine.

Negishi cross-couplings constitute one of the most versatile tools in modern organic synthesis.^{21,51,86} The mechanism of these reactions therefore has attracted a great deal of attention. It is commonly assumed that these reactions start by the oxidative addition of the organic halide to the zero-valent Pd (or Ni) catalyst. The resulting insertion product then undergoes transmetalation by the organozinc reagent and finally yields the coupling product by reductive elimination.^{21b} For these experiments, Pd(dba)₂/tfp (bis(dibenzylideneacetone)palladium/tri-2-furylphosphine) in CH₃CN was employed as catalytic system, which efficiently added ArI⁺. In the presence of BnZnBr, the expected coupling product ArBn⁺ could indeed be detected by ESI mass spectrometry (Figure 8.5).

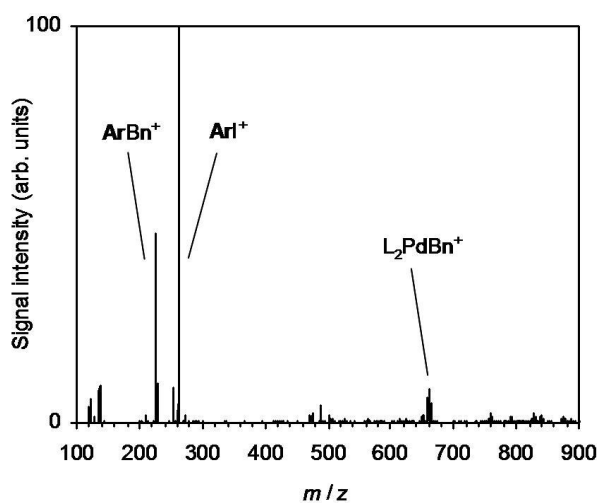
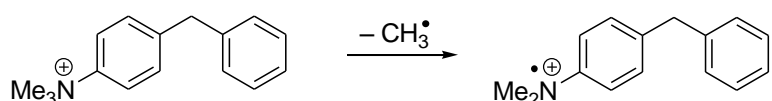


Figure 8.5 Cation-mode ESI mass spectrum of an approx. 2 mM solution of (*p*-iodophenyl)-trimethylammonium iodide (ArI⁺I⁻, **8.5**), BnZnBr (1.2 equiv), Pd(dba)₂ (10 mol%), and the ligand L = tfp (20 mol%) in CH₃CN approx. 15 min after mixing measured with the HCT ion trap.

The identity of this species is confirmed by analysis of its fragmentation pattern (Scheme 8.7) and by a control experiment in which BnZnBr was substituted by *m*-methylbenzylzinc bromide. This resulted in a coupling product of an *m/z* ratio shifted by 14 amu relative to ArBn⁺.



Scheme 8.7. Fragmentation reaction of mass-selected ArBn⁺ (*m/z* = 226).

In addition, smaller amounts of L_2PdBn^+ were produced. Again, this assignment is based on the recorded isotope pattern (Figure 8.6), fragmentation experiments (Eqs. 8.1 and 8.2) and on an observed mass shift of 14 amu when BnZnBr was replaced by *m*-methylbenzylzinc bromide.

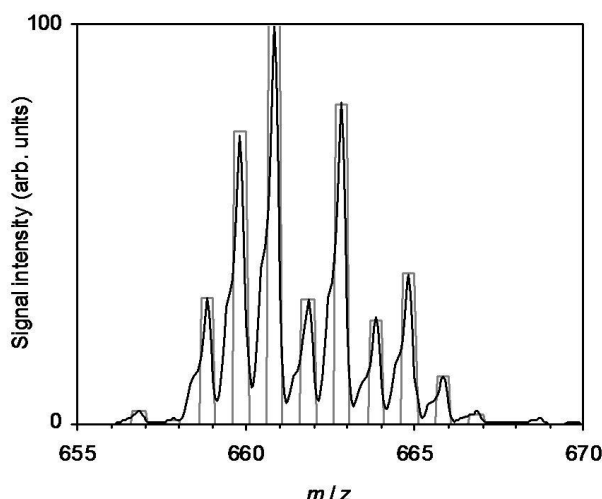
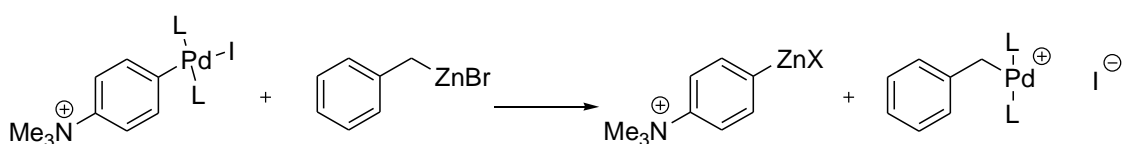


Figure 8.6. Isotope pattern of the complex L_2PdBn^+ with the elemental composition $\text{C}_{31}\text{H}_{25}\text{O}_6\text{P}_2\text{Pd}$ measured with the HCT ion trap (black) and simulated (grey, L = tri-(2-furyl)phosphine).



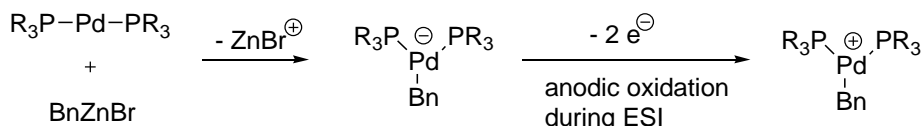
The L_2PdBn^+ complex accumulated with time and increased in signal intensity as a function of catalyst loading (data not shown here). The genesis of the complex L_2PdBn^+ itself is not obvious. One may speculate that in the presence of added ArI^+ it is formed in a metathesis reaction between the insertion product $\text{L}_2\text{ArPdBn}^+$ and BnZnBr (Scheme 8.8).



Scheme 8.8. Possible reaction to form L_2PdBn^+ .

In this case, however, one would also expect to observe ArZnX^+ , $\text{X} = \text{Br}$ and/or I (or degradation products thereof), which was not detected.

Surprisingly, L_2PdBn^+ was even formed to some extent in the reaction of the Pd catalyst with BnZnBr in the absence of aryl iodide ArI^+ . However, in this case the abundance of L_2PdBn^+ was considerably decreased as indicated by the relatively poor signal/noise ratio. As a consequence, additional ions of similarly low absolute signal intensity, such as CuL_n^+ and $(\text{LO})_n\text{ZnBn}^+$ ($\text{LO} = \text{C}_{12}\text{H}_9\text{O}_4\text{P}$) also became visible; the assignments of these species, which may have originated from contaminations, are based on the observed isotope patterns and fragmentation experiments. It might be assumed that L_2PdBn^+ could result, in the absence of added ArI^+ , from the transmetalation of a Pd(0) species. For related Ni(0) phosphine complexes in the presence of organomagnesium and -zinc reagents, Terao and Kambe have suggested the occurrence of transmetalation reactions and formation of nickelate anions.¹³⁷ In analogy, the current experiments might potentially produce a palladate species (Scheme 8.9). This extremely electron-rich species could then possibly afford the observed L_2PdBn^+ cation by anodic oxidation during the ESI process.¹³⁸



Scheme 8.9. Possible genesis of the observed L_2PdBn^+ complex ($\text{R} = 2$ -furyl) by anodic oxidation during ESI.

Negative ion mode ESI mass spectrometric experiments did not detect any palladate species, however, and instead only showed the presence of various zincate complexes (Figure 8.7).

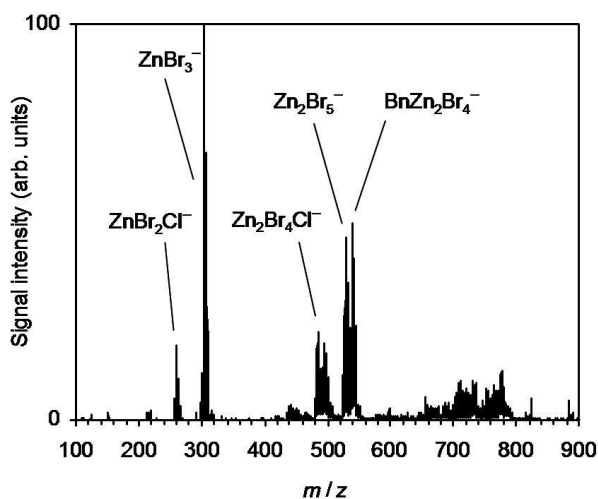


Figure 8.7. Negative ion mode ESI mass spectrum of an approx. 2 mM solution of Pd(dba)₂, tfp (2 equiv), and BnZnBr (2 equiv) in CH₃CN measured with the HCT ion trap. The ions centered around *m/z* 497 corresponded to ZnBnBr₃Cl⁻.

Returning to the actual Negishi cross-coupling reaction between ArI^+I^- and BnZnBr itself, it was questionable whether ESI mass spectrometry could also be used to monitor the temporal evolution of reactants and products and to derive the rate constant(s) of this reaction. To test for this possibility, a mixture of the reactants and the catalyst was prepared and continuously administered into the ESI source of the mass spectrometer while recording the positive ion mode ESI mass spectrum. Averaging every 50-100 scans then gave a time resolution of approx. 10 s. The resulting averaged signal intensities still showed rather high noise levels (Figure 8.8), which directly reflected the relatively poor absolute signal stability typical of the ESI process. Nevertheless, the obtained time profiles clearly exhibit the opposing trends expected for reactants and products. While varying the concentration of the benzylzinc reagent (1.2 - 2.0 equiv relative to ArI^+I^-) did not have a discernible effect, an increase in the catalyst loading strongly accelerated the decay of reactant ArI^+ (Figure 8.8). This finding points to a rate-determining oxidative addition, which is followed by fast transmetalation and reductive elimination steps. The same conclusion can also be derived from the fact that the mass spectra showed the simultaneous presence of reactant ArI^+ and product ArBn^+ but far less of intermediate L_2ArPdI^+ , because it was almost completely consumed by the fast consecutive reaction with BnZnBr (compare Figure 8.5, although in this case the lower concentration of the catalyst helped to suppress the relative signal intensity of L_2ArPdI^+).

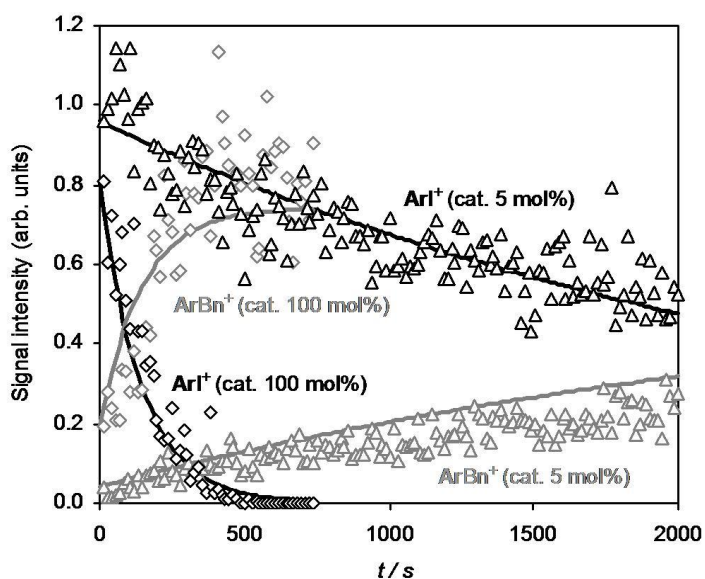


Figure 8.8. Time dependence of the normalized signal intensities of reactant ArI^+ (black) and product ArBn^+ (grey) formed in the Pd-catalyzed cross-coupling reaction with BnZnBr in CH_3CN at room temperature as determined by ESI mass spectrometry. Results of two experiments with different catalyst loadings were shown (diamonds: 100 mol%, triangles: 5 mol% relative to ArI^+). The solid lines represented simulated time profiles based on a second-order rate constant of $k_2 = 3.5 \text{ L mol}^{-1} \text{ s}^{-1}$ (see text for details). Time zero corresponded to the start of the ESI mass spectrometric experiments, which was approx. 2 min after the mixing of the reaction partners.

Note that an alternative tagging mode that attached the charged tag to the phosphine ligand would neither permit the detection of the reactant aryl iodide nor the cross-coupling product and thus would be less useful than the present approach. For a quantitative analysis, it was focused on the decline of reactant ArI^+ , which according to the used model should proceed under pseudo first-order conditions (virtually constant concentration of free Pd catalyst). Indeed, the individual time profiles of the ArI^+ signal intensity could be satisfactorily fitted with mono-exponential functions.¹³⁹ Correlating the corresponding pseudo first-order rate constants with the concentrations of the Pd catalyst in the individual experiments ($c(\text{Pd}(\text{dba})_2) = 10^{-4}$ to $2 \times 10^{-3} \text{ mol L}^{-1}$) then gave a second-order rate constant of $k_2 = 4 \pm 2 \text{ L mol}^{-1} \text{ s}^{-1}$ for the oxidative addition at room temperature. Based on this value, the decline of the ArI^+ signal intensities in Figure 8.8 could be reproduced quite well. The derived k_2 rate constant was also used to predict the increase of the ArBn^+ signal intensities. Here, it was furthermore necessary to introduce a constant scaling factor to account for apparently slightly deviating ESI response factors^{79a,140} of reactant and product ions and/or mass-

dependent ion transmission and detection efficiencies. The agreement between observed and simulated signal intensities of the ArBn^+ coupling product does not equal that observed for the ArI^+ reactant but still is reasonably good.

The oxidative addition of ArI^+ to PdL_2 ($L = \text{tfp}$) in CH_3CN can be compared to the analogous addition of simple PhI to PdL_2 in THF and DMF. The latter reactions are somewhat faster ($k_2(\text{THF}) = 500 \pm 200$ and $k_2(\text{DMF}) = 99 \pm 2 \text{ L mol}^{-1} \text{ s}^{-1}$),¹⁴¹ although the presence of the electron-withdrawing ammonium group in ArI^+ should activate this substrate for the oxidative addition.¹⁴² This comparison suggests that CH_3CN significantly slows down the addition of aryl iodides to zero-valent Pd complexes, presumably by binding to the metal center and blocking of a coordination site. In line with this assessment, CH_3CN is not commonly used as solvent in Negishi cross-coupling reactions,^{21b} although its high polarity and volatility make it ideally suitable for the present model studies.

Conclusion

Zn reacted with ammonium-tagged organic iodides to give C-I bond insertion and the consumption of the latter could be conveniently monitored by ESI mass spectrometry. The detection of the resulting organometallic intermediates by ESI mass spectrometry provides detailed information on their molecular nature. In all cases, the stoichiometry of the observed species is in accordance with the reported chemistry of related systems. Moreover, the proposed charge-tagging approach also lends itself to reactivity studies. Unlike a tagging scheme that attached the charge to a coordinating ligand, the placement of the tag in the organyl substituent permits the tracking of the fate of this moiety and thus, the elucidation of coupling reactions. The feasibility and utility of this approach were demonstrated by analyzing the Pd-catalyzed Negishi cross-coupling of ArI^+ with BnZnBr . The results clearly show that here the oxidative addition was the rate-limiting step, for which a second-order rate constant of $k_2=4 \pm 2 \text{ L mol}^{-1} \text{ s}^{-1}$ was determined.

9 Kinetic Analysis of Palladium-Catalyzed Negishi Cross-Coupling Reactions

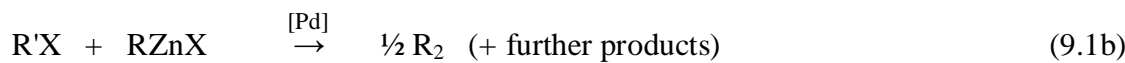
Introduction

Charged tagged organozinc iodides were employed for Negishi cross-coupling reactions in Chapter 8. As the solubility of these reagents in THF is rather low, coupling reactions in acetonitrile were performed, although the use of acetonitrile in Negishi cross-coupling reactions is uncommon. Moreover, the effect of simple salt additives LiX on the efficiency of the palladium-catalyzed reactions could not be investigated via ESI mass spectrometry, as the intensity of the added Li⁺ cations is too high to detect organozinc reagents in the cation-mode, simultaneously. To gain further insight into Negishi cross-coupling reactions, the latter were performed in THF and analyzed by gas-chromatography.

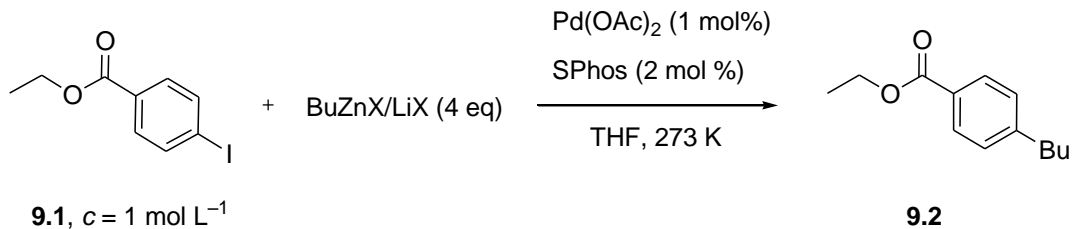
As mentioned in Chapter 8, the cross-coupling reactions are generally believed to follow the catalytic cycle which involves the distinct elementary steps of oxidative addition, transmetalation, and reductive elimination.⁷⁰ Recent studies indicated, however, that the conventional catalytic cycle was oversimplistic and must be extended to describe Negishi cross-coupling reactions correctly.

A first set of observations referred to the effect of simple salt additives.⁹⁰ Several groups reported that the presence of LiX and MgX₂ salts changes the reactivity of RZnX reagents in Pd-catalyzed reactions with organic halides.^{18,86,92,93,106} The authors rationalized this effect by the formation of lithium organozincates, whose increased nucleophilicity supposedly accelerated the transmetalation step. Alternatively, the LiX salts could possibly also act upon the palladium catalyst. Amatore and Jutand have proposed that halide and acetate anions add to Pd(0) centers to form palladate species in Heck and cross-coupling reactions,¹⁴³ in such cases, the salt additive would not influence the transmetalation step, but the oxidative addition. Note that halide effects¹⁴⁴ are well-known for palladium-catalyzed Heck¹⁴⁵ and Stille¹⁴⁶ reactions.

A second finding pointing to the occurrence of reaction pathways beyond the conventional catalytic cycle was the observation of homo-coupling products.¹⁴⁷⁻¹⁵⁴ These synthetically undesired byproducts formed by the combination of two organyl groups from the organyl halide or the organozinc reagent, Eqs. 9.1.a and 9.1.b, respectively. Various mechanisms have been proposed for such reactions.^{148,149,150,152}



For a better understanding of palladium-catalyzed Negishi cross-coupling reactions and a rationalization of the recently observed salt effects and homo-coupling processes, mechanistic studies are necessary. In particular, kinetic analyses appeared indispensable.^{155,156} A kinetic investigation is reported for the model reaction between ethyl 4-iodo-benzoate (ArI, **9.1**) and a series of different butylzinc reagents $\text{BuZnX}/(\text{LiX})_n$, $n = 0 - 2$, with $\text{Pd}(\text{OAc})_2$ as catalyst precursor¹⁵⁷ and the sterically demanding phosphine SPhos¹⁵⁸ as ligand (Scheme 9.2). Note that very similar conditions are successfully used in synthetic applications.^{51,91,99} With a catalyst loading of 1 mol%, the reaction actually proceeded at such a rate that it can no longer be followed by gas-chromatographic analysis. One possibility to slow down the reaction would be to reduce the catalyst concentration. However, very low catalyst loadings could possibly lead to interferences from non-catalyzed background reactions or catalyst degradation processes. Instead, the reaction rate was reduced by lowering the temperature, thereby also decreasing the likelihood of unwanted decomposition reactions.



Scheme 9.2. Model reaction investigated. The given reagent and catalyst concentrations referred to the standard conditions of the kinetic experiments. SPhos = 2-dicyclohexylphosphino-2',6'-dimethoxy-biphenyl.

Results and Discussion

Comparison of different BuZnX reagents. Under standard conditions, the reaction between ArI and BuZnCl went to completion within the sampled time window of $t = 5400 \text{ s}$ and afforded the expected cross-coupling product in $> 95\%$ yield (Figure 9.1), proving the high efficiency of the Negishi reaction. As byproducts, diethyl diphenyl-4,4'-carboxylate (Ar₂, **9.3**) and ethyl benzoate (ArH, **9.4**) were observed, which resulted from homo-coupling and dehalogenation processes.

Because of the low abundance of these byproducts, they are not considered in the present context, but their genesis is discussed below.

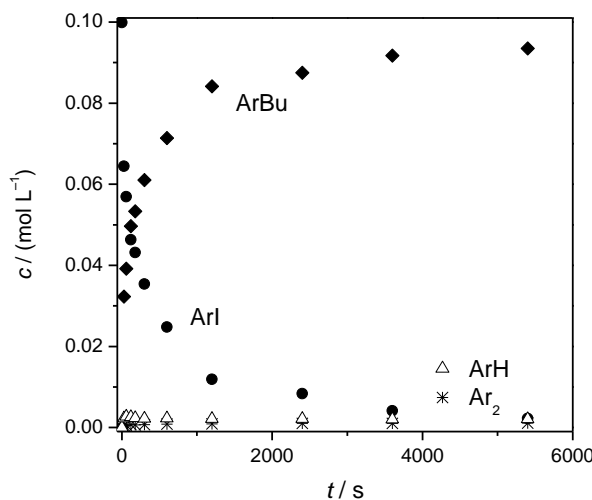


Figure 9.1. Time profiles of the concentrations of reactant ArI (filled circles) and of the products ArBu (cross-coupling product, filled diamonds), ArH (dehalogenation product, open triangles), and Ar₂ (homo-coupling product, stars) formed in the reaction with BuZnCl (0.40 M) in THF at 273 K (catalyst precursor: Pd(OAc)₂/2 SPhos, 1.00 mM).

The analogous reactions of ArI with BuZnBr and Bu₂Zn occurred at very similar rates (Figure 9.2). In contrast, the reaction with BuZnI appeared to be markedly slower.

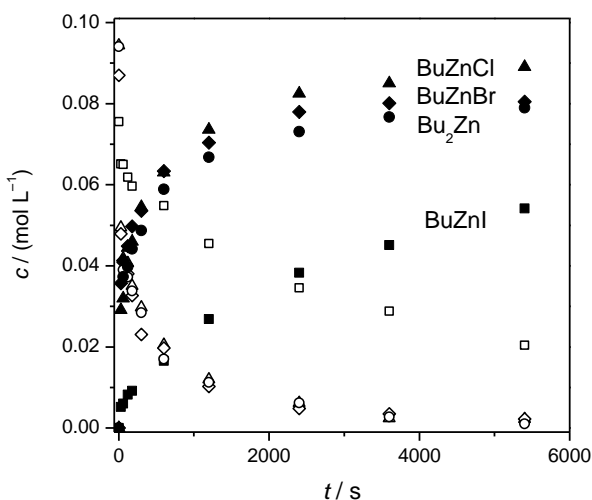


Figure 9.2. Time profiles of the concentrations of reactant ArI (open symbols, decreasing) and the cross-coupling product ArBu (filled symbols, increasing) formed upon reaction with different butylzinc reagents (0.40 M, BuZnCl = triangles, BuZnBr = diamonds, Bu₂Zn = circles, BuZnI = squares) in THF at 273 K (catalyst precursor: Pd(OAc)₂/2 SPhos, 1.00 mM).

Effect of LiX additives. Upon addition of 1 eq of LiCl to the BuZnCl reagent, the cross-coupling reaction was moderately accelerated (Figure 9.3.A). This observation is in accordance with reports from the literature.^{92,93} If LiClO₄ instead of LiCl was added, the effect became smaller. Apparently, the anion and not the Li⁺ cation causes the rate increase.

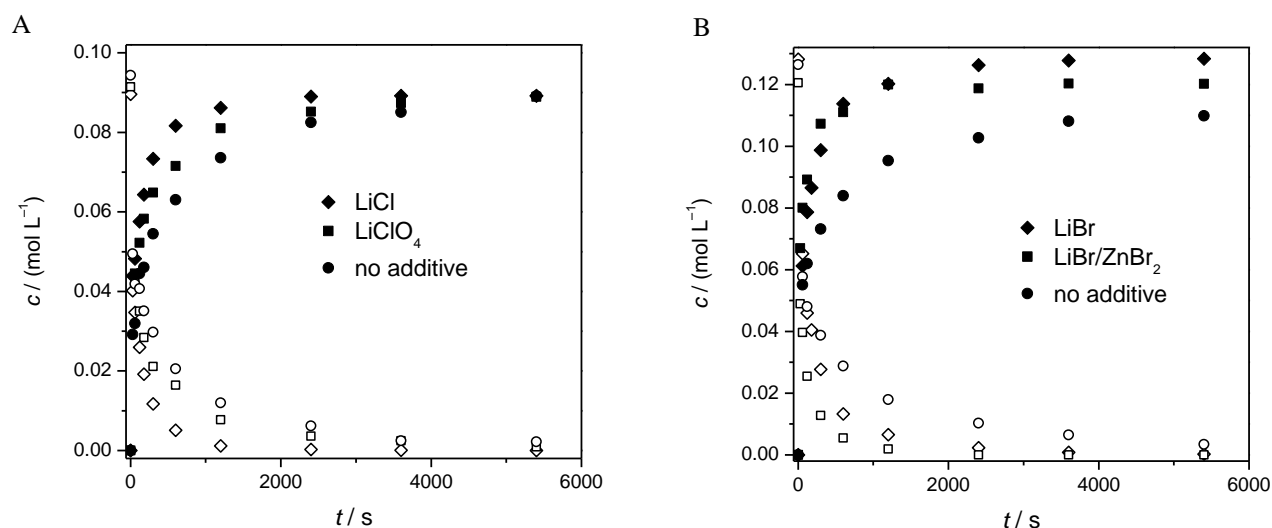


Figure 9.3.A. Time profiles of the concentrations of reactant ArI (open symbols) and of the cross-coupling product ArBu (filled symbols) formed upon reaction with BuZnCl (0.40 M) in the presence of different LiX additives (LiCl = diamonds, LiClO₄ = squares, no additive = circles) in THF at 273 K (catalyst precursor: Pd(OAc)₂/2 SPhos, 1.00 mM). **B.** Time profiles of the concentrations of reactant ArI (open symbols) and of the cross-coupling product ArBu (filled symbols) formed upon reaction with BuZnBr (0.40 M) in the absence (circles, catalyst precursor: Pd(OAc)₂/2 SPhos, 1.00 mM) and presence of LiBr (diamonds, 0.40 M, catalyst precursor: Pd(OAc)₂/2 SPhos, 0.33 mM) and LiBr (0.40 M)/ZnBr₂ (0.10 M) (squares, catalyst precursor: Pd(OAc)₂/2 SPhos, 0.33 mM), respectively, in THF at 273 K.

Compared to simple BuZnBr, the presence of 1 eq of LiBr also led to an acceleration of the model reaction (Figure 9.3.B). This acceleration is not impaired by the addition of extra ZnBr₂ (Figure 9.3.B). In the case of BuZnI, which by itself reacted rather slowly, the treatment with LiI had a particularly strong effect and thus lends itself to a more detailed analysis. An increase of the LiI concentration gave rise to a gradual rate enhancement (Figure 9.4). As a result, the reaction of ArI with BuZnI/LiI proceeded at a rate comparable to those observed for BuZnCl/LiCl and BuZnBr/LiBr.

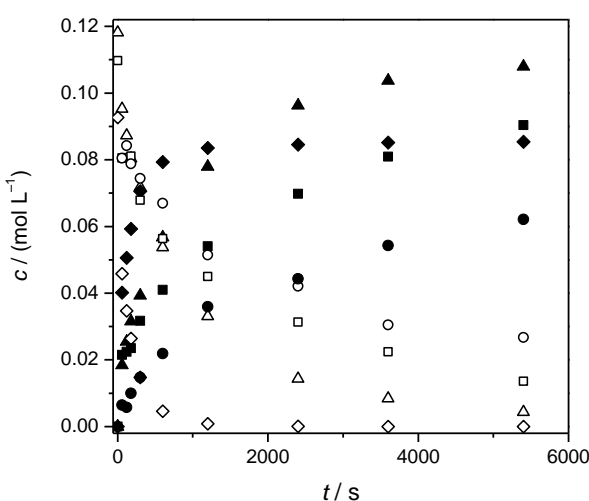


Figure 9.4. Time profiles of the concentrations of reactant ArI (open symbols) and of the cross-coupling product ArBu (filled symbols) formed upon reaction with BuZnI (0.40 M) in the presence of different concentrations of LiI (0.80 M LiI = diamonds, 0.20 M LiI = triangles, 0.05 M LiI = squares, no LiI = circle) in THF at 273 K (catalyst precursor: Pd(OAc)₂/2 SPhos, 1.00 mM).

Rate-determining step. Previous studies of palladium-catalyzed cross-coupling reactions arrived at different results with respect to the nature of the rate-limiting step. For the Pd(PPh₃)₄ catalyzed reaction of aryl bromides with arylzinc reagents, Mayr, Knochel, and coworkers provided data consistent with a rate-determining oxidative addition.¹⁵⁹ In contrast, theoretical calculations by Chass et al. predicted the transmetalation to be the rate-limiting step in the Pd/PEPSSI mediated reaction of alkyl halides with alkylzinc halides.¹⁶⁰ These deviating findings indicate that the rate-determining step cannot be identified a priori, but that each case must be analyzed individually. For the present model reaction, already the qualitative shape of the time profile of reactant ArI contained valuable information. As the BuZnX reagent was present in threefold excess compared to ArI (0.4 versus 0.1 M), its concentration did not significantly change during the course of the reaction. Moreover, the concentration of the catalyst was also expected to remain constant in an ideal scenario (for deviations from this ideal behavior, see below). On the basis of the conventional catalytic cycle (Scheme 9.1), one would therefore expect pseudo-zeroth order kinetics if either the transmetalation or the reductive elimination were the rate-limiting step. In agreement with this assessment, simulations for both cases show essentially linear decreases of the ArI concentration (Figure 9.5). Clearly, this behavior does not match that observed in our experiments. If, in contrast, the oxidative addition is rate-determining, pseudo-first order kinetics result and the simulation accordingly featured an exponential decay (Figure 9.5). For all butylzinc reagents employed, the

latter resembles the measured concentration profiles much more than linear decreases, thus pointing to the oxidative addition as rate-limiting step.

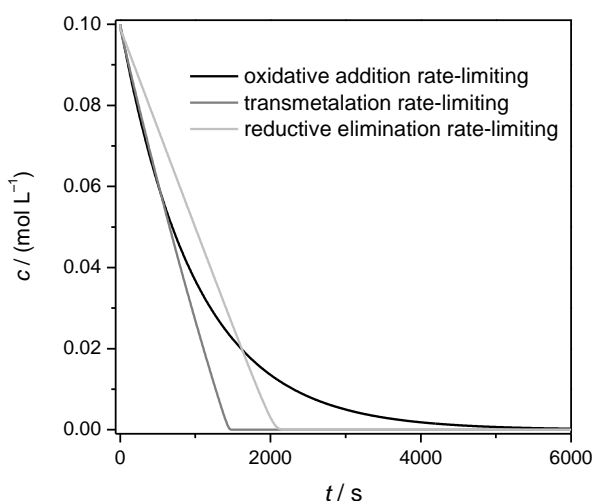


Figure 9.5. Simulated time profile of the concentration of reactant ArI in the model reaction for three different scenarios based on the conventional catalytic cycle (Scheme 1): (a) oxidative addition rate-limiting ($k(\text{ox. add.}) = 1 \text{ M}^{-1} \text{ s}^{-1}$, $k(\text{transmet.}) = 1000 \text{ M}^{-1} \text{ s}^{-1}$, $k(\text{red. elim.}) = 1000 \text{ s}^{-1}$), (b) transmetalation rate-limiting ($k(\text{ox. add.}) = 200 \text{ M}^{-1} \text{ s}^{-1}$, $k(\text{transmet.}) = 0.2 \text{ M}^{-1} \text{ s}^{-1}$, $k(\text{red. elim.}) = 200 \text{ s}^{-1}$), (c) reductive elimination rate-limiting ($k(\text{ox. Add.}) = 50 \text{ M}^{-1} \text{ s}^{-1}$, $k(\text{transmet.}) = 50 \text{ M}^{-1} \text{ s}^{-1}$, $k(\text{red. elim.}) = 0.05 \text{ s}^{-1}$).

To test the hypothesis with respect to the rate-determining step further, kinetic measurements for various concentrations of the butylzinc reagent and the catalyst were performed. Increasing $c(\text{BuZnCl/LiCl})$ from 0.4 to 0.7 M did not accelerate the reaction significantly (Figure 9.6.A), in line with the butylzinc reagent not being involved in the rate-limiting step. The small rate decrease observed for $c(\text{BuZnCl/LiCl})$ did not contradict this interpretation, but presumably mainly reflects the break-down of the approximation of a constant BuZnCl/LiCl concentration (Figure 9.6.A). Variation of the $\text{Pd(OAc)}_2/2\text{SPhos}$ concentration proves that, as expected, the catalyst participates in the rate-determining step. Also note that no cross-coupling products were detected in the absence of the catalyst. In additional experiments the SPhos/ Pd(OAc)_2 ratio was also varied. Somewhat surprisingly, changing the ratio from 2:1 to 4:1 accelerated the cross-coupling reaction, whereas an increase to 8:1 did not have any further effect (Figure 9.6.B). This observation could indicate that an excess of the SPhos ligand is needed to drive the complexation equilibrium with the in situ formed Pd(0) species to saturation. In the present experiments, any complications were avoided by keeping the SPhos/ Pd(OAc)_2 ratio and the absolute catalyst concentration fixed.

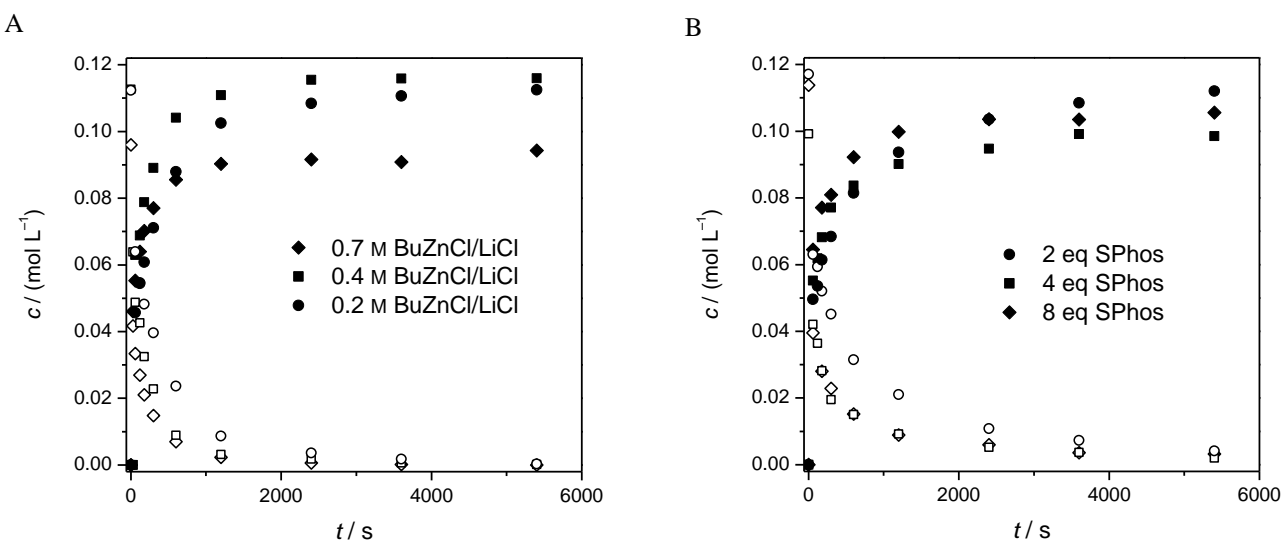


Figure 9.6.A. Time profiles of the concentrations of reactant ArI (open symbols) and of the cross-coupling product ArBu (filled symbols) formed upon reaction with different concentrations of BuZnCl/LiCl ($c = 0.70\text{ M}$ (diamonds), 0.40 M (squares), and 0.20 M (circles)) in THF at 273 K (catalyst precursor: $\text{Pd}(\text{OAc})_2/2\text{ SPhos}$, 1.00 mM). **B.** Time profiles of the concentrations of reactant ArI (open symbols) and of the cross-coupling product ArBu (filled symbols) formed upon reaction with BuZnCl ($c = 0.40\text{ M}$) in presence of catalyst precursor $\text{Pd}(\text{OAc})_2$ ($1.00\text{ mM}/2\text{ SPhos}$ (circles), $\text{Pd}(\text{OAc})_2$ ($1.00\text{ mM}/4\text{ SPhos}$ (squares) and $\text{Pd}(\text{OAc})_2$ ($1.00\text{ mM}/8\text{ SPhos}$ (diamonds) in THF at 273 K .

Homo-coupling and dehalogenation by-products. For the present model system, the homo-coupling and dehalogenation side reactions occurred to only minor extents and did not substantially compromise the yield of the cross-coupling product. Nonetheless, these processes form valuable mechanistic probes and thus deserve a closer analysis. At $t = 0$, i.e., before the addition of the catalyst, the measured concentrations of Ar_2 and ArH were negligible in all cases. This observation shows that these byproducts cannot form in the absence of the catalyst. Upon addition of the latter to a solution of ArI and BuZnCl, the concentration of the dehalogenation product ArH instantaneously shoted up whereas that of the homo-coupling product increased with a short time lag (Figure 9.7). Very similar concentration profiles were also found for reactions with the other butylzinc reagents (data not shown here).

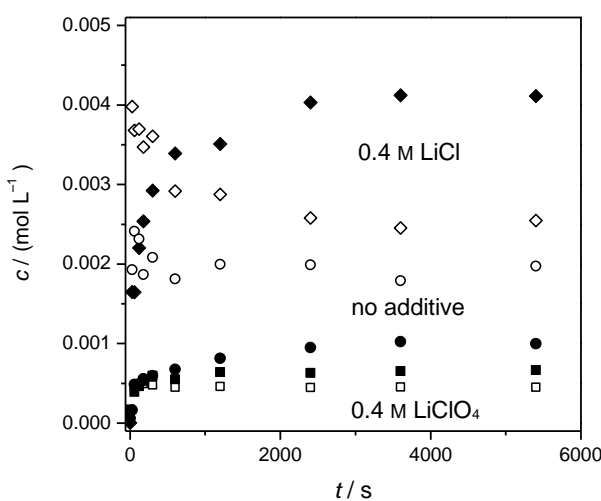
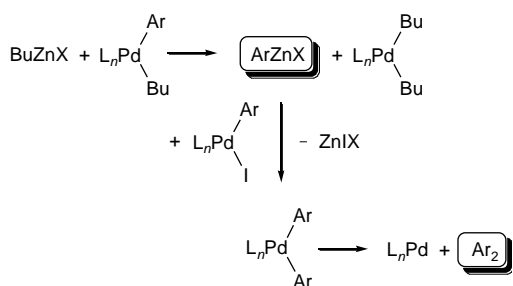


Figure 9.7. Time profiles of the concentrations of the dehalogenation product ArH (open symbols) and of the homo-coupling product Ar_2 (filled symbols) formed upon reaction of ArI with BuZnCl (0.40 M) in the presence of different LiX additives ($\text{LiCl} = \text{diamonds}$, $\text{LiClO}_4 = \text{squares}$, no additive = circles) in THF at 273 K (catalyst precursor: $\text{Pd(OAc)}_2/2\text{ SPhos}$, 1.00 mM). Note that ArH resulted from ArZnCl by a hydrolysis reaction during the aqueous work-up before the gas-chromatographic analysis.

The delayed formation of Ar_2 might indicate that it originated from the dehalogenation product. Most likely, the latter actually corresponded to ArZnX in its native state and furnished the detected ArH species only due to hydrolysis during the aqueous work-up before the gas-chromatographic analysis. For a closely related system, Lei, Wu, and coworkers have confirmed the inferred genesis of ArH by deuterium-labeling experiments.¹⁵² Given that the formation of ArZnX required the presence of the palladium catalyst, it is proposed that it originated from the conventional transmetalated $\text{L}_n\text{Pd}(\text{Ar})\text{Bu}$ intermediate by an aryl/alkyl exchange with BuZnX (Scheme 9.3); this key step resembles an aryl/aryl exchange reaction suggested by Lei, Wu, and coworkers¹⁵² and seems more probable than an aryl/alkyl exchange between $\text{L}_n\text{Pd}(\text{Ar})\text{I}$ and BuZnX . While the concomitantly generated L_nPdBu_2 supposedly underwent reductive elimination,¹⁶¹ ArZnX could transmetalate $\text{L}_n\text{Pd}(\text{Ar})\text{I}$ (formed from the primary oxidative addition of ArI) to yield $\text{L}_n\text{Pd}(\text{Ar})_2$. The latter then released the homo-coupling product Ar_2 in a reductive elimination and regenerated the catalyst. Note that for the $\text{L}_n\text{Pd}(\text{Ar})\text{Bu}$ intermediate, the aryl/alkyl exchange reaction affording ArZnX directly competed with the reductive elimination of the ArBu cross-coupling product. Therefore, increasing the $\text{BuZnX}/\text{catalyst}$ ratio should favor the formation of the dehalogenation product. The measured concentration profiles of ArH indeed clearly followed the predicted trend

(Note that not all data of the dehalogenation and homocoupling product are shown here). As expected, the behavior observed for the coupling product is more complex because its formation involved the reaction with a further palladium species (Scheme 9.3).



Scheme 9.3. Proposed genesis of the byproducts ArZnX and Ar_2 .

A comparison of the reactions employing BuZnCl , BuZnBr , and BuZnI showed that similar levels of dehalogenation and homo-coupling products were afforded. In contrast, Bu_2Zn gave much higher amounts of these byproducts. The presence of LiCl (Figure 9.7), $\text{LiBr}/\text{ZnBr}_2$, and LiI also gave rise to increased levels of ArH and Ar_2 , whereas the treatment with LiClO_4 or additional SPhos had the opposite effect. The presence of LiBr (without added ZnBr_2) somewhat suppressed the dehalogenation reaction, but enhanced the homo-coupling. These different tendencies toward the formation of side products presumably largely reflect the different efficiencies of the aryl/alkyl exchange reactions between the butylzinc reagents and $\text{L}_n\text{Pd}(\text{Ar})\text{Bu}$. For example, the particularly high amount of byproducts observed for the reactions employing Bu_2Zn can be ascribed to its enhanced electron density, which should favor the exchange of a butyl substituent for the less electron-rich aryl group.

Kinetic modeling.^{162,163} Further insight could be gained from a quantitative analysis of the measured concentration profiles. Such an analysis is challenging due to the formidable complexity of the model system. Therefore a stepwise approach was chosen: First, the cross-coupling reaction path was considered and the minor side reactions affording the dehalogenation and homo-coupling products was neglected. In the second step, the derived simplified model was extended by also including the side reactions. The large amount of experimental data finally permitted extensive cross-checks and a critical analysis of the modeling results.

Depending on the nature of the rate-determining step, the conventional catalytic cycle predicts linear or exponential decreases of the ArI concentration in the model reaction (see above). Although

the simple exponential decay (expected for the oxidative addition being rate-limiting) mimics the measured data better than a linear decrease (expected for the transmetalation or the reductive elimination being rate-limiting), it fails to reproduce the experiment in a satisfactory manner (Figure 9.8, light grey line).

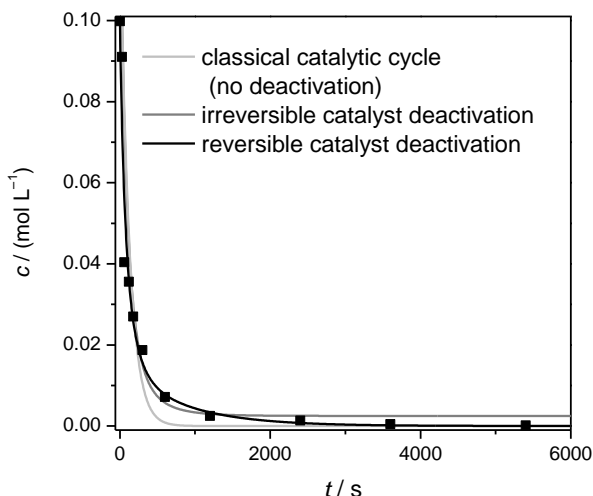
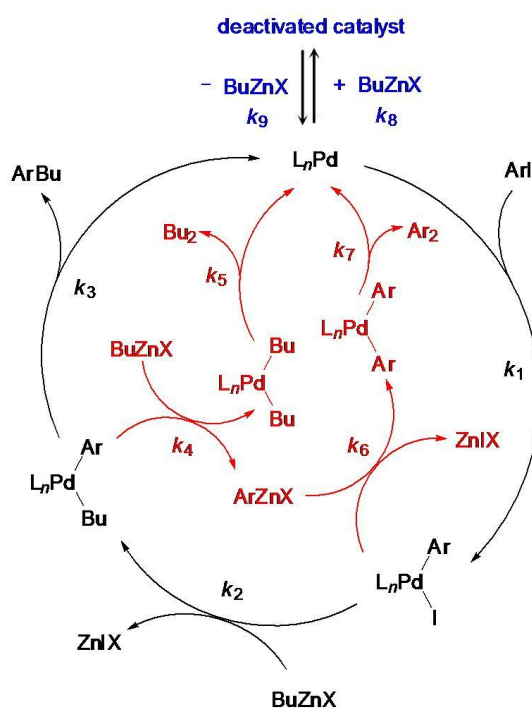


Figure 9.8. Time profile of the concentrations of reactant ArI (filled symbols) in the reaction with BuZnCl/LiCl (0.40 M) in THF at 273 K (catalyst: Pd(OAc)₂/2 SPhos, 1.00 mM). Fits for three different kinetic models are shown: conventional catalytic cycle without catalyst deactivation (Scheme 9.1, light grey line), catalytic cycle modified by irreversible reaction with the butylzinc reagent (grey line), and catalytic cycle modified by reversible reaction with the butylzinc reagent (black line).

The origin of this failure can be traced back to a bimodal nature of the measured concentration profiles. As a close inspection showed, all obtained ArI curves exhibit a steep decrease for the very first data points ($t \leq 120$ s) and then displayed a significantly slower decline for longer reaction times. The initial steep decrease was particularly pronounced for the experiments that employed Bu₂Zn, BuZnCl/LiCl, and BuZnBr/LiBr, and those that use a higher SPhos/Pd(OAc)₂ ratio; in contrast, it was least distinct for the reactions with BuZnI. The question arose whether this behavior could possibly result from an artifact. It was considered both imperfect mixing after addition of the catalyst and an imperfect temperature control. A poor mixing of the reaction solution should lead to a rate decrease, but not to an increase, however, and, thus, cannot explain these observations. For checking for a possible overheating of the the reaction mixture, its temperature was monitored. The temperature actually rose by $\Delta T < 2$ K after the addition of the catalyst and then slowly fell to its initial value again. This rather small change appears insufficient to cause the observed effect.

In further control experiments, the concentration of the active BuZnX reagents was determined after completion of the model reaction and further reactant ArI was added. Iodometric titration³⁹ found the expected amount of BuZnX and, thus, excluded the occurrence of hydrolysis or other decomposition reactions. Upon the addition of further ArI, the cross-coupling restarted again and thereby proves that the catalyst is still active in the reactions with BuZnCl/LiCl and BuZnI/LiI. The renewed reaction appeared to be slower than at the very beginning, though. This behavior points to a partial deactivation of the catalyst directly after its addition to the solution of ArI and the butylzinc reagent; such a deactivation can also explain the consistently found bimodal behavior. The present kinetic experiments alone obviously could not identify the nature of the inferred deactivated catalyst. Previous theoretical calculations on a related Negishi cross-coupling reaction suggest, however, that Pd(0) species could form complexes with zinc compounds.¹⁴³ It seemed possible that similar complexes were also generated in the present experiments, thus leading to the partial deactivation of the catalyst. If an irreversible formation of an inactive, complexed catalyst is assumed, the corresponding fit reproduced the measured data better than the simple exponential decay, but overestimated the ArI concentration at long reaction times (Figure 9.8, dark grey line). Including the reverse reaction (dissociation of the complexed catalyst) in our preliminary kinetic model leads to an almost perfect agreement of the resulting fit with the experiment (Figure 9.8, black line). The same kinetic scheme also affords satisfactory to excellent fits for all other kinetic measurements. The full kinetic model (Scheme 9.4) can now be constructed by combining the conventional catalytic cycle (k_1-k_3) with the reactions causing deactivation of the catalyst (k_8 and k_9) and those affording the dehalogenation and homo-coupling products (k_4-k_7).



Scheme 9.4. Full kinetic scheme used for the modeling.

The obtained fits reproduced the measured kinetic data quite well (Figure 9.9), which perhaps is not surprising, given the considerable flexibility of the model.

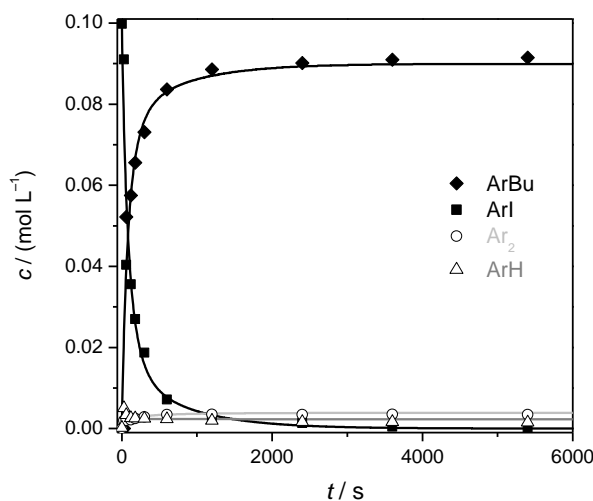


Figure 9.9. Time profiles of the concentrations of reactant ArI (filled square) and of the products ArBu (cross-coupling product, filled diamonds), ArH (dehalogenation product, open triangles), and Ar₂ (homo-coupling product, open circles) formed in the reaction with BuZnCl/LiCl (0.40 M) in THF at 273 K (catalyst precursor: Pd(OAc)₂/2 SPhos, 1.00 mM) together with fits based on the kinetic model defined in Scheme 9.4.

Within the kinetic model, the rate constant of the oxidative addition (k_1) should be the same in all of the experiments. This constancy was fulfilled only very approximately, with $10 \leq k_1 \leq 100 \text{ L mol}^{-1} \text{ s}^{-1}$ for the far majority of the fits. Apparently, the model applied achieved merely a semiquantitative description of the experiment. The rate constants derived for the transmetalation and the reductive elimination (k_2 and k_3 , respectively) are quite high and associated with large uncertainties; this finding corroborated the hypothesis that these reactions are not rate-limiting. Similarly high rate constants with large uncertainties were also obtained for the reactions affording the dehalogenation and homo-coupling products (k_4 - k_7). The rate constants determined for the complexation of the catalyst and the back reaction (k_8 and k_9 , respectively) exhibit comparably smaller relative uncertainties and, thus, permit a meaningful analysis. The ratio k_8/k_9 corresponds to the equilibrium constant K_{complex} , which is of the order of $K_{\text{complex}} \approx 10^2 \text{ L mol}^{-1}$. This value suggests that under the given experimental conditions most of the catalyst is present in its deactivated form (once the equilibrium was reached). The derived constants K_{complex} also seem to depend on the nature of the BuZnX reagent and the presence of salt additives. The addition of LiCl, LiBr, and LiI lowered K_{complex} and thus reduced the extent of catalyst deactivation. This trend is in line with the more pronounced initial steep decrease of the ArI concentration observed in the experiments with added X (X = Cl, Br, and I, see above). Two factors can account for this behavior: (i) The presence of LiX leads to the formation of butylzincate species $\text{Li}^+\text{BuZnX}_2^-$,^{85,93,94,97,110} which may be less likely to deactivate the palladium catalyst by complexation. (ii) The added LiX can stabilize the active catalyst by coordination, thus yielding L_nPdX^- palladate species.¹⁴³ The involvement of palladates, which have been neglected in this kinetic model, may also explain the imperfect consistency of the fitting results.

Conclusion

Kinetic experiments showed that the palladium-catalyzed cross-coupling between ArI and the butylzinc reagents BuZnCl, BuZnBr, and Bu₂Zn yielding ArBu occurred with high efficiency; only the reaction with BuZnI was significantly slower. In agreement with previous reports,^{92,93} the cross-coupling reactions can be accelerated by the addition of lithium halides LiX, whereas LiClO₄ had a smaller effect. The model reaction showed a high chemoselectivity and afforded only small amounts of dehalogenation and homo-coupling byproducts (< 10% except for the case of Bu₂Zn). Concentration-dependent experiments point to the oxidative addition as the rate-determining step of the model reaction. The same result is also derived from a qualitative analysis of the time profiles of

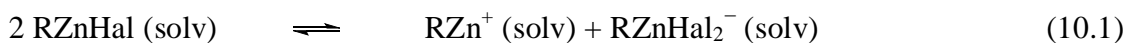
the ArI concentrations. A closer inspection showed that these time profiles are bimodal, with a steep initial decrease and a slower decline at longer reaction times. Such a bimodal nature cannot be explained by the conventional catalytic cycle, but instead indicates the operation of additional processes. The observed reaction slowdown is ascribed to a deactivation of the catalyst after its contact with the BuZnX reagent. If the reversible formation of such deactivated complexes is included in the kinetic model, the observed bimodal behavior is correctly reproduced. In the full kinetic model, not only the reversible catalyst deactivation is incorporated, but also those reactions that gave rise to the dehalogenation and homo-coupling byproducts. The fits calculated with this model describe the measured concentration profiles of all detected species quite well. The internal consistency of the derived rate constants is only modest, however. Possibly, the imperfect performance of the model resulted from the neglect of further reaction pathways. Nonetheless, quantitative analysis fully corroborated the notion that the oxidative addition corresponds to the rate-determining step of the model reaction. It is the $L_nPd(0)$ state upon which the salt additives act, either directly by stabilizing it, or indirectly by impairing its deactivation.

As the present example shows, kinetic experiments performed under realistic reaction conditions can provide valuable information. Spectroscopic studies aiming at the identification of catalytic intermediates promise complementary insight. With the combination of these different approaches, it can thus be hoped to achieve a comprehensive understanding of the Negishi reaction.

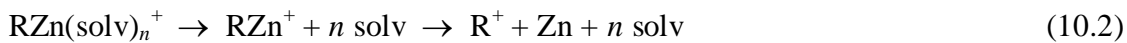
10 Summary

The research topic of this thesis was the detailed characterization of organozinc intermediates. To do so, conventional analytical methods, such as NMR spectroscopy and electrical conductivity measurements, and especially electrospray ionization (ESI) mass spectrometry were employed, the latter being a particularly useful tool to probe ionic intermediates. Tandem mass spectrometry was applied to study the reactivity of mass selected ionic intermediates in the gas phase. Hence, it could be observed how the reactivity of these zinc species was affected by bound solvent molecules, different ligands and aggregation states on a molecular level. The thus gained mechanistic insight will provide a good way to the development of new synthetic methods in the future and catalyst optimization.

As a start, solutions of butylzinc iodide in THF, acetonitrile, and DMF were analyzed by ESI mass spectrometry and micro-solvated $\text{BuZn}(\text{solvent})_n^+$ cations, $n = 1\text{-}3$ were detected, in all cases. Anion-mode mass spectrometry analysis of these solutions in THF and DMF showed presence of the organozincate anions ZnBuI_2^- . Similar results were obtained for the experiments of BnZnBr and RZnI ($\text{R} = \text{Me, } i\text{Pr}$) in THF. It was assumed that these formed ions were generated by disproportionation of neutral RZnX ($\text{R} = \text{Me, } i\text{Pr, Bu, and Bn}$) (Eq. 10.1).



The main driving force for this reaction was believed to be the coordination of the Lewis-basic solvent molecules to the RZn^+ cation. The ability of the different solvents to ionize the butyl zinc iodide compounds decreased in the order DMF > THF > acetonitrile. Upon CID additional insight on the stabilization of the $\text{RZn}(\text{solvent})_n^+$ cation was gained. The cations lost the attached solvent molecules to form bare RZn^+ , which further dissociated into R^+ cation and neutral Zn (Eq. 10.2).



The same behavior was also found for $\text{RZn}(\text{H}_2\text{O})^+$, which originated from the reaction of RZn^+ with background water. To gain further insight into the interaction of organozinc cations with different Lewis bases, the effect of chelating ligands was investigated.

The addition of bidentate chelating ligands (1,2-dimethoxyethane **L1**, *N,N*-dimethyl-2-

methoxyethylamine **L2**, and *N,N,N',N'*-tetramethylethylenediamine **L3**) to THF solutions of butylzinc iodide largely displaced THF from the coordination sphere of the metal center and formed preferentially mononuclear chelate complexes $\text{BuZn}(\text{ligand})^+$. Gas-phase experiments resulted in the fragmentation of $\text{BuZn}(\text{ligand})^+$ by elimination of butene and formation of the hydridozinc cations $\text{ZnH}(\text{ligand})^+$ (Eq. 10.3).

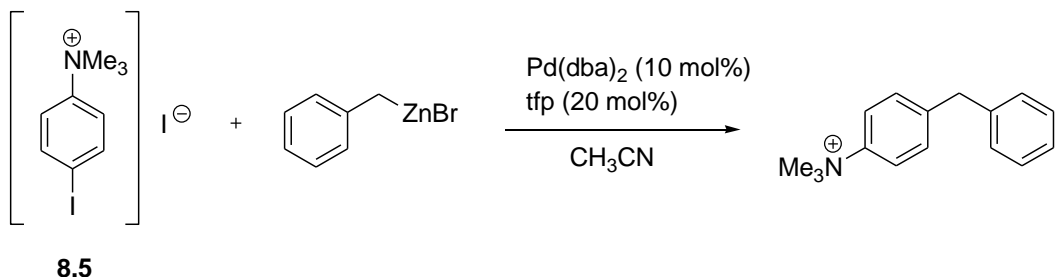


This fragmentation behavior was in stark contrast to that of the micro-solvated $\text{BuZn}(\text{solvent})_n^+$ complexes and proved that the chelating ligands bound much more strongly to the zinc center than the probed solvents. It could be suggested that the energy gained from the chelation exceeded the barrier associated with the elimination of butene. This difference in reactivity resembled the situation in organozinc solution chemistry, where chelating ligands were needed to activate dialkylzinc compounds for the nucleophilic addition to aldehydes.

Next, a combination of ESI mass spectrometry, electrical conductivity measurements, and NMR spectroscopy was used to investigate the effect of LiCl on solutions of organylzinc halides RZnX ($\text{R} = \text{Bu, Bn, Ph}$; $\text{X} = \text{halogen}$) and dibutylzinc in THF. In the case of RZnX , the addition of LiX ($\text{X} = \text{Cl}$) led to a steep rise of the ESI signal intensities of RZnX_2^- . Besides, the electrical conductivities strongly increased and the NMR absorptions of the α -H atoms of BuZnX shifted upfield. These results consistently pointed to the formation of lithium organozincates $\text{Li}^+\text{RZnX}_2^-$. As the most common syntheses of RZnX reagents involve stoichiometric amounts of LiX salts, $\text{Li}^+\text{RZnX}_2^-$ complexes are supposedly widespread and may hold the key to understanding the marked effects of LiCl on the reactivity of organozinc halides. In contrast, it was found that Bu_2Zn had a much lower tendency to add LiCl and form ate complexes. This result was in line with the weak effect of LiCl on the reactivity of diorganozinc compounds reported in the literature.⁹⁵ The used analytical methods were also applied for the investigation of the LiCl effect on solutions of $i\text{PrMgCl}$. The situation was in this case far more complex. Although the electrical conductivities strongly increased upon addition of LiCl, the α -H atoms of $i\text{PrMgCl}$ just shifted insignificantly and the analyses of $i\text{PrMgCl}$ solutions by ESI mass spectrometry resulted only in the detection of inorganic magnesium halides. These results did not allow a satisfying statement of the aggregation of this magnesium reagent.

Furthermore, several geminal diiodides were prepared from the corresponding iodides and their reactions with zinc in DMF were analyzed by ESI mass spectrometry. The measurements resulted in the detection of organozinc cations and anions. Upon CID the formation of a neutral fragment corresponding to a formal carbene was observed. The detection of a carbene would support the carbenoid character of the organozinc compounds, which was already assumed for the Simmons-Smith reagents.

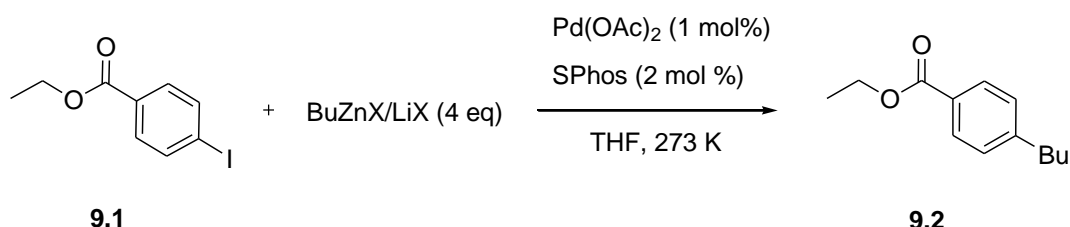
Organic iodides bearing a cationic quaternary ammonium group at a remote position were synthesized and allowed to react with zinc. The resulting charge-tagged organometallics could be detected by ESI mass spectrometry, which provided detailed information on their stoichiometry and coordination sphere. Moreover, the proposed charge-tagging approach also lent itself to reactivity studies. A Pd-catalyzed Negishi cross-coupling of an ammonium-tagged organyl iodide with benzylzinc bromide was performed (Scheme 10.1) and the consumption of the electrophile and the formation of the product could be conveniently monitored by ESI mass spectrometry.



Scheme 10.1. Reaction of **8.5** with benzylzinc bromide as test system for monitoring cross-coupling reaction using ESI mass spectrometry.

The results clearly showed that here the oxidative addition was the rate-limiting step and the second-order rate constant could be determined.

At last, gas chromatography was used to study the kinetics of the palladium/SPhos-catalyzed Negishi cross-coupling reaction of ethyl 4-iodo-benzoate with various butylzinc reagents in THF (Scheme 10.2).



Scheme 10.2. Model reaction investigated.

Concentration-dependent experiments as well as kinetic modeling consistently pointed to the oxidative addition as the rate-determining step of these reactions. The bimodal nature of the measured kinetic profiles moreover indicates that the contact with the butylzinc reagents partially deactivates the catalyst. Salt additives, such as LiCl, LiBr, and LiI, counteract this deactivation and, thus accelerate the cross-coupling reaction. Added salts also affect the formation of dehalogenation and homo-coupling byproducts, which are observed in only rather small abundance, though.

11 References and Notes

- 1 S. P. Palii, D. V. Zagorevskii, in *The Chemistry of Organozinc Compounds*, (Eds.: Z. Rappoport, I. Marek), Wiley, Chichester, **2006**, pp. 163.
- 2 E. Frankland, *Liebigs Ann. Chem.* **1849**, 71, 171.
- 3 E. Frankland, *Liebigs Ann. Chem.* **1849**, 71, 213.
- 4 D. Seyferth, *Organometallics* **2001**, 20, 2940.
- 5 V. Grignard, *Compt. Rend. Acad. Sci. Paris* **1900**, 130, 1322.
- 6 (a) S. Reformatsky, *Chem. Ber.* **1887**, 20, 1210. (b) S. Reformatsky, *Chem. Ber.* **1895**, 28, 2842. (c) A. Fürstner, *Angew. Chem. Int. Ed.* **1993**, 32, 164.
- 7 (a) H. E. Simmons, R. D. Smith, *J. Am. Chem. Soc.* **1958**, 80, 5323. (b) H. E. Simmons, T. L. Cairns, A. Vladuchick, C. M. Hoiness, *Org. React.* **1973**, 20, 1. (c) J. Furukawa, N. Kawabata, J. Nishimma, *Tetrahedron Lett.* **1966**, 7, 3353. (d) M. Nakamura, A. Hirai, E. Nakamura, *J. Am. Chem. Soc.* **2003**, 125, 2341. (e) E. Nakamura, K. Sekiya, I. Kuwajima, *Tetrahedron Lett.* **1987**, 28, 337.
- 8 H. Hunsdiecker, H. Erlbach, E. Vogt, *German Patent 722467*, **1942**.
- 9 (a) K. Tagaki, N. Hayama, S. Inokawa, *Bull. Chem. Soc. Jpn.* **1980**, 53, 3691. (b) K. Tagaki, *Chem. Lett.* **1994**, 469. (c) K. Tagaki, Y. Shimoishi, K. Sasaki, *Chem. Lett.* **1994**, 23, 2055. (d) T. N. Majid, P. Knochel, *Tetrahedron Lett.* **1990**, 31, 4413.
- 10 M. Gaudemar, *Bull. Soc. Chim. Fr.* **1962**, 974.
- 11 S. C. Berk, M. C. P. Yeh, N. Jeong, P. Knochel, *Organometallics* **1990**, 9, 3053.
- 12 (a) K. Takagi, *Chem. Lett.* **1993**, 469. (b) R. Ikegami, A. Koresawa, T. Shibata, K. Takagi, *J. Org. Chem.* **2003**, 68, 2195.
- 13 C. S. Dexter, R. F. W. Jackson, *Chem. Commun.* **1998**, 75.
- 14 H. Fillon, C. Gosmini, J. Périchon, *J. Am. Chem. Soc.* **2003**, 125, 3867.
- 15 S. Huo, *Org. Lett.* **2003**, 5, 423.
- 16 (a) R. D. Rieke, *Science* **1989**, 246, 1260. (b) L. Zhu, R. M. Wehmeyer, R. D. Rieke, *J. Org. Chem.* **1991**, 56, 1445.
- 17 (a) A. Krasovskiy, V. Malakhov, A. Gavryushin, P. Knochel, *Angew. Chem. Int. Ed.* **2006**, 45, 6040. (b) H. Ren, G. Dunet, P. Mayer, P. Knochel, *J. Am. Chem. Soc.* **2007**, 129, 5376. (c) N. Boudet, S. Sase, P. Sinha, C.-Y. Liu, A. Krasovskiy, P. Knochel, *J. Am. Chem. Soc.*

- 2007, 129, 12358.
- 18 For an earlier investigation, see: Z. Huang, M. Qian, D. J. Babinski and E. Negishi, *Organometallics* **2005**, 24, 475.
- 19 P. Knochel, H. Leuser, L.-Z. Gong, S. Perrone, F. F. Kneisel in *Handbook of Functionalized Organometallics, Vol. 1* (Ed.: P. Knochel), Wiley-VCH, Weinheim, **2005**, pp. 251.
- 20 (a) E. Negishi, S. Baba, *J. Chem. Soc., Chem. Commun.* **1976**, 596. (b) E. Negishi, S. Baba, *J. Am. Chem. Soc.* **1977**, 98, 6729. (c) E. Negishi, A. O. King, N. Okukado, *J. Org. Chem.* **1977**, 42, 1821. (d) E. Negishi, *J. Organomet. Chem.* **2002**, 653, 64.
- 21 (a) M. R. Netherton, G. C. Fu, *Adv. Synth. Catal.* **2004**, 346, 1525. (b) A. C. Frisch, M. Beller, *Angew. Chem. Int. Ed.* **2005**, 44, 674. (c) E. Negishi, Q. Hu, Z. Huang, G. Wang, N. Yin, in *The Chemistry of Organozinc Compounds*, (Eds.: Z. Rappoport, I. Marek), Wiley, Chichester, **2006**, pp. 457. (d) V. B. Phapale, D. J. Cárdenas, *Chem. Soc. Rev.* **2009**, 38, 1598. (e) S. Calimsiz, M. Sayah, D. Mallik, M. G. Organ, *Angew. Chem. Int. Ed.* **2010**, 49, 2014.
- 22 (a) E. Negishi, Z. Huang, G. Wang, S. Mohan, C. Wang, H. Hattori, *Acc. Chem. Res.* **2008**, 41, 1474. (b) G. C. Fu, *Acc. Chem. Res.* **2008**, 41, 1551. (c) T. Thaler, B. Haag, A. Gavryushin, K. Schober, E. Hartmann, R. M. Gschwind, H. Zipse, P. Mayer, P. Knochel, *Nature Chem.* **2010**, 2, 125 (d) A. Krasovskiy, C. Duplais, B. H. Lipshutz, *Org. Lett.* **2010**, 12, 4742. (g) N. Hadei, G. T. Achonduh, C. Valente, C. J. O'Brien, M. G. Organ, *Angew. Chem. Int. Ed.* **2011**, 50, 3896. (h) A. Krasovskiy, B. H. Lipshutz *Org. Lett.* **2011**, 13, 3822.
- 23 C. Elschenbroich, *Organometallics*, Wiley-VCH, Weinheim, **2006**, 3rd ed.
- 24 M. Yamashita, J. B. Fenn, *J. Phys. Chem.* **1984**, 88, 4451.
- 25 (a) D. A. Plattner, *Int. J. Mass Spectrom.* **2001**, 207, 125. (b) P. Chen, *Angew. Chem. Int. Ed.* **2003**, 42, 2832. (c) L. S. Santos, L. Knaack, J. O. Metzger, *Int. J. Mass Spectrom.* **2005**, 246, 84. (d) C. A. Müller, C. Markert, A. M. Teichert, A. Pfaltz, *Chem. Comm.* **2009**, 1607. (e) J. C. Traeger, *Int. J. Mass Spectrom.* **2000**, 200, 387.
- 26 (a) L. A. Hammad, G. Gerdes, P. Chen, *Organometallics* **2005**, 24, 1907. (b) M.-E. Moret, P. Chen, *Organometallics* **2007**, 26, 1523.
- 27 R. B. Cole, *J. Mass Spectrom.* **2000**, 35, 763.
- 28 (a) K. Koszinowski, P. Böhrer, *Organometallics* **2009**, 28, 100. (b) K. Koszinowski, P. Böhrer, *Organometallics* **2009**, 28, 771.
- 29 J. H. Gross, *Mass Spectrometry*, Springer-Verlag, Berlin Heidelberg, **2004**.

- 30 M. Dole, L. L. Mack, R. L. Hines, R. C. Mobley, L. D. Ferguson, M. B. Alice, *J. Chem. Phys.* **1968**, *49*, 2240.
- 31 (a) J. B. Fenn, M. Mann, C. K. Meng, S. F. Wong, C. M. Whitehouse, *Science* **1989**, *246*, 64. (b) J. B. Fenn, *J. Am. Soc. Mass Spectrom.* **1993**, *4*, 524.
- 32 N. B. Cech, C. G. Enke, *Mass Spectrom. Rev.* **2001**, *20*, 362.
- 33 E. de Hoffmann, V. Stroobant, *Mass Spectrometry*, 3rd ed., Wiley Chichester, **2007**.
- 34 R. A. J. O'Hair, *Chem. Commun.* **2006**, 1469.
- 35 K. Koszinowski, *J. Am. Chem. Soc.* **2010**, *132*, 6032.
- 36 A. Putau, K. Koszinowski, *Organometallics* **2010**, *29*, 3593. Addition/correction: A. Putau, K. Koszinowski, *Organometallics* **2010**, *29*, 6841.
- 37 H. M. McNair, J. M. Miller, *Basic Gas Chromatography*, 2nd ed., Wiley-VCH, Weinheim, **2009**.
- 38 S. Cacchi, F. La Torre, D. Misti, *Synthesis* **1977**, *5*, 301.
- 39 A. Krasovskiy, P. Knochel, *Synthesis* **2006**, *5*, 890.
- 40 I. Rilatt, R. F. W. Jackson, *J. Org. Chem.* **2008**, *73*, 8694.
- 41 F. F. Kneisel, dissertation, LMU Munich, 2003.
- 42 H. K. Hofstee, J. Boersma, J. D. van der Meulen, G. J. M. van der Kerk, *J. Organomet. Chem.* **1978**, *153*, 245.
- 43 P. R. Markies, G. Schat, O. S. Akkermann, F. Bickelhaupt, *J. Organomet. Chem.* **1992**, *430*, 1.
- 44 (a) 2-*D,D*-butyl bromide was bought at Dr. Ehrenstorfer GmbH, Augsburg. (b) C. Müller, diploma thesis, LMU Munich, 2009.
- 45 Calculations of the temperature-dependent changes in sample volumes and, thus, in concentrations were based on data from: C. Carvajal, K. J. Tölle, J. Smid, M. Szwarc, *J. Am. Chem. Soc.* **1965**, *87*, 5548.
- 46 W. Lin, L. Chen, P. Knochel, *Tetrahedron* **2007**, *63*, 2787.
- 47 P. J. Garreg, B. Samuelsson, *J. Chem. Soc. Chem. Commun.* **1979**, 978.
- 48 J. A. Bull, A. B. Charette, *J. Org. Chem.* **2008**, *73*, 8097.
- 49 M. Müller, M. Brönstrup, O. Knopff, V. Schulze, R. W. Hoffmann, *Organometallics* **2003**, *22*, 2931.
- 50 J. Pliml, M. Borovička, M. Protiva, *Collect. Czech. Chem. Commun.*, **1958**, *23*, 704.

- 51 G. Manolikakes, M. A. Schade, C. Muñoz Hernandez, H. Mayr, P. Knochel *Org. Lett.* **2008**, *10*, 2765.
- 52 K. Mitsudo, T. Shiraga, D. Kagen, D. Shi, J. Y. Becker, H. Tanaka *Tetrahedron* **2009**, *65*, 8384.
- 53 Z. Rappoport, I. Marek, *The Chemistry of Organozinc Compounds*, Wiley, Chichester, **2006**.
- 54 (a) P. Knochel, R. D. Singer, *Chem. Rev.* **1993**, *93*, 2117. (b) P. Knochel, *Synlett* **1995**, 393.
- 55 P. Knochel, J. J. A. Perea, P. Jones, *Tetrahedron* **1998**, *54*, 8275.
- 56 (a) K. Soai, *Enantiomer* **1999**, *4*, 591. (b) C. Gosmini, Y. Rollin, J. Y. Nédélec, J. Périchon, *J. Org. Chem.* **2000**, *65*, 6024.
- 57 (a) H. Fillon, E. Le Gall, C. Gosmini, J. Périchon, *Tetrahedron Lett.* **2002**, *43*, 5941. (b) I. Kazmierski, C. Gosmini, J.-M. Paris, J. Périchon, *Synlett* **2006**, 881.
- 58 (a) R. F. W. Jackson, R. J. Moore, C. S. Dexter, J. Elliott, C. E. Mowbray, *J. Org. Chem.* **1998**, *63*, 7875. (b) N. Kurono, K. Sugita, S. Takasugi, M. Tokuda, *Tetrahedron* **1999**, *55*, 6097. (c) C. S. Dexter, R. F. W. Jackson, J. Elliott, *J. Org. Chem.* **1999**, *64*, 7579. (d) C. Hunter, R. F. W. Jackson, H. K. Rami, *J. Chem. Soc., Perkin Trans 1* **2000**, 219. (e) S. Peng, F.-L. Qing, Y.-Q. Li, C.-M. Hu, *J. Org. Chem.* **2000**, *65*, 694. (f) A. M. Egorov, *J. Phys. Org. Chem.* **2006**, *19*, 664.
- 59 R. Duddu, M. Eckhardt, M. Furlong, H. P. Knoess, S. Berger, P. Knochel, *Tetrahedron* **1994**, *50*, 2415.
- 60 I. Rilat, L. Caggiano, R. F. W. Jackson, *Synlett* **2005**, *18*, 2701.
- 61 C. S. Dexter, C. Hunter, R. F. W. Jackson, J. Elliot, *J. Org. Chem.* **2000**, *65*, 7417.
- 62 L. Caggiano, R. F. W. Jackson, A. J. H. M. Meijer, B. T. Pickup, K. A. Wilkinson, *Chem. Eur. J.* **2008**, *14*, 8798.
- 63 M. Driess, K. Merz, R. Schoenen, *Organometallics* **2007**, *26*, 2133.
- 64 The given value refers to the benzylic radical, see: G. C. Eiden, F. Weinhold, J. C. Weisshaar, *J. Chem. Phys.* **1991**, *95*, 8665. The ionization energy of the cycloheptatrienyl radical is even lower, $IE = 6.28$ eV, see: T. Koenig, J. C. Chang, *J. Am. Chem. Soc.* **1978**, *100*, 2240.
- 65 R. D. Lide (ed.), *CRC Handbook of Chemistry and Physics*, 88th ed., CRC Press, Boca Raton, **2008**.
- 66 The given value refers to the 1-butyl radical: J. C. Schultz, F. A. Houle, J. L. Beauchamp, *J. Am. Chem. Soc.* **1984**, *106*, 3917. The ionization energy of the tert-butyl radical is even

- lower: F. A. Houle, J. L. Beauchamp, *J. Am. Chem. Soc.* **1979**, *101*, 4067.
- 67 Fragmentation of the organozincate ion yields I⁻ and BuZnI, as already reported in 28b.
- 68 The bromine present in these species originated from the use of 1,2-dibromomethane for the zinc activation (see Experimental Section)
- 69 S. E. Denmark, G. L. Beutner, *Angew. Chem. Int. Ed.* **2008**, *47*, 1560.
- 70 C. Elschenbroich, *Organometallchemie*, 6th ed., Teubner Verlag, Wiesbaden, **2008**.
- 71 (a) R. M. Fabicon, A. D. Pajerski, H. G. Richey, Jr., *J. Am. Chem. Soc.* **1993**, *115*, 9333. (b) A. D. Pajerski, J. E. Chubb, R. M. Fabicon, H. G. Richey, Jr., *J. Org. Chem.* **2000**, *65*, 2231.
- 72 (a) H. G. Richey, Jr., B. A. King, *J. Am. Chem. Soc.* **1982**, *104*, 4672. (b) E. P. Squiller, R. R. Whittle, H. G. Richey, Jr., *J. Am. Chem. Soc.* **1985**, *107*, 432. (c) H. G. Richey, Jr., D. M. Kushlan, *J. Am. Chem. Soc.* **1987**, *109*, 2510. (d) A. D. Pajerski, M. Parvez, H. G. Richey, Jr., *J. Am. Chem. Soc.* **1988**, *110*, 2660.
- 73 (a) R. M. Fabicon, A. D. Pajerski, H. G. Richey, Jr., *J. Am. Chem. Soc.* **1991**, *113*, 6680. (b) R. M. Fabicon, M. Parvez, H. G. Richey, Jr., *Organometallics* **1999**, *18*, 5163. (c) H. Tang, M. Parvez, H. G. Richey, Jr., *Organometallics* **2000**, *19*, 4810.
- 74 C. Reichhardt, *Solvents and Solvent Effects in Organic Chemistry*, 3rd ed., Wiley-VCH, Weinheim, **2003**.
- 75 J. E. Fleckenstein, K. Koszinowski, *Chem. Eur. J.* **2009**, *15*, 12745.
- 76 (a) M. Kitamura, S. Suga, K. Kawai, R. Noyori, *J. Am. Chem. Soc.* **1986**, *108*, 6071. (b) R. Noyori, M. Kitamura, *Angew. Chem. Int. Ed.* **1991**, *30*, 49. (c) K. Soai, S. Niwa, *Chem. Rev.* **1992**, *92*, 833.
- 77 (a) Y. L. Bennani, S. Hanessian, *Chem. Rev.* **1997**, *97*, 3161. (b) J.-C. Kizirian, *Chem. Rev.* **2008**, *108*, 140.
- 78 R. Noyori, S. Suga, K. Kawai, S. Okada, M. Kitamura, N. Oguni, M. Hayashi, T. Kaneko, Y. Matsuda, *J. Organomet. Chem.* **1990**, *382*, 19.
- 79 (a) L. Tang, P. Kebarle, *Anal. Chem.* **1993**, *65*, 3654. (b) I. Leito, K. Herodes, M. Huopolainen, K. Virro, A. Künnapas, A. Kruve, R. Tanner, *Rap. Comm. Mass Spectrom.* **2008**, *22*, 379.
- 80 (a) R. E. Linney, D. K. Russell, *J. Mater. Chem.* **1993**, *3*, 587. (b) K. Maejima, H. Kawabata, S. Fujita, *Jpn. J. Appl. Phys.* **2008**, *47*, 1098. (c) Y. S. Kim, Y. S. Won, H. Hagelin-Weaver, N. Omenetto, T. Anderson, *J. Phys. Chem. A* **2008**, *112*, 4246.

- 81 (a) K. Maejima, H. Kawabata, S. Fujita, *Japan. J. of Appl. Phys.* **2008**, *47*, 1089. (b) Y. S. Kim, Y. S. Won, H. Hagelin-Weaver, N. Omenetto, T. Anderson, *J. Phys. Chem. A* **2008**, *112*, 4246.
- 82 This work was done in collaboration with C. Müller and K. Koszinowski.
- 83 S. Alridge, A. J. Downs, *Chem. Rev.* **2001**, *101*, 3305.
- 84 J. Spielmann, D. Piesik, B. Wittkamp, G. Jansen, S. Harder, *Chem. Commun.* **2009**, 3455.
- 85 C.-Y. Liu, X. Wang, T. Furuyama, S. Yasuike, A. Muranaka, K. Morokuma, M. Uchiyama, *Chem. Eur. J.* **2010**, *16*, 1780.
- 86 M. G. Organ, S. Avola, I. Dubovyk, N. Hadei, E. A. B. Kantchev, C. B. O'Brien, C. Valente, *Chem. Eur. J.* **2006**, *12*, 4749.
- 87 (a) H. Ochiai, M. Jang, K. Hirano, H. Yorimitsu, K. Oshima, *Org. Lett.* **2008**, *10*, 2681. (b) Y. Asada, S. Yasuda, H. Yorimitsu, K. Oshima, K. *Organometallics* **2008**, *27*, 6050.
- 88 K. B. Urkalan, M. S. Sigman, *J. Am. Chem. Soc.* **2009**, *131*, 18042.
- 89 D. Glynn, J. Shannon, S. Woodward, *Chem. Eur. J.* **2010**, *16*, 1053.
- 90 E. Hevia, R. E. Mulvey, *Angew. Chem. Int. Ed.* **2011**, *50*, 6448.
- 91 For a recent report of a negative effect of lithium halides on the reactivity of RZnX, however, see: A. Joshi-Pangu, M. Ganesh, M. R. Biscoe, *Org. Lett.* **2011**, *13*, 1218.
- 92 G. T. Achonduh, N. Hadei, C. Valente, S. Avola, C. J. O'Brien, M. G. Organ, *Chem. Commun.* **2010**, *46*, 4109.
- 93 H. N. Hunter, N. Hadei, V. Blagojevic, P. Patschinski, G. T. Achonduh, S. Avola, D. K. Bohme, M. G. Organ, *Chem. Eur. J.* **2011**, *17*, 7845.
- 94 I. S. MacIntosh, C. N. Sherren, K. N. Robertson, J. D. Masuda, C. C. Pye, J. A. C. Clyburne, *Organometallics* **2010**, *29*, 2063.
- 95 F. F. Kneisel, M. Dochnahl, P. Knochel, *Angew. Chem. Int. Ed.* **2004**, *43*, 1017.
- 96 J. Estager, P. Nockemann, K. R. Seddon, M. Swadźba-Kwaśny, S. Tyrrell, *Inorg. Chem.* **2011**, *50*, 5258.
- 97 J. E. Fleckenstein, K. Koszinowski, *Organometallics* **2011**, *30*, 5018.
- 98 For selected recent examples, see: (a) S. Sase, M. Jaric, A. Metzger, V. Malakhov, P. Knochel, *J. Org. Chem.* **2008**, *73*, 7380. (b) G. Manolikakes, M. Dong, H. Mayr, J. Li, P. Knochel, *Chem. Eur. J.* **2009**, *15*, 1324. (c) T. Zhang, X. Gao, H. B. Wood *Tetrahedron Lett.* **2011**, *52*, 311.
- 99 Also note that the shift to smaller zincates corresponds to an increase of the Cl:Zn ratio, thus

- reflecting the change in the overall composition of the solution. A similar correlation has been reported for ZnCl_2^- containing ionic liquids, see ref. 96.
- 100 (a) M. Hojo, T. Ueda, Z. Chen, M. Nishimura, *J. Electroanal. Chem.* **1999**, *468*, 110. (b) D. Das, *J. Solution Chem.* **2008**, *37*, 947.
- 101 However, similar arguments cannot explain why $\text{BuZnBr}/(\text{LiCl})_n$ displays higher conductivities than $\text{BuZnI}/(\text{LiCl})_n$. Clearly, the situation here is more complex.
- 102 R. M. Fuoss, C. A. Kraus, *J. Am. Chem. Soc.* **1933**, *55*, 2387.
- 103 Note that the $(\text{THF})\text{ZnCl}_3^-$ complexes are too weakly bound to survive the ESI process, however.
- 104 M. Uchiyama, M. Kameda, O. Mishima, N. Yokoyama, M. Koike, Y. Kondo, T. Sakamoto, *J. Am. Chem. Soc.* **1998**, *120*, 4934–4946.
- 105 The related EtZnI has been shown to be monomeric in THF: M. H. Abraham, P. H. Rolfe, *J. Organomet. Chem.* **1967**, *7*, 35.
- 106 E. Hevia, J. Z. Chua, P. García-Álvarez, A. R. Kennedy, M. D. McCall, *Proc. Natl. Acad. Sci.* **2010**, *107*, 5294.
- 107 S. E. Denmark, J. P. Edwards, S. R. Wilson, *J. Am. Chem. Soc.* **1992**, *114*, 2592.
- 108 (a) J. Boersma, J. G. Noltes, *J. Organomet. Chem.* **1967**, *8*, 551. (b) D. F. Evans, G. V. Fazakerley, *J. Chem. Soc. (A)* **1971**, *182*. (c) A. J. Blake, J. Shannon, J. C. Stephens, S. Woodward, *Chem. Eur. J.* **2007**, *13*, 2462.
- 109 (a) F. M. Piller, P. Appukkuttan, A. Gavryushin, M. Helm, P. Knochel, *Angew. Chem. Int. Ed.* **2008**, *47*, 6802. (b) F. M. Piller, A. Metzger, M. A. Schade, B. A. Haag, A. Gavryushin, P. Knochel, *Chem. Eur. J.* **2009**, *15*, 7192.
- 110 (a) A. Krasovskiy, P. Knochel, *Angew. Chem. Int. Ed.* **2004**, *43*, 3333. (b) A. Krasovskiy, B. F. Straub, P. Knochel, *Angew. Chem. Int. Ed.* **2006**, *45*, 159. (c) H. Ren, P. Knochel, *Chem. Commun.* **2006**, 726. (d) C.-Y. Liu, P. Knochel, *Org. Lett.* **2005**, *7*, 2543. (e) F. Kopp, A. Krasovskiy, P. Knochel, *Chem. Commun.* **2004**, 2288.
- 111 P. Schmid, bachelor thesis, LMU Munich, 2010.
- 112 H. Ren, A. Krasovskiy, P. Knochel, *Org. Lett.* **2004**, *6*, 4215.
- 113 S. Petrie, *Environ. Chem.* **2005**, *2*, 25.
- 114 P. J. Heard, in *The Chemistry of Organomagnesium Compounds*, (Eds.: Z. Rappoport, I. Marek), Wiley, Chichester, **2008**, pp. 131.
- 115 M. A. Schade, J. E. Fleckenstein, P. Knochel, K. Koszinowski, *J. Org. Chem.* **2010**, *75*,

- 6848.
- 116 (a) J. Furukawa, N. Kawabata, *Adv.Organomet. Chem.* **1974**, *12*, 83. (b) A. Hoveyda, D. A. Evans, G. C. Fu, *Chem. Rev.* **1993**, *93*, 1307. (c) W. B. Motherwell, C. J. Nutley, *Contemp. Org. Synth.* **1994**, *1*, 219.
- 117 (a) H. E. Simmons, R. D. Smith, *J. Am. Chem. Soc.* **1959**, *81*, 4256. (b) A. B. Charette, A. Beauchemin, *Org. React.* **2001**, *58*, 1. (c) H. Lebel, J.-F. Marcoux, C. Molinaro, A. B. Charette, *Chem. Rev.* **2003**, *103*, 977.
- 118 H. E. Simmons, R. D. Smith, *J. Am. Chem. Soc.* **1959**, *81*, 4256.
- 119 (a) J. Furukawa, N. Kawabata, J. Nishimura, *Tetrahedron Lett.* **1966**, 3353. (b) J. Furukawa, N. Kawabata, J. Nishimura, *Tetrahedron* **1968**, *24*, 53.
- 120 (a) E. P. Blanchard, H. E. Simmons, *J. Am. Chem. Soc.* **1964**, *86*, 1337. (b) H. E. Simmons, E. P. Blanchard, R. D. Smith, *J. Am. Chem. Soc.* **1964**, *86*, 1347. (c) G. Wittig, F. Wingler, *F. Chem. Ber.* **1964**, *97*, 2146. (d) U. Burger, R. Huisgen, *Tetrahedron Lett.* **1970**, 3057. (e) S. Miyano, J. Yamashita, H. Hashimoto, *Bull. Chem. Soc. Jpn.* **1972**, *45*, 1946.
- 121 A. B. Charette, J-F. Marcoux, *J. Am. Chem. Soc.* **1996**, *118*, 4539.
- 122 A. B. Charette, J-F. Marcoux, F. J. Béöanger-Gariépy, *J. Am. Chem. Soc.* **1996**, *118*, 6792.
- 123 Internship K. Böck, 2009.
- 124 R. Brückner, *Reaktionsmechanismen*, 3rd ed., Elsevier GmbH Spektrum Akademischer Verlag, München, **2004**, pp. 116.
- 125 J. C. Traeger, *Int. J. Mass Spectrom.* **2000**, *200*, 387.
- 126 (a) R. Colton, J. C. Traeger, *Inorg. Chim. Acta* **1992**, *201*, 153. (b) I. Ahmed, A. M. Bond, R. Colton, M. Jurcevic, J. C. Traeger, J. N. Walter, *J. Organomet. Chem.* **1993**, *447*, 59.
- 127 D. J. F. Bryce, P. J. Dyson, B. K. Nicholson, D. G. Parker, *Polyhedron* **1998**, *17*, 2899.
- 128 (a) C. Hinderling, C. Adlhart, P. Chen, *Angew. Chem. Int. Ed.* **1998**, *37*, 2685. (b) C. Adlhart, P. Chen, *Helv. Chim. Acta* **2000**, *83*, 2192. (c) C. Adlhart, C. Hinderling, H. Baumann, P. Chen, *J. Am. Chem. Soc.* **2000**, *122*, 8204.
- 129 C. Adlhart, P. Chen. *Helv. Chim. Acta* **2000**, *86*, 941.
- 130 A. Dorcier, P. J. Dyson, U. Rothlisberger, R. Scopelliti, I. Tavernelli, *Organometallics* **2005**, *24*, 2114.
- 131 J. M. Basset, D. Bouchu, G. Godard, I. Karamé, E. Kuntz, F. Lefebre, N. Legagneux, C. Lucas, D. Michelet, J. B. Tommasino, *Organometallics* **2008**, *27*, 4300.
- 132 For a recent review, see: D. M. Chisholm, J. S. McIndoe, *Dalton Trans.* **2008**, 3933.

- 133 E. Crawford, T. Lohr, E. M. Leitao, S. Kwok, J. S. McIndoe, *Dalton Trans.* **2009**, 9110.
- 134 Prepared by Dr. M. A. Schade according to: H. Kobayashi, T. Sonada, K. Takuma, N. Honda, T. Nakata, *J. Flourine Chem.* **1985**, 27, 1.
- 135 One may speculate that the long-range electrostatic potential of the charged tag could direct water molecules into the proximity of the Zn-C bond and thus accelerate its protolysis. Note that a similar argument does not hold for the previously observed $\text{ZnR}(\text{THF})_n^+$ and RZnHal_2^- species because their equilibrium concentration is supposedly low in comparison to neutral ZnRHal .
- 136 F. Dreicker, J. Oomens, A. J. H. M. Meijer, B. T. Pickup, R. F. W. Jackson, M. Schäfer, *J. Org. Chem.* **2010**, 75, 1203.
- 137 J. Terao, N. Kambe, *Bull. Chem. Soc. Jpn.* **2006**, 79, 663.
- 138 G. J. Van Berkel, *J. Mass Spectrom.* **2000**, 35, 773.
- 139 All fits were performed by K. Koszinowski.
- 140 C. G. Enke, *Anal. Chem.* **1997**, 69, 4885.
- 141 C. Amatore, A. Jutand, F. Khalil, *Arkivoc* **2006**, 38.
- 142 (a) J. F. Fauvarque, F. Pflüger, M. Troupel, *J. Organomet. Chem.* **1981**, 208, 419. (b) A. Jutand, A. Mosleh, *Organometallics* **1995**, 14, 1810.
- 143 (a) C. Amatore, M. Azzabi, A. Jutand, *J. Am. Chem. Soc.* **1991**, 113, 8375. (b) C. Amatore, A. Jutand, *J. Am. Chem. Soc.* **1993**, 115, 9531. (c) C. Amatore, E. Carré, A. Jutand, M. A. M'Barki, G. Meyer, *Organometallics* **1995**, 14, 5605. (d) C. Amatore, A. Jutand, *J. Organomet. Chem.* **1999**, 576, 254. (e) C. Amatore, A. Jutand, *Acc. Chem. Res.* **2000**, 33, 314.
- 144 M. Lautens, K. Fagnou, *Angew. Chem. Int. Ed.* **2002**, 41, 26.
- 145 (a) W. Cabri, I. Candiani, S. DeBernardinis, F. Francalanci, S. Penco, R. Santi, *J. Org. Chem.* **1991**, 56, 5796. (b) J. G. de Vries, *Dalton Trans.* **2006**, 421.
- 146 (a) A. M. Echavarren, J. K. Stille, *J. Am. Chem. Soc.* **1987**, 109, 5478. (b) S. Verbeeck, C. Meyers, P. Franck, A. Jutand, B. U. W. Maes, *Chem. Eur. J.* **2010**, 16, 12831. (c) F. Proutiere, F. Schoenebeck, *Angew. Chem. Int. Ed.* **2011**, 50, 8192.
- 147 N. A. Bumagin, A. B. Ponomaryov, I. P. Beletskaya, *J. Organomet. Chem.* **1985**, 291, 129.
- 148 E. Negishi, T. Takahashi, K. Akiyoshi, *J. Organomet. Chem.* **1987**, 334, 181.
- 149 Y. Okamoto, K. Yoshioka, T. Yamana, H. Mori, *J. Organomet. Chem.* **1989**, 369, 285.
- 150 R. van Asselt, C. J. Elsevier, *Organometallics* **1994**, 13, 1972.

- 151 M. G. Organ, H. Ghasemi, C. Valente, *Tetrahedron* **2004**, *60*, 9453.
- 152 Q. Liu, Y. Lu, J. Liu, G. Li, Y.-D. Wu, A. Lei, *J. Am. Chem. Soc.* **2009**, *131*, 10201.
- 153 E. G. Dennis, D. W. Jeffery, M. V. Perkins, P. A. Smith, *Tetrahedron* **2011**, *67*, 2125.
- 154 A. Krasovskiy, B. Lipshutz, *Org. Lett.* **2011**, *13*, 3818.
- 155 E. Negishi, T. Takahashi, S. Baba, D. E. Van Horn, N. Okukado, *J. Am. Chem. Soc.* **1987**, *109*, 2393.
- 156 (a) J. A. Casares, P. Espinet, B. Fuentes, G. Salas, *J. Am. Chem. Soc.* **2007**, *129*, 3508. (b) M. García-Melchor, B. Fuentes, A. Lledós, J. A. Casares, G. Ujaque, P. Espinet, *J. Am. Chem. Soc.* **2011**, *133*, 13519.
- 157 The active Pd(0) catalyst forms by reduction in situ: C. Amatore, A. Jutand, M. A. M'Barki, *Organometallics* **1992**, *11*, 3009.
- 158 S. D. Walker, T. E. Barder, J. R. Martinelli, S. L. Buchwald, *Angew. Chem. Int. Ed.* **2004**, *43*, 1871.
- 159 Z.-B. Dong, G. Manolikakes, L. Shi, P. Knochel, H. Mayr, *Chem. Eur. J.* **2010**, *16*, 248.
- 160 G. A. Chass, C. J. O'Brien, N. Hadei, E. A. B. Kantchev, W.-H. Mu, D.-C. Fang, A. Hopkinson, I. G. Csizmadia, M. G. Organ, *Chem. Eur. J.* **2009**, *15*, 4281.
- 161 The high volatility of the expected Bu₂ product prohibited its detection in these experiments.
- 162 All fits were performed by K. Koszinowski. All fitting calculations were performed with the program Gepasi 3.30. Calculations were repeated several times and with different starting values to ensure convergence of the fitting results. In the preliminary kinetic model (used to calculate k_1 , k_8 , and k_9 as input values for the full kinetic model), the kinetic scheme was simplified by approximating the reductive elimination step as instantaneous. For all modeling calculations, the experimental data were normalized to give the proper mass balance ($c(\text{ArI}) + c(\text{ArBu}) + c(\text{ArH}) + 2 c(\text{Ar}_2) = 0.1 \text{ M}$) needed for successful fitting; these normalized data were also shown in the corresponding figures (in contrast, the experimental data displayed in all of the other figures are not normalized). The error introduced by this procedure is considered negligible in comparison to the numerical uncertainties of the fitting results.
- 163 (a) P. Mendes, *Comput. Applic. Biosci.* **1993**, *9*, 563. (b) P. Mendes, *Trends Biochem. Sci.* **1997**, *22*, 361. (c) P. Mendes, D. B. Kell, *Bioinformatics* **1998**, *14*, 869. (d) Also see: <http://www.gepasi.org/gepasi.html>.

12 Curriculum Vitae

Personal

Name: Julia Elisabeth Fleckenstein

Date of birth: 27. November 1980

Place of birth: Würzburg

Citizenship: German

Publications

Microsolvated and Chelated Butylzinc Cations: Formation, Relative Stability, and Unimolecular Gas-Phase Chemistry

J. E. Fleckenstein, K. Koszinowski, *Chem. Eur. J.* **2009**, *15*, 12745.

Charged Tags as Probes for Analyzing Organometallic Intermediates and Monitoring Cross-Coupling Reactions by Electrospray Ionization Mass Spectrometry

M. A. Schade, J. E. Fleckenstein, P. Knochel, K. Koszinowski, *J. Org. Chem.* **2010**, *75*, 6848.

Lithium Organozincate Complexes LiRZnX_2 : Common Species in Organozinc Chemistry

J. E. Fleckenstein, K. Koszinowski, *Organometallics* **2011**, *30*, 5018.
